The University of Sheffield

Bio-Inspired Collective Decision-Making in Game Theoretic Models and Multi-Agent Systems

A thesis submitted in partial fulfilment of the requirements for the degree of Doctor of Philosophy

L Stella

2019

The University Of Sheffield.

The University of Sheffield

Faculty of Engineering

Department of Automatic Control and Systems Engineering

Bio-Inspired Collective Decision-Making in Game Theoretic Models and Multi-Agent Systems

A thesis submitted in partial fulfilment of the requirements for the degree of Doctor of Philosophy

Leonardo Stella

August 2019

Acknowledgements

Firstly, I am truly grateful to Prof. Dario Bauso for his unwavering support throughout the duration of my studies. If this thesis has been completed, it is thanks to his guidance, patience and understanding and most importantly for being the person who managed to talk me into pursuing a PhD in the first place. It has been exceptional to work with a person of his scientific excellence. I would also like to thank Dr. Roderich Gross for his unconditioned help. I am grateful for accepting me as his student during my studies and for his generous and gratuitous support towards the completion of my studies.

I would like to acknowledge the Automatic Control and Systems Engineering directorate for giving me the chance of joining the department and for granting me the funding for this research. I would like to express my thanks to the University of Sheffield for the stimulating environment, albeit competitive and challenging, allowing me to pursue my goals and make a lot of important experiences for my future career.

I would like to dedicate this thesis to someone that probably suffered the most from my absence, my loyal friend Simba. This thesis is also dedicated to my family and specifically to my parents who stoically and unconditionally supported me throughout my entire life. I owe it to them, if I achieved what I achieved. I would also like to thank them for taking care of Simba while I was away.

I would like to express my gratitude to Prof. Andrea Genovese and Patrizia Baldi for the opportunity to make a great secondment experience at Softeco under the supervision of Alessandro Barisone and Andrea Gorini, who I thank for their guidance and tutoring. I would like to thank all the staff at Sheffield for accepting me as a GTA, specifically Ben Taylor, Tara Baldacchino, Viktor Fedun, and Giuliano Punzo. I am grateful to the organisers of the GEC and EYH weeks, giving me the chance to work as a facilitator, and the staff of the Future Learn course in robotics for the experience as a mentor.

Finally, I would like to acknowledge all the amazing people I met and spent time with during the past three years and, despite being hard to thank all of them individually, I think it's mandatory to mention them at the very least. Unlike the wise master said, *"stat rosa pristina nomine; nomina nuda tenemus"* (yesterday's rose endures in its name; we hold empty names), here the names are more than empty. In my memory, they carry the significance of the time I spent with the people bearing them. Therefore, I would like to express my most sincere gratitude to Han, Francesco, Yung Ting, Federico, Matthew, Riccardo, Matteo, Omar, Sinisa, Kacper, Romain, Buket, Isaac, Zhenglin, Sarah, Jing, Qi, Verna, César, Rachel.

Last but not least, I must also extend my thanks to all of my colleagues and friends at Sheffield, whose company and sharing has helped to make it far more than just a workplace.

Declaration

I hereby declare that the present thesis was composed by myself in its entirety, and the work contained herein is my own except when stated otherwise in the text. The work included in Chapter 2 and 3 was done in collaboration with Prof. Dario Bauso, while part of Chapter 4 was done in collaboration with my actual first supervisor, Dr. Roderich Gross, and part with Prof. Dario Bauso. Part of the work in Chapter 2 has been published in the peer-reviewed journals *IEEE Control Systems Letters* and part in *Automatica*. Chapter 3 was presented at two conferences, namely *MED* and *CDC*. Finally, part of Chapter 3 and part of Chapter 4 have been submitted to the peer-reviewed journal *IEEE Transaction of Automatic Control*, for which the manuscript is still under review at the time of submission of this thesis. A list of all the mentioned publication can be found in the next pages.

Abstract

Collective decision-making can be investigated in a variety of different contexts, from opinion dynamics to swarm robotics. In the context of honeybee swarms, the evolutionary dynamics corresponding to the honeybee consensus problem can be studied via game theoretic tools. Evolutionary game theory provides the necessary tools to capture the relevant aspects for the decision-making process, whereas mean-field game theory serves well as a framework to analyse the optimal response of a large number of interacting players, even in the case of adversarial disturbance, where the aim is to ensure the robustness of the system to worst-case deterministic perturbations. The interactions among players, often originating in the corresponding real system from a social or physical structure, e.g. humans or animals for social and nodes of a power network for physical, can be captured by means of a network. In this thesis, the model originating in the context of bio-inspired collective decision-making is formulated in a game theoretic framework. The study of the corresponding consensus problem is carried out by analysing the stability property of the system and the corresponding optimal strategies in the presence of an adversarial disturbance. A threshold is identified to prevent a situation of deadlock, which happens when the population is stuck in a scenario where no option has predominantly taken over. The analysis is then extended to compartmental models, which share similarities with the original system and gives insight on asymmetric evolutions of the system. Through this link, other relevant applications are considered, such as duopolistic competition in marketing and virus propagation in smart grids. Finally, structured environments are explored as an extension to the original model, and the structure is captured by means of undirected graphs or of the Barabási-Albert scale-free (SF) complex network model.

List of Publications

Parts of the work present in this thesis have been reported in the following journal publications and conference proceedings:

Journal Publications

1. L. Stella and D. Bauso, "Bio-inspired Evolutionary Dynamics on Complex Networks under Uncertain Cross-inhibitory Signals", *Automatica*, vol. 100, pp. 61-66, 2019. Available: 10.1016/j.automatica.2018.11.005.
2. L. Stella and D. Bauso, "Bio-Inspired Evolutionary Game Dynamics in Symmetric and Asymmetric Models", *IEEE Control Systems Letters*, vol. 2, no. 3, pp. 405-410, 2018. Available: 10.1109/lcsys.2018.2838445.

Conference Proceedings

1. L. Stella and D. Bauso, "On the nonexistence of stationary solutions in bio-inspired collective decision making via mean-field game", in *IEEE 56th Annual Conference on Decision and Control (CDC)*, Melbourne, VIC, Australia, 2017, pp. 787-792.
2. L. Stella and D. Bauso, "Stationary and initial-terminal value problem for collective decision making via mean-field games", in *25th Mediterranean Conference on Control and Automation (MED)*, Valletta, Malta, 2017, pp. 1125-1130.
3. L. Stella and D. Bauso, "Evolutionary Game Dynamics for Collective Decision Making in Structured and Unstructured Environments", in *20th IFAC World Congress*, Toulouse, France, 2017, vol 50, no. 1, pp. 11914-11919.

Contents

List of Figures

List of Tables

CHAPTER 1

Introduction

This thesis is the result of the work of research carried out by the PhD candidate at the University of Sheffield, department of Automatic Control and Systems Engineering. This thesis is submitted in partial fulfilment of the requirements for the degree of Doctor of Philosophy. The dissertation consists of five chapters, namely the Introduction, three chapters for the main body and the Conclusion. Chapter 2, Chapter 3 and Chapter 4 constitute the main body of this thesis.

1.1 Overview

Each chapter of the main body describes a collective decision-making problem in a different framework, first evolutionary game theory, then mean-field game theory and finally structured/stochastic interactions. The models corresponding to each framework are formulated and studied in detail. Although the aforementioned models are investigated separately in each chapter, they constitute a whole due to the fact that they share a common ground and because they originate from the same source, at least in the general formulation. Each model is then linked to a different discipline or context. This multidisciplinary approach constitutes one original aspect of this work. The common source of these models can be traced back to the problem of finding a new nest in the context of swarms of honeybees, see [91], and, in general, in the study of social insects such as wasps, ants, bees and termites, see [108]. The properties that motivate the study of such bio-inspired collective decision-making problem can be linked to multi-agent system properties such as: scalability, i.e. the number of agents can be increased *ad libitum*, e.g. this is the case for swarm robotics; robustness, i.e. system performance

is not compromised by perturbations or adversarial disturbances; and resilience, i.e. the system is not disrupted even in case of small failures of a number of its parts.

To understand the problem, a general overview should be given: the ground in which this research moves involves a swarm of bees that has to choose between two options. The choice is crucial for the survival of the swarm and it depends on multiple factors, e.g. size of the entrance or exposure of the nest to rain. Scout bees advertise the position and quality of the possible nest options by means of the so-called *waggle dance*. At the same time, competing scouts try to disrupt the other bees' waggle dance by sending a cross-inhibitory stop signal. In the rest of the thesis, many of the proposed applications and examples cover this scenario in more detail by bridging the gap between the theoretical models and the honeybee swarm consensus problem. Additional applications are also proposed.

The literature studies the model originating in the context of honeybee swarms in the framework of swarm robotics and value-sensitive decision-making, see [19] and [80]. Especially in the latter, the authors concentrate mostly on the case where the two options have equal value. In this scenario, they report results in terms of deadlock avoidance and in terms of the analysis of the corresponding bifurcation diagrams which depend on the value of the cross-inhibitory signal. The model proposed in this thesis aims to extend the original system to the case where the options have different values and the signal changes over time, stressing a different perspective based on the Lyapunov's direct method for stability analysis and control design. For a general overview of the honeybee swarm model, the reader is referred to [81], [82], [101]. In recent times, the interest for these bio-inspired problems has grown in the control community, as reported in [45] and [94] in general terms, or in [90] and [113] for a perspective on consensus and swarm dynamics, or in [84] for a focus on decision-making.

Game theory provides the framework that is used to investigate the above problem. Technically, game theory studies the strategic interactions of rational individuals, in a cooperative or competing context. To make a parallelism with multi-agent systems, a game can be described as a multi-agent decision problem in a strategic setting. In this setting, the players' actions are interdependent, which makes this approach different from decision theory. The formal establishment of game theory can be traced back to 1944 when von Neumann and Morgenstern published "Theory of games and economic behaviour", see [76]. Game theory has grown in popularity really fast since then, and

has been applied to a variety of domains, spanning from social sciences to formal sciences. Evolutionary game theory was developed in response to the interest in the natural sciences to study natural systems. For a general overview on game theory, the reader is referred to [52], [75], [79]. In the context of collective decision-making, a game perspective is provided in [88]. The problem of finding consensus and the corresponding game are studied in [112]. In the following, a brief description of the content of each chapter is provided.

1.2 Core Contributions

In order to highlight the importance of this work, a summary of core contributions is given in this section. The relationship between the different contributions is indicated explicitly to allow the reader to better follow the development of the work in the next chapters. A list of core contributions follows:

1. ***Formulation of a model to explain the behavioural traits of honeybee swarms in a game theoretic framework***. For the first contribution, the model originating in the context of honeybee swarms is reframed using evolutionary game theory. A new notion of game dynamics, i.e *Expected Gain Comparison*, is formulated and then applied to the game, with the aim to match the transition rates of the initial model with the payoff matrix of the corresponding game model. The strategic aspects of the game are investigated in the macroscopic and microscopic dynamics, i.e. the study of the population as a whole and from the perspective of a reference player.

2. ***Extension of the model to symmetric and asymmetric cases, including conditions for local asymptotic stability of the equilibria***. The second contribution involves the extension of the game model to the case where parameters are symmetric or asymmetric, namely the parameters are equal for both options, e.g. $\gamma := \gamma_1 = \gamma_2$, or different, e.g. $\gamma_1 \neq \gamma_2$, respectively. The case where also the structure of the game is no longer symmetric is considered, namely the transitions between states 1 and 3 are no longer possible, i.e. $\sigma_2 = 0$, $\alpha_2 = 0$. A stability analysis is carried out for each case where the equilibrium points of each system

are identified and studied in terms of local asymptotic stability.

3. ***Study of the individual and collective behaviour that leads to deadlock or consensus based on a threshold on the cross-inhibitory signal via Lyapunov stability analysis***. The third contribution generalises the results found in the literature for deadlock on the value of the cross-inhibitory signals. The threshold is generalised in terms of the parameters of the model rather than specific values coming from the honeybee swarm example. In order to formulate this general threshold, a new perspective based on Lyapunov stability analysis is given. This is then extended to the structured case in the last chapter.

4. ***Study of absolute stability and passivity for the collective system under time-varying and uncertain cross-inhibitory parameter via the Kalman-Yakubovich-Popov lemma***. In the fourth contribution, the problem of uncertain time-varying cross-inhibitory parameter is tackled by isolating the nonlinearities in a feedback loop. The only assumption is that the uncertain parameter is bounded. When the system has symmetric structure, absolute stability is preserved, whereas when the structure is asymmetric, passivity of the system is proved.

5. ***Formulation of a mean-field game model and the corresponding stationary solutions in the robust case***. The fifth contribution extends the game model to a mean-field game framework, where the transition rates are derived from the players' controls and an adversarial disturbance. The mean-field Nash equilibrium is found and stationary solutions are investigated with respect to their stability properties. When the disturbance is the worst-case deterministic signal, the robust mean-field game is studied and a basin of attraction is found under certain conditions for the parameters.

6. ***Study of the impact on stability of different interaction topologies***. The last major contribution includes results on the impact of interaction topologies and stochastic dynamics on transient response and steady-state. When the topology is modelled through complex networks, it is proved that a higher connectivity would

result in a faster transient response and higher values of uncommitted agents at steady-state at equilibrium. When the topology is modelled through an undirected graph with adjacency matrix A, similar results are established with a link to compartmental models such as the susceptible-infected-recovered (SIR) model.

1.3 Applications

This section illustrates some possible applications for this research, in practical contexts such as opinion dynamics or virus propagation. A more detailed discussion of each application is given in Chapter 4, where the model is specialised and the meaning of the parameters is explained for each application context.

Duopolistic Competition in Marketing. In this context, two manufacturers sell the same product in a market and each manufacturer has a share of this market. The analogy with the nest options is that the population has to choose one product, either from the first manufacturer or from the second. Part of the population can also decide not to buy any of the two products. The model proposed in this thesis can describe this scenario in an appropriate way, including also an advertising effort to make the potential customers buy one of the products or to prevent them to buy the opposing one by disrupting the other manufacturer's advertisement. In the structured case, the topology models the interactions among customers and it is shown that by increasing the connectivity the equilibrium shifts toward a higher number of undecided customers.

Opinion Dynamics. This application models the scenario where two political parties compete for a voting campaign, e.g. an election or a referendum. The voters are given two options, e.g. left and right, but they can also choose not to vote. The model describes the persuaders' effort to make people vote for their party and to prevent them from voting for the opposing party. When the voters' interactions are modelled via a network topology, it can be seen that the more the connections, the more voters remain undecided at steady state.

Virus Propagation in Smart Grids. Linking the original formulation of the model to compartmental models such as the SIR (susceptible-infected-recovered) and the SIS

(susceptible-infected-susceptible) models for the asymmetric case, it is easy to see an analogy with virus propagation. The problem is tackled within the context of smart grids, where the interaction topology plays a crucial role in the system evolution, whether the system is compromised or not. Different kinds of cyber-attacks are considered, e.g. continuous low-rate attacks and sequential attacks. By using a model for coupled oscillator, it can be shown that the connectivity has a negative impact in that it makes the node more prone to be infected. However, a higher connectivity mitigates the impact of the infection through the coupling strength. A practical scenario on a real network is discussed in a case study in Chapter 4.

1.4 Summary

Chapter 2 introduces the evolutionary game model which extends the evolutionary dynamics originating in the context of the collective decision-making problem for a swarm of honeybees. First, the original model is reframed into the corresponding evolutionary game dynamics. The evolutionary game model is then specialised to three different cases and, in each of the these cases, the corresponding Markov chain has different transition rates which depend on the different parameters involved in the decision-making process. These cases include a more general model with asymmetric parameters, a model with symmetric parameters and, finally, a model with asymmetric structure. The dynamics with asymmetric structure share similarities with well-known compartmental models such as the Susceptible-Infected-Recovered (SIR) model. The players' goal is to reach consensus on one option and this mimics the same behaviour that honeybees exhibit when choosing a nest. In order to achieve this, players can send a signal to other players with the aim of disrupting the advertisement of the opposing option. Especially in the case of symmetric options, the value of this signal is crucial to avoid deadlocks and preserve stability. Furthermore, the evolution of the system under a time varying signal is investigated and results in terms of absolute stability and passiveness are presented, both constituting novel aspects with respect to the literature.

Chapter 3 introduces a more general mean-field game model which extends the evolutionary dynamics presented in the first chapter. The study of the macroscopic and microscopic dynamics is carried out independently first, and then in a unified framework where both dynamics characterise the initial-terminal value problem and therefore the

Nash equilibrium. Given a large population of small decision makers, the macroscopic dynamics describe the evolution of the population as a whole. On the other hand, the microscopic dynamics show the evolution of a reference player's response in terms of his/her strategic approach. The stationary solutions are presented and studied in the special case where the difference between the value function for the uncommitted state and the value function for each option is considered. Within this context, the presence of a basin of attraction is investigated and results in terms of periodic orbits are given. Finally, the link to the initial model is provided, showing that the mean-field game is a generalisation of the initial problem when parameters are set as in the honeybee swarm scenario.

Chapter 4 extends the models proposed in the previous chapters to a structured environment, under a multi-agent modelling framework. The study of the structure is twofold: in the first case, the structure is captured by a complex network, while in the second the interactions are modelled by means of an undirected graph. In both cases, the impact of the connectivity is throughly analysed, providing results in terms of stability for all the equilibrium points of the system. For the first case, the effects of a higher connectivity are measured in terms of a faster transient response and of a larger number of uncommitted agents at steady-state. The link for other applications, such as opinion dynamics and duopolistic competition, is presented in a separate section. A detailed analysis of a case study involving a real network is given in the context of virus propagation in smart grids. The impact of the structured environment is measured in terms of the resistance of the nodes to the infection. Furthermore, the original 2-option model is extended to the n-option case under stochastic perturbations in the context of nudge theory. Finally, an initial study on buffer networks is provided. This study is carried out in the setting of a swarm of robots, where each node of the network models the actual buffer of a robot and the corresponding routing problem is considered.

CHAPTER 2

Evolutionary Game Theoretic Framework for Consensus Problems

2.1 Introduction

The problem of finding consensus in a population of individuals is tackled in this chapter. Inspired by the biological studies on honeybee swarms, the problem involves a large number of players that have to choose one of two possible options in a collective way. A key aspect for the evolutionary dynamics involves two behaviours that are significant to achieve consensus: the waggle dance and the cross-inhibitory stop signal. The first behaviour is used to attract undecided individual to one's option, whereas the second behaviour is used to force individuals committed to the opposite option to become undecided again.

The original model is reframed in the context of evolutionary game theory. After studying the system in more general terms, two variants are introduced. These variants, which are denominated 'symmetric parameters' and 'asymmetric structure', are investigated in detail and the stability analysis is carried out for each of them. In the case of the asymmetric structure, the asymmetric system bridges the gap between the original problem and compartmental models such as the Susceptible-Infected-Recovered (SIR) model. Both variants, i.e. symmetric case and asymmetric case, are then extended to the context of uncertain time varying parameters. In this context, the system is then proved to be absolutely stable for symmetric parameters or passive for asymmetric structure.

2.1.1 Literature Review

Evolutionary game theory was originally developed as a mathematical application to biological contexts, with the aim to study the dynamics of a given population of animals. The main idea was that the number of offspring, referred to as *fitness*, was indeed linked to a strategic aspect of evolution. In general terms, given a population of individuals, whether they are animals or humans, all the individuals belonging to that population behave in different ways, i.e. make different decisions. In the biological interpretation of the evolution, the offspring genetically inherits these behavioural decisions from their ancestors. This procedure is referred to as *phenotypic gambit*. Over time, the frequency of each decision can change due to the response from the rest of the population. The frequency of a given strategy evolves according to how successful the strategy is. Successful strategies correspond to higher payoffs because they are linked to a greater number of offspring. Therefore the individuals choosing a successful strategy will become dominant in the considered population. For a general survey on the literature of evolutionary game theory, see [52], [53], [71], [77], [78], [89], and plenty of references therein.

In more formal terms, an evolutionary game consists of a population of decision makers under a game theoretic framework, where each individual adjusts his/her strategies over time in response to the strategies played by the other participants in the game. The term *population profile* refers to the vector that models the probability in which each strategy is played in the population. In an evolutionary game, an evolutionarily stable strategy (ESS) is the analogous concept of the Nash equilibrium in classical game theory. Evolutionary games can be distinguished into two types, i.e. pairwise contests and games against the field, albeit some evolutionary games can include interactions between both. A pairwise contest consists of a scenario where a reference player plays against an opponent chosen at random in the population. The payoff depends on the strategies selected by both players. This kind of games is similar to games in classical game theory. The other type, i.e. games against the field, does not involve a couple of players directly, where one plays with another, but rather a reference player playing with the rest of the population. Therefore, the payoff is not necessarily linear in the probabilities since it depends on which strategies all the players in the population choose. These latter games are often called "frequency-dependent selection", see [105].

Evolutionary game theory was initially developed by R. A. Fisher, see [38], in 1930. Fisher's aim was to investigate the approximate equality of the sex ratio in mammals

and explain the evolution and stability of this ratio. Fisher's findings showed that the equality could be explained in terms of the individuals' fitness: each individual would benefit from an equal distribution of males and females in maximising the expected number of grandchildren. However, since Fisher's argument was not explicitly stated in game theoretic terms, the first formal approach in the field, an application of game theory to evolutionary biology, is attributable to in R.C. Lewontin in 1961, see [66].

Later, in 1972, the concept of ESS was introduced by J. M. Smith, see [92], who investigated the stability and its link to the notion of evolution rather than to rationality as in classical game theory. In the following year, the same concept became widespread, when it was used by Smith and Price to describe the scenario in which two animals of the same species fight for supremacy, dominance right and territory, see [93]. The proposed analysis showed that an injury is unlikely or impossible in such conflicts due to individual selection and for the fact that evolutionary stability involves diversity in the population, i.e. individuals' different approaches to each contest.

Evolutionary game theory has also been used to describe and explain the emergence of multiple phenomena in nature. As an example, consider the fighting behaviours that lead to supremacy and territoriality as in [93]. Another example is the so-called *kin selection*, in the context of biological altruism. The idea involves an altruistic behaviour of an organism that is willing to share food with others at its own cost. However, these altruistic organisms discriminate in who they share food with; in fact they do not share food with the all the other individuals in the population, but only with their relatives. In terms of the evolution, this means that the relatives are likely to be genetically similar and thus the altruistic gene would be favoured by natural selection under a certain condition called *Hamilton's rule*, from the name of W. D. Hamilton who published two seminal papers on the topic, see [47], [48]. Real life examples of biological altruism include worker bees that provide food for their queen and never mate, and vampire bats that feed other individuals who failed to feed during the night's hunt.

The model proposed in this chapter belongs to the class of nonlinear discrete-state continuous-time systems. The model combines the evolutionary game approach and the mathematical framework in epidemiology. A central role in the study of evolutionary games is played by 6 families of game dynamics, see [52] and the references therein. Of interest for the proposed model are the replicator dynamics and the dynamics based on pairwise comparison. Replicator dynamics are the most common functional expression

for the fitness in an evolutionary game. Replicator dynamics are non-innovative, i.e. they cannot generate new strategies, while the dynamics based on pairwise comparison are innovative dynamics.

The framework in epidemiology refers to the so-called compartmental models, studied by Kermack and McKendrick in 1927 in an early work, i.e. [60]. Compartmental models provides a set of techniques which are widely used to model infectious diseases. The key point involves a simplification of the model by dividing the population into compartments or classes. The individuals in the same compartment is assumed to have similar characteristics and thus behave in the same way. The SIS (Susceptible-Infected-Susceptible) model refers to the family of diseases that can periodically infect an individual without granting them immunity. The most widely known model is the SIR (Susceptible-Infected-Recovered) model, see [51]. In the SIR model, when an infected individual recovers from the disease, he/she cannot be infected again from the same virus. For the derivation of an exact analytical solution to the SIR model, see [49].

These models have been widely used to predict the outcome of the epidemic under consideration, i.e. how the virus propagates in the population, the percentage of the infected individuals at any given time and the speed of the virus spreading. More recently, they have been used under a network topology to describe the internet and the World-Wide Web (WWW), see [72] and the references therein. The model in structured environment is the focus of Chapter 4.

2.1.2 Summary and Contributions

The focus of this chapter is to the study the evolutionary game dynamics inspired by honeybees and to carry out the stability for each equilibrium point of the corresponding system. The word *consensus* refers to the situation in which the population converges to one of the options, possibly when the number of individuals committed to this option goes above a certain threshold. A large population of indistinguishable players has to reach consensus on one of three options. It is worth emphasising that the proposed setting differ from the standard evolutionary dynamics where the original model was proposed, because of the evolutionary game approach.

The main contributions presented in this chapter are highlighted in the following. First, the original model is reframed in the framework of evolutionary game dynamics, where the study of the Lyapunov stability is carried out. Additionally, the model is

specialised in symmetric and asymmetric structure, and the dynamics are studied by taking into account the compartmental models such as the SIR epidemic model. Finally, the study of the cross-inhibitory coefficient is carried out under the assumption that this coefficient is treated as a time varying disturbance, as opposed to a constant signal. This approach yields novel results in terms of the absolute stability and passivity of the corresponding system.

2.1.3 Structure

Chapter 2 is organised as follows. In Section 2.2, the general model is introduced and parameters are asymmetric, i.e. the two options have different values and therefore the transition rates are different. This means that the parameter for the waggle dance, for instance, has a different value for each of the two options. In Section 2.3, the model under symmetric parameters is introduced, which corresponds to the case where the options have the same intrinsic value and so do the parameters. In Section 2.4, some transitions between states are no longer allowed which leads to an asymmetric structure which can be linked to the compartmental models in epidemiology. In each of the last two sections, a formulation of the model is presented first; secondly, the stability analysis is carried out; thirdly, the problem of uncertain cross-inhibitory coefficients is tackled; and, finally, the numerical analysis is introduced to corroborate the theoretical results.

2.2 General Model

A nonlinear discrete-state continuous-time system is considered. A large population of players has to reach consensus on one of two possible options in a distributed way. While players can choose to commit to either option, they cannot change their decision directly from one option to the other. A player committed to either option can abandon their commitment to their option and move to the uncommitted state before choosing to commit to the other one. Additionally, with the aim to achieve consensus, players benefit from choosing the more popular option.

Figure 2.1 shows the Markov chain corresponding to each of the three models described in the following. In the case of asymmetric parameters, namely $r_1 \neq r_2$, $\gamma_1 \neq \gamma_2$, $\alpha_1 \neq \alpha_2$ and $\sigma_1 \neq \sigma_2$, the corresponding model is displayed in Fig. 2.1 (top-left). The Markov chain in Fig. 2.1 (top-right) refers to the case of symmetric parameters,

namely $r := r_1 = r_2$, $\gamma := \gamma_1 = \gamma_2$, $\alpha := \alpha_1 = \alpha_2$ and $\sigma := \sigma_1 = \sigma_2$. The Markov chain in Fig. 2.1 (bottom) refers to the asymmetric structure, which does not allow players to move from state 1 to state 3. In general, these Markov chains describe each scenario from the corresponding macroscopic perspective. This means that the population as a whole is considered rather than individual players. This is why the number of players is not important in this context, and instead the portion of the population of each state is considered, namely x_1 for the players choosing strategy 1, x_2 for the players choosing strategy 2 and and x_3 for the players choosing strategy 3. When the number of players is assumed to tend to infinity, this is similar to the mean-field case in Chapter 3. Due to the way the model is defined in this context, concepts like proximity are not included here but are taken into consideration for the structured case in Chapter 4.

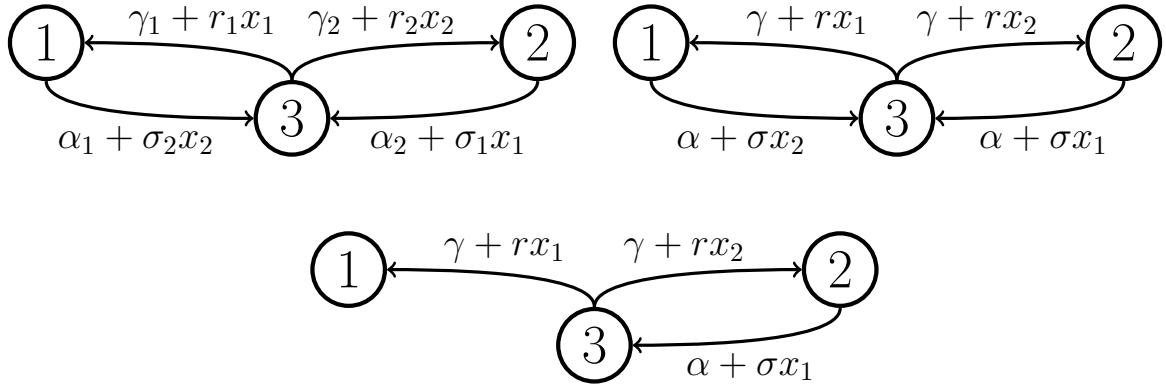

Figure 2.1: Markov chain representations relating to the asymmetric parameters, namely $r_1 \neq r_2$, $\gamma_1 \neq \gamma_2$ etc., in (2.6) (top-left), the symmetric parameters, i.e. $r := r_1 = r_2$, etc., in (2.9) (top-right), and the asymmetric structure in (2.17) (bottom), describing the transition rates between different states.

The most general model to be considered is when the structure is symmetric but the parameters are not. The two options correspond to states 1 and 2, while state 3 represents the uncommitted part of the population. A player who is in state 1 can recruit uncommitted players, by means of an effort, i.e. $r_1 \geq 0$, or $r_2 \geq 0$ if the player is in state 2. Moreover, committed players can send cross-inhibitory signals to players committed to a different option, and the strength of this signal is modelled through $\sigma_1 \geq 0$ and $\sigma_2 \geq 0$. The parameter σ_1 models the signals sent from players who choose strategy 1 towards those who choose strategy 2. The other parameter σ_2 models the opposite scenario. It is worth clarifying that the three terms *strategy*, *state* and *decision* can be

and are used interchangeably due to the structure of the game under consideration.

Each player chooses within a set of three pure strategies, i.e. committing to option 1, or to option 2 and being uncommitted. Table 2.1 illustrates the framework described so far, where the reference player is the row player and the column player can be any other player in the population.

Table 2.1: Normal-form table for the two-player game.

	Option 1	**Option** 2	**Uncommitted**
Option 1	r_1, r_1	$-\sigma_2$, $-\sigma_1$	0
Option 2	$-\sigma_1$, $-\sigma_2$	r_2, r_2	0
Uncommitted	0	0	0

The non-zero entries of Table 2.1 simulate a *coordination game*, whereby the row player benefits from matching the column player's strategy. More formally, coordination games are a class of games with multiple pure strategy Nash equilibria in which players benefit from choosing the same strategies. When both players choose the same strategy, they earn r_1 and r_2 for matching strategy 1 or 2, respectively. Otherwise the row player looses σ_1 or σ_2 if playing strategy 2 or 1 while the column player plays the other strategy and vice versa. Uncommitted players neither gain nor lose anything in random-matching with opponents. The presented framework models a *crowd-seeking* scenario where the benefit of choosing strategy 1 or 2 depends on the frequency of that strategy.

Before introducing the model, some preliminaries are due. Let the frequency of strategy i, namely the portion of the population who has selected that strategy, be defined by $x_i(t) \in \mathbb{R}_0^+$, $\sum_{i=1}^{3} x_i = 1$, for $i = 1, 2, 3$. For simplicity, the notation x_i will be used in place of $x_i(t)$. Let $\mathbf{x} = [x_1, x_2, x_3]^T$ be the vector of all strategies. Let $A \in \mathbb{R}^{3\times 3}$ be the payoff matrix defined according to the normal-form table above as:

$$A = \begin{pmatrix} r_1 & -\sigma_2 & 0 \\ -\sigma_1 & r_2 & 0 \\ 0 & 0 & 0 \end{pmatrix}, \tag{2.1}$$

where r_1, r_2, σ_1 and σ_2 have the previously defined meaning.

The evolution of the frequencies of each strategy is in accordance with the following

game dynamics which links to the notion of innovative dynamics as in [52]. Let $\rho_{ij}(\mathbf{x}) \in \mathbb{R}_0^+$ be the transition rate from i to j:

$$\dot{x}_i = \sum_j x_j \rho_{ji} - x_i \sum_j \rho_{ij}. \tag{2.2}$$

The following is the definition of *expected gain comparison* given x.

Definition 1. ***(Expected gain comparison)*** *Given a payoff matrix $A = (a_{ij})$, by changing from strategy j to i the expected gain pairwise payoff comparison is defined as*

$$E_{ji}(x) = \sum_{k=1}^{n} (a_{ik} - a_{jk})_+ x_k + b_{ji}, \tag{2.3}$$

where $(a_{ik} - a_{jk})_+$ denotes the positive part of $a_{ik} - a_{jk}$, and b_{ji} is an offset.

It is worth noting that equation (2.3) can be linked to Kahneman and Tversky's prospect theory through a weighting function which assigns zero weight to the probability of unfavourable events in a risk-seeking scenario, see [57]. One major difference with the work of Kahneman and Tversky is that the offset is not considered in their work, whereas it is used in this model to capture individual decisions that are not influenced by the players in the other states. The above definition models the expected revenue obtained by considering the probability of a payoff increase only and ignoring payoff decreases in correspondence to a unilateral change of strategy.

Example 1. *Let the general payoff matrix be the following:*

$$A = \begin{pmatrix} a_{11} & a_{12} & a_{13} \\ a_{21} & a_{22} & a_{23} \\ a_{31} & a_{32} & a_{33} \end{pmatrix}.$$

Given the above payoff matrix, the game dynamics associated with the expected gain comparison has the following transition rates:

$$\begin{aligned}
\rho_{31} &= x_1(a_{11} - a_{31})_+ + x_2(a_{12} - a_{32})_+ + x_3(a_{13} - a_{33})_+ + \gamma_1, \\
\rho_{13} &= x_1(a_{31} - a_{11})_+ + x_2(a_{32} - a_{12})_+ + x_3(a_{33} - a_{13})_+ + \alpha_1, \\
\rho_{32} &= x_1(a_{21} - a_{31})_+ + x_2(a_{22} - a_{32})_+ + x_3(a_{23} - a_{33})_+ + \gamma_2, \\
\rho_{23} &= x_1(a_{31} - a_{21})_+ + x_2(a_{32} - a_{22})_+ + x_3(a_{33} - a_{23})_+ + \alpha_2.
\end{aligned}$$

In the above, the offset is taken as $b_{31} = \gamma_1$, $b_{13} = \alpha_1$, $b_{32} = \gamma_2$, and $b_{23} = \alpha_2$.

By assuming $\rho_{ij} = E_{ij}(x)$, each ρ_{ij} in equation (2.2) can be replaced with the expression of the right-hand side of (2.3). Therefore, the transition rates can be derived by using the payoff matrix in (2.1) as:

$$\begin{aligned} \rho_{31} &= x_1(r_1)_+ + x_2(-\sigma_2)_+ + \gamma_1 &&= r_1x_1 + \gamma_1, \\ \rho_{13} &= x_1(-r_1)_+ + x_2(\sigma_2)_+ + \alpha_1 &&= \sigma_2x_2 + \alpha_1, \\ \rho_{32} &= x_1(-\sigma_1)_+ + x_2(r_2)_+ + \gamma_2 &&= r_2x_2 + \gamma_2, \\ \rho_{23} &= x_1(\sigma_1)_+ + x_2(-r_2)_+ + \alpha_2 &&= \sigma_1x_1 + \alpha_2, \end{aligned} \tag{2.4}$$

where the offset b_{ij} is set to γ_1, α_1, γ_2 and α_2 for each transition rate, respectively. The offset can be interpreted as the way in which players spontaneously choose to commit or to abandon an option. That said, the general model is derived as in the following:

$$\begin{cases} \dot{x}_1 = x_3(r_1x_1 + \gamma_1) - x_1(\alpha_1 + \sigma_2x_2), \\ \dot{x}_2 = x_3(r_2x_2 + \gamma_2) - x_2(\alpha_2 + \sigma_1x_1), \\ \dot{x}_3 = x_1(\alpha_1 + \sigma_2x_2) + x_2(\alpha_2 + \sigma_1x_1) - x_3(r_1x_1 + \gamma_1) - x_3(r_2x_2 + \gamma_2). \end{cases} \tag{2.5}$$

The formulation of system (2.5) can be reduced to a two-dimensional system by using the conservation of mass, i.e. $\dot{x}_3 = -\dot{x}_1 - \dot{x}_2$, as:

$$\begin{cases} \dot{x}_1 = (1 - x_1 - x_2)(r_1x_1 + \gamma_1) - x_1(\alpha_1 + \sigma_2x_2), \\ \dot{x}_2 = (1 - x_1 - x_2)(r_2x_2 + \gamma_2) - x_2(\alpha_2 + \sigma_1x_1). \end{cases} \tag{2.6}$$

2.3 Symmetric Parameters

Different parameters, as discussed so far, are used to describe the fact that each option has a different inner value, making one more appealing than the other or vice versa. The problem where all options have the same value (or, in other words, when the options are almost indistinguishable in terms of quality) is what motivates the following study. In this case, the parameters become: $r := r_1 = r_2$, $\gamma := \gamma_1 = \gamma_2$, $\alpha := \alpha_1 = \alpha_2$ and $\sigma := \sigma_1 = \sigma_2$. Therefore, the payoff matrix $A_s \in \mathbb{R}^{3\times3}$ for symmetric parameters is defined as:

$$A_s = \begin{pmatrix} r & -\sigma & 0 \\ -\sigma & r & 0 \\ 0 & 0 & 0 \end{pmatrix}. \tag{2.7}$$

By following the same reasoning as for the asymmetric parameters, the transition rates can be derived by using the payoff matrix in (2.7) as:

$$\begin{aligned} \rho_{31} &= rx_1 + \gamma, \qquad & \rho_{13} &= \sigma x_2 + \alpha, \\ \rho_{32} &= rx_2 + \gamma, \qquad & \rho_{23} &= \sigma x_1 + \alpha, \end{aligned} \tag{2.8}$$

leading to the following model:

$$\textit{Symmetric parameters} \begin{cases} \dot{x}_1 = (1 - x_1 - x_2)(rx_1 + \gamma) - x_1(\alpha + \sigma x_2), \\ \dot{x}_2 = (1 - x_1 - x_2)(rx_2 + \gamma) - x_2(\alpha + \sigma x_1). \end{cases} \tag{2.9}$$

2.3.1 Local Asymptotic Stability

In this section, the stability analysis of system (2.9) under symmetric parameters is carried out. First, the equilibrium points of the system are found and then local asymptotic stability is studied.

Theorem 1. *Given an initial state* $\hat{\mathbf{x}} = (\hat{x}_1, \hat{x}_2, \hat{x}_3)$*, the equilibria* $x^* = (x_1^*, x_2^*, x_3^*)$ *of game dynamics (2.9) are:*

- ***Case 1****. When* $x_1 = x_2$*,*

  $$x^* = \left(\tfrac{(r-2\gamma-\alpha)+\hat{\Delta}}{2(2r+\sigma)}, \tfrac{(r-2\gamma-\alpha)+\hat{\Delta}}{2(2r+\sigma)}, 1 - \tfrac{(r-2\gamma-\alpha)+\hat{\Delta}}{2r+\sigma} \right),$$

  where $\hat{\Delta} = \sqrt{(r - 2\gamma - \alpha)^2 + 4\gamma(2r + \sigma)}$.
- ***Case 2****. When* $x_3 = \alpha/r$*,*

  $$x^* = \left(\tfrac{1-\frac{\alpha}{r}+\sqrt{(1-\frac{\alpha}{r})^2+\frac{4\alpha\gamma}{\sigma r}}}{2}, 1 - \tfrac{1-\frac{\alpha}{r}+\sqrt{(1-\frac{\alpha}{r})^2+\frac{4\alpha\gamma}{\sigma r}}}{2} - \tfrac{\alpha}{r}, \tfrac{\alpha}{r} \right).$$

- ***Case 3****. When* $x_1 = x_2$ *and* $x_3 = \alpha/r$*,*

  $$x^* = \left(\sqrt{\tfrac{\alpha\gamma}{r\sigma}}, \sqrt{\tfrac{\alpha\gamma}{r\sigma}}, \tfrac{\alpha}{r} \right) = \left(\tfrac{r-\alpha}{2r}, \tfrac{r-\alpha}{2r}, \tfrac{\alpha}{r} \right).$$

Proof. See Section 2.6. □

Corollary 1. *Let* $\alpha \to 0$*, the equilibria converge to* $(1, 0, 0)$ *in* ***Case 2*** *and to* $(\frac{1}{2}, \frac{1}{2}, 0)$ *in* ***Case 3****.*

It is worth noting that the equilibrium point $(1, 0, 0)$ corresponds to convergence to option 1, whereas $(\frac{1}{2}, \frac{1}{2}, 0)$ means that the players are uniformly distributed between the two options. Finally, an equilibrium point such $(0, 1, 0)$ corresponds to consensus on

option 2. Cases 1 and 3 refer to equilibrium points that are symmetric, i.e. the same number of individuals are committed to option 1 and 2. The next result establishes local asymptotic stability of the symmetric equilibrium described in Case 1.

Theorem 2. *Given an initial state* $\hat{\mathbf{x}} = (\hat{x}_1, \hat{x}_2, \hat{x}_3)$*, the symmetric equilibrium point in Case 1 is locally asymptotically stable if and only if*

$$\sigma \leq \frac{4r\alpha\gamma}{(r-\alpha)^2}. \tag{2.10}$$

Proof. See Section 2.6. □

Remark 1. *In the special case where* $\alpha = \frac{1}{r}$ *and* $\gamma = r$*, the above result is in accordance with the threshold value reported in equation (4) in [80].*

2.3.2 Uncertain Cross-Inhibitory Coefficient

In this section, the cross-inhibitory coefficient is no longer considered constant. Instead, it is a time varying signal $\sigma(t)$ with a pre-specified amplitude. By isolating the non-linearity related to the uncertain cross-inhibitory coefficient in the feedback loop, the stability of the whole system is proved not to be compromised. Specifically, absolute stability is ensured by using the Kalman-Yakubovich-Popov lemma, see Chapter 10.1 in [58].

The following assumption introduces the sector nonlinerarities, by providing a lower bound and an upper bound for the values taken by the time varying cross-inhibitory coefficient. This fact is in accordance with the physical interpretation of the coefficient as an effort to persuade players committed to the other option to abandon their strategy.

Assumption 1. *Let the cross-inhibitory coefficient* $\sigma(t)$ *be in* $[0, \tilde{k}]$*, where* $\tilde{k} > 0$ *is the upper bound of the strength of the signal.*

The focus of this work is not to investigate a specific value of $\tilde{k}$ but rather the fact that the strength of the signal changes over time, similarly to the honeybee swarm model. If given the need to specify a value, a good approximation for a value of $\tilde{k}$ would be the value in (2.10) or the ones later on used in the numerical analysis. To depict a plausible scenario in the case of symmetric parameters, system (2.9) can be rewritten by taking into account the assumption that $x := x_1 = x_2$. For analogy with the previous models, both equations are written in terms of $\dot{x}_1$ and $\dot{x}_2$, despite being

the same equation repeated twice, one for each state. Therefore, the following set of equations describe the system dynamics when they evolve in the manifold defined by $x_1 = x_2$:

$$\begin{aligned} \dot{x}_1 &= (1-2x)(rx+\gamma) - x(\sigma x + \alpha), \\ \dot{x}_2 &= (1-2x)(rx+\gamma) - x(\sigma x + \alpha). \end{aligned} \tag{2.11}$$

The corresponding bidimensional first-order system of (2.11) can be calculated as in the following:

$$\begin{aligned} \begin{bmatrix} \dot{x}_1 \\ \dot{x}_2 \end{bmatrix} &= \underbrace{\begin{bmatrix} r - 2rx - \gamma - \alpha & -\gamma \\ -\gamma & r - 2rx - \gamma - \alpha \end{bmatrix}}_{A} \begin{bmatrix} x_1 \\ x_2 \end{bmatrix} + \underbrace{\begin{bmatrix} \gamma \\ \gamma \end{bmatrix}}_{k} - \underbrace{\begin{bmatrix} \sigma \\ \sigma \end{bmatrix}}_{b} x^2, \\ y &= \underbrace{\begin{bmatrix} 1 & 1 \end{bmatrix}}_{c} \begin{bmatrix} x \\ x \end{bmatrix}. \end{aligned} \tag{2.12}$$

The matrix is denoted as matrix A, the constant vector $[\gamma \quad \gamma]^T$ as k (external input), the vector $[\sigma \quad \sigma]^T$ as b and the vector $[1 \quad 1]$ as c^T. By isolating the nonlinearities in $\psi(t)$, the transfer function associated with the above system is the following:

$$G(s) \quad = c^T[s\mathbb{I}^2 - A]^{-1}b \quad = \tfrac{1}{a_1^2 - a_2^2} \begin{bmatrix} a_1 & -a_2 \\ -a_2 & a_1 \end{bmatrix}, \tag{2.13}$$

where $a_1 = s + 2rx + \gamma + \alpha - r$ and $a_2 = \gamma$.

Figure 2.2 depicts the feedback scheme associated with systems (2.12)-(2.13), where the nonlinearity isolated in the feedback loop is represented by $\psi(t)$ and k is the external input vector.

Building on the Kalman-Yakubovich-Popov lemma, absolute stability is linked to strictly positive realness of $Z(s) = \mathbb{I}^2 + KG(s)$ where $K \in \mathbb{R}^{2\times 2}$ is the matrix whose entries are $k \in [0, \tilde{k}]$, and $G(s)$ is the transfer function of system (2.12). It is useful to note that the above calculation for $Z(s)$ can be done in the scalar version due to the assumption $x_1 = x_2$. However, to preserve the analogy with the general formulation of the bidimensional model, it is proved as in the following. In order to ensure absolute stability, matrix A in (2.12) must be Hurwitz, i.e. the trace of the matrix must be negative and the determinant must be positive. Both conditions must be investigated to prove that matrix A is Hurwitz. The first condition (negative trace), i.e.

$$Tr(A) = r - 2rx - \gamma - \alpha < 0,$$

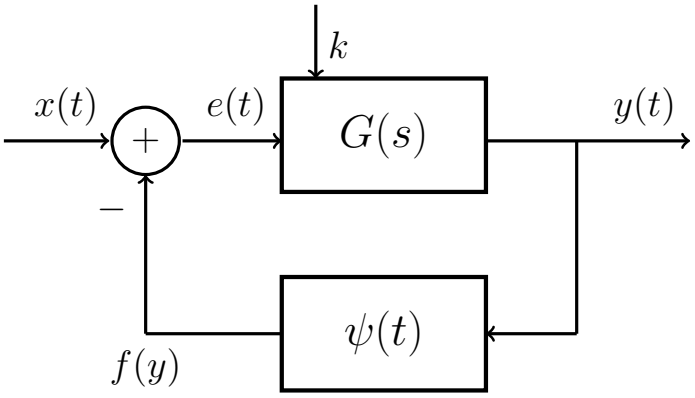

Figure 2.2: Feedback scheme used to isolate the nonlinearity related to the uncertain cross-inhibitory coefficient.

holds true in both cases that derive from the above assumption $x_1 = x_2$. The assumption implies, in turn, that $0 \leq x \leq 0.5$. Specifically, the trace is negative for $x = 0$ when $r < \gamma + \alpha$, and for $x = 0.5$, it is always negative. Furthermore, the second condition (positive determinant), i.e.

$$\Delta(A) = 2rx + \gamma + \alpha - r + \gamma = 2rx + 2\gamma + \alpha - r > 0,$$

is satisfied when $x = 0.5$, and holds true for $2\gamma + \alpha > r$ in the worst case.

Finally, matrix $Z(s)$ can be obtained as follows:

$$\begin{aligned} Z(s) &= \mathbb{I}^2 + KG(s) = \begin{bmatrix} 1 & 0 \\ 0 & 1 \end{bmatrix} + \begin{bmatrix} \frac{a_1k - a_2k}{a_1^2 - a_2^2} & \frac{-a_2k + a_1k}{a_1^2 - a_2^2} \\ \frac{-a_2k + a_1k}{a_1^2 - a_2^2} & \frac{a_1k - a_2k}{a_1^2 - a_2^2} \end{bmatrix} \\ &= \begin{bmatrix} 1 + \frac{k}{a_1 + a_2} & \frac{k}{a_1 + a_2} \\ \frac{k}{a_1 + a_2} & 1 + \frac{k}{a_1 + a_2} \end{bmatrix} = \frac{1}{s + \zeta} \begin{bmatrix} s + \zeta + k & k \\ k & s + \zeta + k \end{bmatrix}, \end{aligned} \tag{2.14}$$

where $\zeta = 2rx + 2\gamma + \alpha - r$. Absolute stability of system (2.12) is established in the following result.

Theorem 3. *Let system (2.12) be given and assume that matrix A is Hurwitz. Furthermore, consider the sector nonlinearity as in Assumption 1. Then, when $k < \tilde{k}$, $Z(s)$ is strictly positive real and the system (2.12) is absolutely stable.*

Proof. See Section 2.6. □

Remark 2. *Theorem 3 proves absolute stability for symmetric parameters under a time varying signal. Recall that a system is said to be absolutely stable if the system is globally stable for any $\sigma(t)$ within the conic sector. It is worth noting that the same result would apply to a structured system, in which the parameter describing the interactions among the individuals in the population, denoted by ψ_k in Chapter 4, is approximated by 1.*

2.3.3 Numerical Analysis

In this section, a set of simulations is presented to show the stability properties of system (2.9). Let the time horizon be $T = 500$. The cross-inhibitory signal is set to $\sigma = 3$, $r = \gamma = v$, where v is defined as the intrinsic value of both options and it is set to $v = 1$. These parameters are chosen to be consistent with the ones in the literature. Additionally, some parameters are set in. such a way to corroborate the theoretical results in the different scenarios, e.g. parameter α. The initial condition on the population distribution is $\hat{\mathbf{x}} = (0.8, 0.2, 0)$.

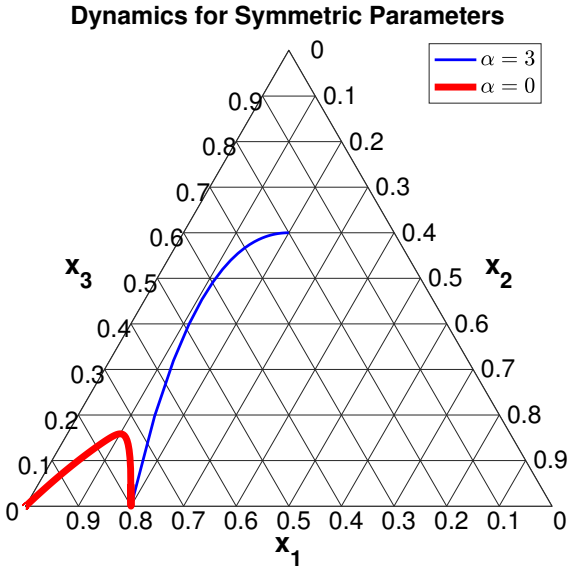

Figure 2.3: Plot in barycentric coordinates, showing the behaviour of system (2.9).

Two different scenarios can be identified. In the first one, let $\alpha = 3$. In accordance with Theorem 2, the equilibrium point in Case 1 is locally is asymptotically stable, since the condition in (2.10), i.e. $3 \leq (4 * 3)/(1 - 3)^2 = 3$, holds true. The equilibrium point can be computed explicitly by substituting the values of all parameters in the equation

of Case 1 as:

$$x^* = \Big(\frac{(1-2-3)+6}{2(2+3)}, \frac{(1-2-3)+6}{2(2+3)}, 1-2\frac{(1-2-3)+6}{2(2+3)}\Big) = (0.2, 0.2, 0.6).$$

This scenario is depicted in Fig. 2.3 (blue line) in barycentric coordinates, where it can be seen that the dynamics converge to the equilibrium point calculated above. The time evolution is shown in Fig. 2.4 (top).

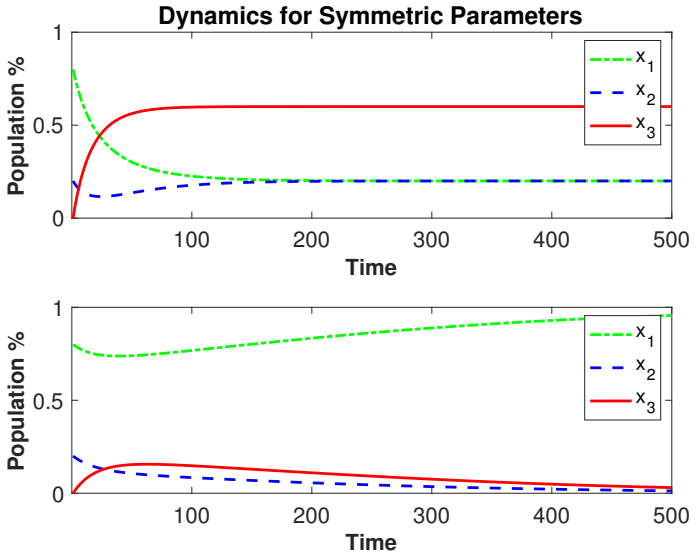

Figure 2.4: Time plot of system (2.9), for $\alpha = 3$ (top) and $\alpha = 0$ (bottom).

In the second scenario, the equilibrium point of Case 1 is no longer stable. In this scenario, let $\alpha = 0$. The equilibrium point is therefore $x^* = (0.358, 0.358, 0.284)$. According to Theorem 2, the equilibrium is unstable, since the condition in (2.10) does not hold, i.e. $3 \leq 0$. Fig. 2.3 (red line) shows, in barycentric coordinates, that the dynamics diverge from the calculated equilibrium and converge to another point, i.e. (1,0,0). The same can be seen in the time plot of Fig. 2.4 (bottom).

2.4 Asymmetric Structure

In this section, the main difference with the previous models is that the structure is asymmetric, and therefore the cross-inhibitory signal is sent only by players in state 1 to players in state 2. Additionally, players choosing strategy 1 cannot spontaneously

abandon their commitment, so α influences only state 2. Parameters γ and r have the usual meaning. The payoff matrix $A_{as} \in \mathbb{R}^{3\times 3}$ simplifies as:

$$A_{as} = \begin{pmatrix} r & -\sigma & 0 \\ 0 & r & 0 \\ 0 & 0 & 0 \end{pmatrix}. \tag{2.15}$$

In the case of asymmetric structure, by using the payoff matrix in (2.15), the transition rates can be derived as:

$$\rho_{31} = rx_1 + \gamma, \qquad \rho_{32} = rx_2 + \gamma, \qquad \rho_{23} = \sigma x_1 + \alpha. \tag{2.16}$$

The above transition rates lead to the following model:

$$\textit{Asymmetric structure} \begin{cases} \dot{x}_1 = (\gamma + rx_1)x_3, \\ \dot{x}_2 = (\gamma + rx_2)x_3 - (\sigma x_1 + \alpha)x_2, \\ \dot{x}_3 = (\sigma x_1 + \alpha)x_2 - (\gamma + rx_1)x_3 - (\gamma + rx_2)x_3. \end{cases} \tag{2.17}$$

The above system is not given in a two-dimensional form in order to highlight the similarities with the Susceptible-Infected-Recovered (SIR) model. In particular, each state can be linked to one of the states in the SIR model. States x_1 and x_2 represent the percentage of recovered (R) and susceptible (S) players, respectively, while x_3 can be viewed as the percentage of infected players (X). Parameter γ is the rate at which individuals recover from the infection completely or partially. In other words, such γ involves transitions to the recovered and the susceptible states. In the original formulation of the SIR model, players cannot become susceptible again after being infected. However, system (2.17) can be obtained by combining the SIR dynamics with the Susceptible-Infected-Susceptible (SIS) model. Parameter σ is the rate at which the infection is spread by the autoimmune individuals among the population. In the general formulation of the SIR model, the dynamics evolve according to the following:

$$\begin{cases} \dot{R} = \mu X, \\ \dot{S} = -\lambda \bar{k} X S, \\ \dot{X} = -\mu X + \lambda \bar{k} X S, \end{cases} \tag{2.18}$$

where μ is the rate at which individuals decay into the recovered class, λ is the rate at which the infection spreads among the population, and $\bar{k}$ is the number of contacts of the individuals.

2.4.1 Local Asymptotic Stability

In this section, the stability analysis is carried out on two equilibrium points, i.e. $(1, 0, 0)$ and $(0, 0, 1)$, due to the structure of system (2.17). The first equilibrium point represents consensus on option 1 and can be linked to the case where the epidemic is removed from the population, i.e. all individuals recover from the virus. The second equilibrium point involves the largest percentage of undecided players, which can be translated in the consensus problem as a higher risk of no consensus in the population. The link to the SIR model can be established to the spread of the epidemic in the population, with the meaning that the individuals do not recover from the infection. The following result states the stability properties of both equilibrium points.

Theorem 4. *Given an initial state $\hat{\mathbf{x}} = (\hat{x}_1, \hat{x}_2, \hat{x}_3)$, the asymmetric structure defined by the equations in (2.17) have the following stability properties:*

- ***(i)** The following vector $x^* = (x_1^*, x_2^*, x_3^*) = (1, 0, 0)$ is an asymptotically stable equilibrium point.*
- ***(ii)** If $\gamma = 0$, the following vector $x^* = (x_1^*, x_2^*, x_3^*) = (0, 0, 1)$ is another equilibrium point for the system. It is unstable for $r > \alpha$ and a saddle point for $r < \alpha$.*

Proof. See Section 2.6. □

Remark 3. *The physical interpretation of Theorem 4 can be given by linking it to compartmental models. The equilibrium point in **(i)** is the only one which is locally asymptotically stable, meaning that, at steady-state, the dynamics converge towards the recovered state for small perturbations. Additionally, the equilibrium point in **(ii)** shows that dynamics diverge for any values of r and α. This means that the population always recovers from the epidemic.*

2.4.2 Uncertain Cross-Inhibitory Coefficient

In this section, the system in the case of asymmetric structure is analysed in the presence of uncertain cross-inhibitory coefficient. It can be shown that stability properties are not compromised even if the cross-inhibitory coefficient $\sigma(t)$ is uncertain and changes over time, taking values within a pre-specified set. The feedback scheme used in this section is the same as in the case of symmetric parameters and is shown in Fig. 2.2.

System (2.17) is now generalised to include asymmetric parameters. Additionally, r and α are assumed to be negligible. The robustness analysis is given for the model described by the following set of equations:

$$\begin{aligned}\dot{x}_1 &= \gamma_1(1 - x_1 - x_2),\\ \dot{x}_2 &= -\sigma_1 x_1 x_2 + \gamma_2(1 - x_1 - x_2).\end{aligned} \tag{2.19}$$

As in the previous sections, the equilibrium points are studied in the case of constant cross-inhibitory signal, first. The following result shows the stability properties of each equilibrium point.

Theorem 5. *Given an initial state $\hat{\mathbf{x}} = (\hat{x}_1, \hat{x}_2, \hat{x}_3)$, the following points $x^* = (1, 0, 0)$ and $x^* = (0, 1, 0)$ are equilibrium points for system (2.19). The equilibrium point $(1, 0, 0)$ is asymptotically stable, while the equilibrium point $(0, 1, 0)$ is a saddle point.*

Proof. See Section 2.6. □

In the rest of this section, the sector nonlinearity is assumed to be as in Assumption 1. The corresponding bidimensional first-order system of (2.19) is given in the following:

$$\begin{aligned}\begin{bmatrix}\dot{x}_1\\ \dot{x}_2\end{bmatrix} &= \underbrace{\begin{bmatrix}-\gamma_1 & -\gamma_1\\ -\gamma_2 & -\gamma_2\end{bmatrix}}_{A}\begin{bmatrix}x_1\\ x_2\end{bmatrix} + \underbrace{\begin{bmatrix}\gamma_1\\ \gamma_2\end{bmatrix}}_{k} - \underbrace{\begin{bmatrix}0\\ \sigma_1\end{bmatrix}}_{b} x_1 x_2,\\ y &= \underbrace{\begin{bmatrix}0 & 1\end{bmatrix}}_{c}\begin{bmatrix}x_1\\ x_2\end{bmatrix}.\end{aligned} \tag{2.20}$$

The matrix is denoted as matrix A, the constant vector $[\gamma_1 \quad \gamma_2]^T$ as k, the vector $[0 \quad \sigma_1]^T$ as b and the vector $[0 \quad 1]$ as c^T. The transfer function for the above system is the following:

$$G(s) = c^T[s\mathbb{I}^2 - A]^{-1}b = \tfrac{(s+\gamma_1)\sigma_1}{s(s+\gamma_1+\gamma_2)}. \tag{2.21}$$

Theorem 6. *Let system (2.20) be given. Furthermore, let the sector nonlinearity be given as in Assumption 1. Then, $G(s)$ is positive real and system (2.20) is passive. Moreover, if a positive definite storage function $V(x)$ is given, then, by linearising around $(1, 0, 0)$ and shifting the origin of the system to that point, the origin is stable.*

Proof. See Section 2.6. □

Remark 4. *The above result shows that by isolating the nonlinearities, even in the case of time varying signals, the stability of the origin can be preserved. This is achieved by showing that the system is passive. Note that the term passive means that the system does not produce energy. Then, stability can be proved by finding a positive definite storage function, which is a real-valued function with explicit upper bounds on the increment of the state of the system.*

2.4.3 Numerical Analysis

This section includes three sets of simulations to corroborate the theoretical results on the role of the cross-inhibitory stop signal σ. The first two sets illustrate the properties of system (2.17), and the third one show the behaviour of system (2.19) under uncertain cross-inhibitory coeffecient. In all the three sets, let the time horizon be $T = 500$. To better visualise the impact of the coefficient, in the last set only the first 100 time instants are shown.

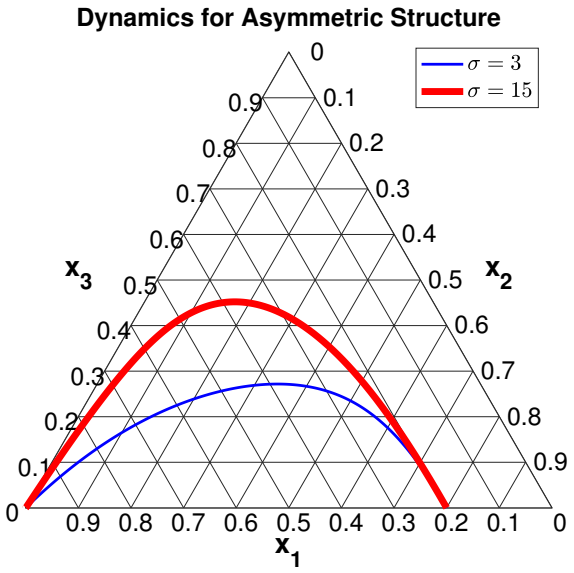

Figure 2.5: Plot in barycentric coordinates, showing the behaviour of system (2.17).

In the first set of simulations, the cross-inhibitory signal is set to $\sigma = 3$ and $\sigma = 15$, while $r = \gamma = 1/\alpha = v$, and $v = 1$ is defined as the intrinsic value of both options, as before. The initial condition on the distributions is $\hat{\mathbf{x}} = (0.2, 0.8, 0)$. The plot of the

population distribution in barycentric coordinates is displayed in Fig. 2.5, where the blue line refers to the case with $\sigma = 3$ and the red line to the case in which $\sigma = 15$. Figure 2.6 shows the time evolution of the system for $\sigma = 3$ (top) and $\sigma = 15$ (bottom). The plots show that a higher value of σ leads to a faster response of the first two state components. Moreover, the system converges to the equilibrium point $(1, 0, 0)$, which is asymptotically stable in accordance with Theorem 4.

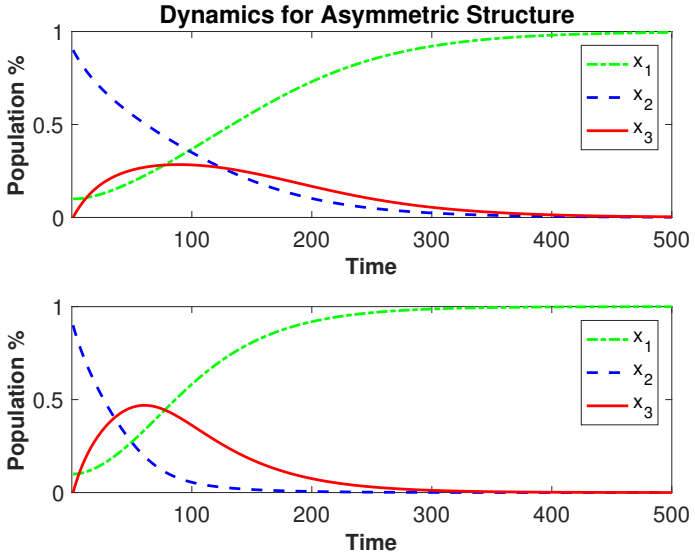

Figure 2.6: Time plot of system (2.17), for $\sigma = 3$ (top) and $\sigma = 15$ (bottom).

In the second set of simulations, the cross-inhibitory signal is set to $\sigma = 3$. Let $\gamma = 0$, $r = 1$ and $\alpha \in \{0.5, 3\}$. The dynamics are depicted in Figure 2.7 for $\alpha = 0.5$ (top) and $\alpha = 3$ (bottom). To show that the equilibrium point $(0, 0, 1)$ is unstable or a saddle, the initial condition is set around the equilibrium point $(0, 0, 1)$ as $\hat{\mathbf{x}} = (0, 0.15, 0.85)$. In accordance with Theorem 4, the plot shows that the dynamics diverge from this equilibrium point and converge to the only stable equilibrium, i.e. $(1, 0, 0)$.

The last set of simulations shows the case where the cross-inhibitory signal is no longer a constant value, as in (2.19). Let $\gamma = 0$, $r = 1$ and $\alpha \in \{0.5, 3\}$. The system behaviour is shown in Fig. 2.8 for $\hat{\sigma} = 0.5$ (blue line) and $\hat{\sigma} = 15$ (red line). The coefficient evolves as $\sigma(t) = \hat{\sigma} + (\hat{\sigma}k)sin(t\hat{\sigma})$, where $k = 0.4$. In accordance with Theorem 6, the plot shows that the dynamics are not affected by the uncertain signal and the stability of the system is ensured.

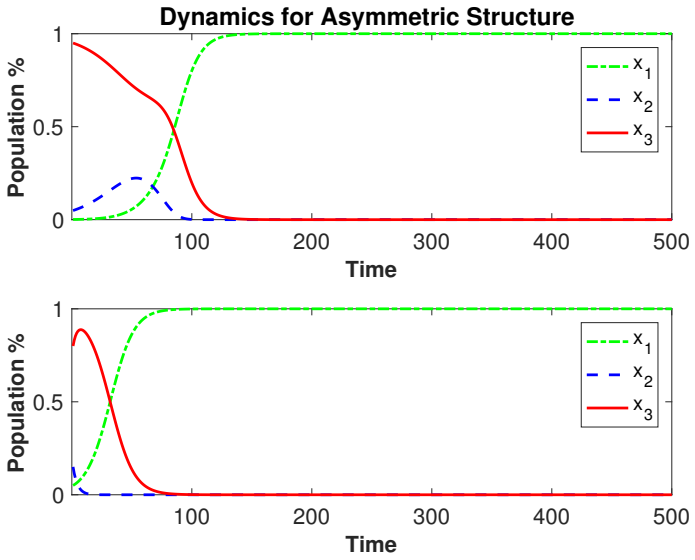

Figure 2.7: Behaviour around the equilibrium point $\mathbf{x}^* = (0, 0, 1)$ for $\alpha = 0.5$ (top) and $\alpha = 3$ (bottom) for system (2.17).

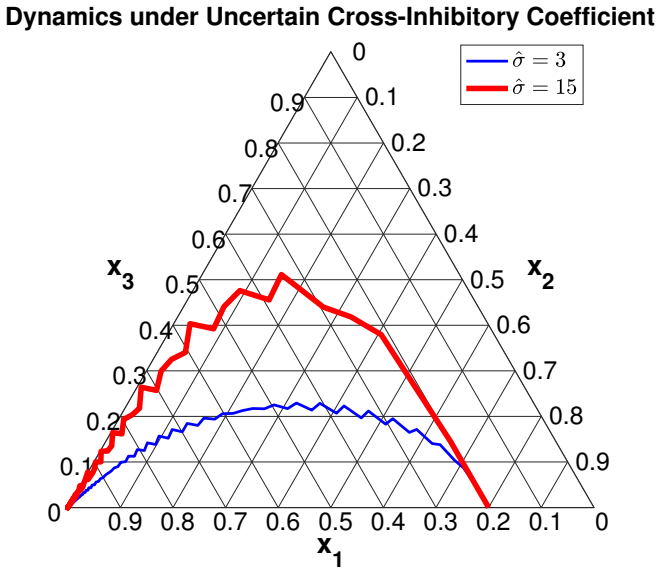

Figure 2.8: Plot in barycentric coordinates, showing the behaviour of system (2.19) under uncertain cross-inhibitory coefficient.

2.5 Summary and Discussion

In this chapter, the model originating in the context of honeybees was reframed in the form of a game. Instead of modelling the microscopic dynamics by looking at the

choices of individual players, the macroscopic dynamics are considered in the form of the population distribution across three states, namely x_1, x_2 and x_3. The first two states represent the options available to the players, whereas x_3 represents the portion of the population that didn't choose either option/strategy 1 nor option/strategy 2. When the model is specialised in the symmetric and asymmetric cases, it can be linked to compartmental models such as the susceptible-infected-recovered (SIR) model. For the asymmetric structure, the transition from state 1 to state 3 is no longer permitted, namely parameters α_1 and σ_2 are set to zero.

Although the parameters were assigned specific values in the simulations (coming mostly from the literature), the theoretical formulation of the model shows how they influence the final values of equilibrium points of the system as explicitly stated in Theorem 1 and Theorem 4. Furthermore, the parameters influence the stability properties of these equilibria, as proved in Theorem 2 and Theorem 5. The simulations corroborate the theoretical results by showing that the dynamics converge to the equilibrium point (the ones that are asymptotically stable) for both the symmetric and the asymmetric case. When showing that an equilibrium point is no longer stable, parameters are chosen in such a way to be consistent with the threshold in (2.10).

The scenario where the number of players tends to infinity is investigated in the next chapter, namely Chapter 3. In the mean-field game, the perspective of a reference player is taken into account and the problem where the player has to control his/her state in the presence of an adversarial disturbance is tackled. The scenario where the players' position is taken into account in terms of the interactions with other players is studied in Chapter 4 via a network topology. Furthermore, the formulation of a model where the number of players is fixed is given. In the structured case, results include different dynamics for different connectivity values, to assess the impact of the connectivity. This means faster transient response and higher number of uncommitted players at steady-state.

2.6 Proofs

The main tool used in this section is Lyapunov's linearisation method, see [58]. For hyperbolic equilibrium points, the Hartman-Grobman theorem was used. The Hartman-Grobman theorem states that the behaviour of a dynamical system near a hyperbolic

equilibrium point is topologically equivalent to the behaviour of its linearisation in the neighbourhood of the equilibrium point, see [96]. In simple words, the stability properties hold true when going from the linear to the nonlinear system. Hyperbolicity is the property for which no eigenvalue of the linearisation evaluated at the equilibrium point has real part equal to zero. It is worth recalling that, for a second order system, an equilibrium point (or fixed point) is asymptotically stable if and only if all eigenvalues have strictly negative real part, a saddle point when one eigenvalue has positive real part and the other one has negative real part, or an unstable node when both eigenvalues have positive real part. Lastly, for the study of stability under uncertain coefficients, the Kalman-Yakubovich-Popov lemma was used, which establishes an equivalence between the conditions in the frequency domain, an input-output relationship in the time domain, and conditions on the state-space representation, see [20], [58].

Proof of Theorem 1

The equilibrium points of system (2.9) are studied by imposing $\dot{x}_1 = \dot{x}_2 = 0$ to obtain the following equation:

$$(x_3 r - \alpha)(x_1 - x_2) = 0,$$

which leads to two solutions: $x_1 = x_2$ and $x_3 = \alpha/r$. The first solution is studied in Case 1 and the second solution in Case 2. Case 3 analyses the scenario in which both hold true.

[**Case 1**] When $x_1 = x_2 = x$, the equilibrium point is the root of a second degree polynomial, which is derived as

$$\begin{aligned}\dot{x} &= (1-2x)(rx+\gamma) - x(\alpha+\sigma x)\\ &= rx + \gamma - 2rx^2 - 2\gamma x - \alpha x - \sigma x^2\\ &= (2r+\sigma)x^2 - (r - 2\gamma - \alpha)x - \gamma = 0,\end{aligned}$$

under the conditions $\dot{x}_1 = 0$ and $x_1^* + x_2^* + x_3^* = 1$. By excluding the one with the minus sign, the roots of the above polynomial, and therefore the equations characterising the equilibrium point, are given by:

$$\begin{aligned}x_1^* &= \frac{(r-2\gamma-\alpha)+\sqrt{(r-2\gamma-\alpha)^2+4\gamma(2r+\sigma)}}{2(2r+\sigma)} = x_2^*,\\ x_3^* &= 1 - \frac{(r-2\gamma-\alpha)+\sqrt{(r-2\gamma-\alpha)^2+4\gamma(2r+\sigma)}}{2r+\sigma}.\end{aligned}$$

[**Case 2**] When $x_3 = \alpha/r$, the following equation follows from setting $\dot{x}_1 = 0$:

$$\dot{x}_1 = \alpha x_1 + \frac{\alpha}{r}\gamma - \alpha x_1 + \sigma x_1 - \sigma x_1^2 - \frac{\alpha}{r}\sigma x_1 = 0,$$

which can be rearranged in the form of a second-order polynomial as:

$$x_1^2 - (1 - \frac{\alpha}{r})x_1 - \frac{\alpha\gamma}{r\sigma} = 0.$$

From the roots of the above polynomial, the equilibrium point when $x_3 = \alpha/r$ can be obtained as:

$$x_1^* = \frac{1-\frac{\alpha}{r}+\sqrt{(1-\frac{\alpha}{r})^2+\frac{4\alpha\gamma}{\sigma r}}}{2},$$
$$x_2^* = 1 - \frac{1-\frac{\alpha}{r}+\sqrt{(1-\frac{\alpha}{r})^2+\frac{4\alpha\gamma}{\sigma r}}}{2} - \frac{\alpha}{r}, \qquad x_3^* = \frac{\alpha}{r}.$$

[**Case 3**] A special case is when both conditions, i.e. $x_3 = \alpha/r$ and $x_1 = x_2$, hold. Then, it follows:

$$\begin{aligned} \dot{x} &= \tfrac{\alpha}{r}(rx + \gamma) - x(\alpha + \sigma x) \\ &= \alpha x + \tfrac{\gamma\alpha}{r} - \alpha x - \sigma x^2 = \sigma x^2 - \tfrac{\gamma\alpha}{r} = 0. \end{aligned}$$

Due to condition $x_1 = x_2$, the above leads to $x_1^* = x_2^* = \sqrt{\frac{\alpha\gamma}{r\sigma}}$. By also considering the other condition $x_3 = \alpha/r$, the value of x_1 (or x_2) is equivalent to the whole population minus the value of x_3 and then divided by 2, i.e. $x_1 = \frac{1-\alpha/r}{2} = \frac{r-\alpha}{2r}$. From the previous equations, the following value for σ can be obtained as:

$$\frac{(r-\alpha)^2}{4r^2} = \frac{\alpha\gamma}{r\sigma} \quad \Rightarrow \quad \sigma = \frac{4r\alpha\gamma}{(r-\alpha)^2}. \tag{2.22}$$

Proof of Theorem 2

To study the stability of the equilibrium point in Case 1, the Jacobian matrix around an equilibrium point, i.e. $x^* = (x, x, 1-2x)$ where $x := x_1 = x_2$, is calculated as:

$$J = \left[\begin{array}{cc} r - 3rx - \gamma - \alpha - \sigma x & x(-r-\sigma) - \gamma \\ x(-r-\sigma) - \gamma & r - 3rx - \gamma - \alpha - \sigma x \end{array} \right]\Bigg|_{x^*}. \tag{2.23}$$

The equilibrium point is a saddle node, when the following condition for the determinant Δ of the Jacobian holds: $\Delta := J_{11}J_{22} - J_{12}J_{21} = J_{11}^2 - J_{12}^2 < 0$, . The latter is true when $x(r+\sigma)+\gamma > 3rx+\gamma+\alpha+\sigma x-r$, which in turn implies $-2rx > \alpha - r$. The latter yields $x < \frac{r-\alpha}{2r}$. From Case 3, under the same conditions, the equation $x = \sqrt{\frac{\alpha\gamma}{r\sigma}}$ holds true. By taking a similar argument, the equilibrium point is asymptotically stable when the following holds:

$$\sigma \leq \frac{4r\alpha\gamma}{(r-\alpha)^2}. \tag{2.24}$$

Proof of Theorem 3

In order to prove that $Z(s)$ is strictly positive real, the following conditions must hold true:

- $Z(s)$ is Hurwitz, i.e poles of all elements of $Z(s)$ have negative real parts;
- $Z(j\omega) + Z(-j\omega) > 0, \quad \forall \omega \in \mathbb{R}$;
- $Z(\infty) + Z^T(\infty) > 0$.

For the first condition to be true, all the poles must be negative, i.e. $r - 2rx - 2\gamma - \alpha < 0$. This condition holds true, due to the conditions on the trace and determinant of matrix A. For the second condition, the following must hold:

$$\begin{aligned} Z(j\omega) + Z(-j\omega) &= \tfrac{1}{j\omega+\zeta} \begin{bmatrix} j\omega+\zeta+k & k \\ k & j\omega+\zeta+k \end{bmatrix} \\ &\quad + \tfrac{1}{-j\omega+\zeta} \begin{bmatrix} -j\omega+\zeta+k & k \\ k & -j\omega+\zeta+k \end{bmatrix}, \end{aligned} \tag{2.25}$$

where, again, $\zeta = 2rx + 2\gamma + \alpha - r$. It follows:

$$\begin{aligned} Z(j\omega) + Z(-j\omega) &= \begin{bmatrix} \frac{j\omega+\zeta+k}{j\omega+\zeta} & \frac{k}{j\omega+\zeta} \\ \frac{k}{j\omega+\zeta} & \frac{j\omega+\zeta+k}{j\omega+\zeta} \end{bmatrix} + \begin{bmatrix} \frac{-j\omega+\zeta+k}{-j\omega+\zeta} & \frac{k}{-j\omega+\zeta} \\ \frac{k}{-j\omega+\zeta} & \frac{-j\omega+\zeta+k}{-j\omega+\zeta} \end{bmatrix} \\ &= \begin{bmatrix} z_{11} & z_{12} \\ z_{21} & z_{22} \end{bmatrix}, \end{aligned} \tag{2.26}$$

where

$$\begin{aligned} z_{11} = z_{22} &= \tfrac{\omega^2 - j\omega\zeta - j\omega k + j\omega\zeta + \zeta^2 + \zeta k + \omega^2 + j\omega\zeta + j\omega k - j\omega\zeta + \zeta^2 + \zeta k}{\zeta^2+\omega^2}, \\ z_{12} = z_{21} &= \tfrac{-j\omega k + \zeta + k + j\omega k + \zeta k}{\zeta^2+\omega^2}. \end{aligned}$$

Thus, the second condition can be rewritten as:

$$Z(j\omega) + Z(-j\omega) = \begin{bmatrix} \frac{2\omega^2+2\zeta^2+2\zeta k}{\zeta^2+\omega^2} & \frac{2\zeta+k}{\zeta^2+\omega^2} \\ \frac{2\zeta+k}{\zeta^2+\omega^2} & \frac{2\omega^2+2\zeta^2+2\zeta k}{\zeta^2+\omega^2} \end{bmatrix} > 0, \tag{2.27}$$

which is verified for all ω. Lastly, due to the symmetry of $Z(s)$, the third condition implies that $2Z(\infty) > 0$. Note that the off-diagonal entries converge to zero in the limit, whereas the entries on the main diagonal converge to 1 in the limit. Therefore, in the limit, matrix $Z(s)$ converges to an identity matrix, and, therefore, the third condition holds true. Absolute stability can now be proved by showing that there exists a Lyapunov function such as $V(x) = x^T P x$. The expression of $\dot{V}(t, x)$ can be derived as

in the following:

$$\begin{aligned} \dot{V}(t,x) &= \dot{x}^T P x + x^T P \dot{x} \\ &= x^T A^T P x + x^T P A x - \psi^T B^T P x - x^T P B \psi, \end{aligned} \tag{2.28}$$

where ψ is equivalent of writing $\psi(t,y)$. For the condition on the sector nonlinearity, it follows that $-2\psi^T(\psi - Ky) \geq 0$. Since matrices P and K are symmetric, equation (2.28) can now be specialised to the case where A is symmetric and $B = C = \mathbb{I}^2$ as:

$$\begin{aligned} \dot{V}(t,x) &\leq x^T(A^T P + PA)x - 2x^T P B\psi - 2\psi^T(\psi - Ky) \\ &= 2x^T A P x - 2x^T P \psi + 2\psi^T K x - 2\psi^T \psi \\ &= 2x^T A P x + 2x^T(K - P)\psi - 2\psi^T \psi. \end{aligned} \tag{2.29}$$

To show that the right-hand side of (2.29) is negative, a square term is constructed by imposing the following:

$$2AP = -L^T L - \epsilon P, \qquad K - P = \sqrt{2} L^T, \tag{2.30}$$

where $\epsilon > 0$ is a constant and matrix $P = P^T > 0$. Now, (2.29) can be rewritten as:

$$\begin{aligned} \dot{V}(t,x) &\leq -\epsilon x^T P x - x^T L^T L x + 2\sqrt{2} x^T L^T \psi - 2\psi^T \psi \\ &= -\epsilon x^T P x - [Lx - \sqrt{2}\psi]^T [Lx - \sqrt{2}\psi] \\ &\leq -\epsilon x^T P x. \end{aligned} \tag{2.31}$$

From Kalman-Yakubovich-Popov lemma, P, L and ϵ can be obtained solving (2.30), as $Z(s)$ is positive real. This concludes the proof.

Proof of Theorem 4

The equilibrium points of system (2.17) are studied by imposing $\dot{x}_1 = \dot{x}_2 = 0$. The two equilibria are found by setting $x_3 = x_2 = 0$ in **(i)** and $x_1 = x_2 = 0$ in **(ii)**. In the first case, it follows that $x^* = (1,0,0)$, whereas in the second case, $x^* = (0,0,1)$ follows. The Jacobian matrices are now calculated to check the stability of each equilibrium point:

$$J_1 = \begin{bmatrix} -\gamma - r & -\gamma - r \\ -\gamma & -\gamma - \sigma - \alpha \end{bmatrix}\Bigg|_{x^*}, \qquad J_2 = \begin{bmatrix} r & 0 \\ 0 & r - \alpha \end{bmatrix}\Bigg|_{x^*}, \tag{2.32}$$

where J_1 and J_2 are calculated in $(1,0,0)$ and $(0,0,1)$, respectively. For J_1, the trace T_1 and determinant Δ_1 are calculated as:

$$T_1 = -2\gamma - r - \sigma - \alpha, \qquad \Delta_1 = (\gamma + r)(\gamma + \sigma + \alpha), \tag{2.33}$$

where T_1 is always negative and Δ_1 is always positive. This implies that $x^* = (1, 0, 0)$ is an asymptotically stable point. For J_2, the corresponding equilibrium point is unstable or a saddle point, which follows from the following:

$$T_2 = 2r - \alpha, \qquad \Delta_2 = r^2 - r\alpha, \tag{2.34}$$

which states that the equilibrium point is unstable when $r > \alpha$, since the trace and the determinant are positive; on the contrary, when $\alpha/2 < r < \alpha$ or $r < \alpha/2$, the determinant is negative and the trace is positive or negative, respectively. Thus, it is a saddle point.

Proof of Theorem 5

System (2.19) admits two equilibrium points, i.e. $x^* = (1, 0, 0)$ or $x^* = (0, 1, 0)$. As before, by applying the Lyapunov linearisation method, the stability of these equilibrium points is studied in the following. First, the Jacobian matrices are given by the following:

$$J_3 = \begin{bmatrix} -\gamma_1 & -\gamma_1 \\ -\gamma_2 & -\gamma_2 - \sigma_1 \end{bmatrix}\Bigg|_{x^*}, \quad J_4 = \begin{bmatrix} -\gamma_1 & -\gamma_1 \\ -\gamma_2 - \sigma_1 & -\gamma_2 \end{bmatrix}\Bigg|_{x^*}, \tag{2.35}$$

where J_3 is calculated in $(1, 0, 0)$ and J_4 in $(0, 1, 0)$. For J_3 the trace and determinant are:

$$T_3 = -\gamma_1 - \gamma_2 - \sigma_1, \qquad \Delta_3 = -\gamma_1(-\gamma_2 - \sigma_1) - \gamma_1\gamma_2 = \gamma_1\sigma_1, \tag{2.36}$$

where T_3 is always negative and Δ_3 is always positive. Thus the equilibrium point $x^* = (1, 0, 0)$ is asymptotically stable. Analogously, for J_4, the trace and determinant are given by:

$$T_4 = -\gamma_1 - \gamma_2, \qquad \Delta_4 = \gamma_1\gamma_2 - \gamma_1(\gamma_2 + \sigma_1) = -\gamma_1\sigma_1, \tag{2.37}$$

where both T_4 and Δ_4 are negative. Therefore the equilibrium point $x^* = (0, 1, 0)$ is a saddle point.

Proof of Theorem 6

The idea is to check whether the transfer function is positive real, to ensure stability of system (2.19). To be positive real, the following conditions must hold true:

(1) $G(s)$ is stable, i.e. no poles $\text{Re}\{s\} > 0$.

(2) $\text{Re}\{G(j\omega)\} \geq 0$, i.e. $-\pi/2 \leq G(j\omega) \leq \pi/2$.

Condition **(1)** can be easily verified, since the real part of both poles of the transfer function in (2.21), i.e. $s = 0$ and $s = -\gamma_1 - \gamma_2$, is equal to or less than zero. Condition **(2)** can be verified by inspection. A graphical representation is available in Fig. 2.9.

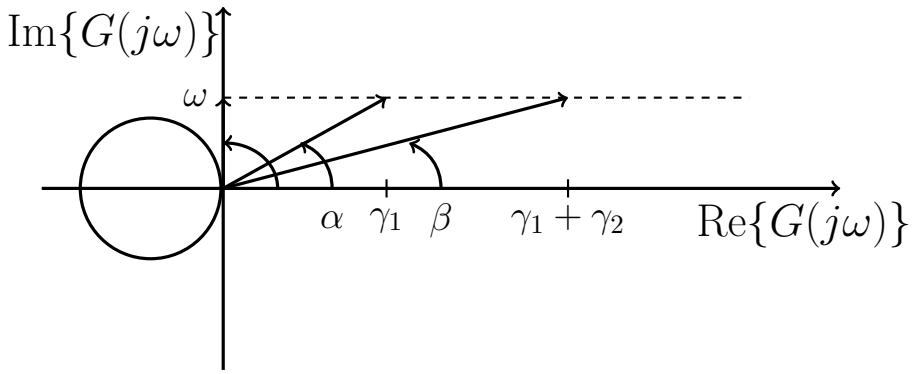

Figure 2.9: Graphical representation for condition **(2)**, i.e. $-\pi/2 \leq G(j\omega) \leq \pi/2$.

From the figure, it can be seen that, for a fixed $\omega > 0$, the condition translates into $\alpha - \beta - \pi/2 \geq -\pi/2$, which is always verified. Similarly, for a fixed $\omega < 0$, we have $-\alpha + \beta + \pi/2 \leq \pi/2$, which is always verified as well. Thus, $G(s)$ is positive real and system (2.19) is passive.

Now, in order to prove stability of the origin of system (2.19), e.g. $\dot{x} = f(x, 0)$, a positive definite storage function $V(x)$ must be found. The storage function candidate is the following:

$$V(x) = \frac{1}{2} x^T P x, \tag{2.38}$$

where $P = P^T > 0$. From the passivity of the system, it follows:

$$u^T x \geq \frac{\partial V}{\partial x} f(x, u). \tag{2.39}$$

Finally, by shifting the origin of the system to the equilibrium point and substituting in the above equation, it follows:

$$\frac{\partial V}{\partial x} f(x, 0) \leq 0. \tag{2.40}$$

Thus, the origin of the system is stable. This concludes the proof.

CHAPTER 3

Mean-Field Games and Stationary Solutions for Collective Decision-Making

3.1 Introduction

In Chaper 2, the formulation of the game was given in the symmetric case and asymmetric case, and the stability of both systems was investigated. Furthermore, the scenario where the cross-inhibitory signal is no longer a constant signal was studied and absolute stability and passivity was proved to be preserved for the symmetric and asymmetric case, respectively. When the population tend to an infinite number of players, the initial model can be reframed within mean-field game theory, which is the focus of this chapter.

In this chapter, the collective decision-making problem originating in the context of honeybees is investigated in the framework of mean-field game theory. The motivation for this study comes from the fast-growing interest in mean-field games. The original problem is also suitable to be generalised in a mean-field game framework. The mean-field game component is defined by the optimisation that the players do by taking into account the behaviour of the whole population. In other words, while in the evolutionary game setting players compare the payoffs to establish which strategy is more successful, in the mean-field game framework players perform a 'global' optimisation through the knowledge of how the entire population behave.

3.1.1 Literature Review

Mean-field game theory was originally developed by Lasry and Lions, see [63], [64], [65], and independently by Huang, Caines and Malhamé, see [54], [55], [56]. Lasry and Lions introduced mean-field game theory as an extension to mean-field theory in physics and statistical mechanics where the complexity of the behaviour in high-dimensional models is approximated by an average over all the components in the system. At the same time, Huang, Caines and Malhamé developed this theory by extending stochastic dynamic games to a large number of players and approximating their behaviour by averaging across all the players' strategies.

Further developments of the theory includes the concept of *oblivious equilibrium*, see [106], an approximation of the mean-field equilibrium for stochastic dynamic games with the aim to reduce the computational complexity of solving such games. The authors in [106] provide also an error bound to compare the oblivious equilibrium in the case of a growing number of players. For a survey on mean-field games, the reader is referred to [41]. Mean-field games can be also seen as the successors of *anonymous games* and *aggregative games*, where the notion of mass interaction was already a main feature, see [44].

Mean-field games theory applies to a variety of domains, spanning from economics to engineering, from physics to biology; for examples in each of these domains, the reader is referred to [3], [9], [12], [46]. When the problem has a linear quadratic structure, the author in [5] provides explicit solutions in terms of mean-field equilibria. Otherwise, numerical approximations and discretisation methods can be used as one of several solution schemes proposed in recent times, see [1]. Other approximation techniques come from the results for long-time convergence in [42], due to a variational formulation of the current models. In recent times, there have been multiple developments in the numerical analysis of finite state mean-field games, e.g. see [43].

When the optimisation problem takes into consideration the adversarial disturbance in the worst-case scenario, robustness is investigated in the corresponding mean-field game. An introduction on robust mean-field games can be found in [11] and for a further study, the reader is referred to [8], [10]. Robustness is also discussed in [98] and [7], in the case of risk-sensitive games and in the case of the consensus problem, respectively.

Finite state mean-field games were first introduced in [39] for discrete time, where

the authors consider the study by Lasry and Lions and extend their work to the exponential convergence of the initial-terminal value problem to equilibrium. The corresponding finite state mean-field games in continuous time were later introduced in [40], where convergence to stationary solutions in the case of d-state model is proved. Additionally, the authors study the $(N+1)$-player problem and the convergence of the model as $N \to \infty$ under the assumption of concave costs.

Convergence to the stationary solutions was studied in [27] for state-dependent Markov chains in problems of distributed optimal resource allocation, where the aim is to design optimal sharing algorithms for different contexts. Similarly to [27], the Markov chain taken into account is place-dependent, in the sense that the transition probabilities are function of the states. Additionally, the probability vector sums to one, due to the conservation of mass, and satisfy the Kolmogorov equations. Differently, the methodology used in this chapter treats the study of the stationary solutions when the population distribution is at equilibrium, from the Kolmogorov equations studied in Chapter 2. And then, it investigates the behaviour of the value function when the equilibrium point in the population distribution is locally asymptotically stable. In its simplicity, this approach is an element of novelty compared to the literature.

An extensive literature explores biochemical reactions and the corresponding Markov processes, see [34], [35] for an overview on the topic. The model presented here can be linked to such a biochemical process when the reaction has three possible states and the number of molecules that react are large in number (if one wants to see the similarities with the mean-field game). In the Markov process, when the probability depends on the population distribution, the system can be reduced to a nonlinear model, bilinear to be more precise. This is the case treated in Chapter 2, and also the case investigated in this chapter, but here the number of players tends to infinity. A similar case but with more than three states is studied in [31], where the master model is obtained for a generic n-state bio-chemical reaction.

Additional contributions on robustness and structural properties are presented in [14], and further in [15]. The authors in [14] tackle the problem of local stability for systems that admit a BCD-decomposition under different value of the positive parameters d_i, namely the diagonal entries of a matrix D containing the partial derivatives for the system. Whilst the authors provide a sufficient condition to check the co-positivity of a sum of squares (SOS) polynomial, they also provide a necessary and sufficient condition

for finding quadratic Lyapunov functions by means of a LMI-based convex optimisation. The authors in [15] propose an efficient algorithm to compute the signed steady-state input-output influences for biomolecular systems. They also check the outcome for a structurally zero influence, showing that this scenario boils down to perfect adaptation or zero influence. Finally, when uncertain parameters are subject to given interval bounds, quantitative results on the maximum and minimum output variations are provided. This literature could provide interesting insights in the case of robustness for the bio-inspired model of honeybees in presence of uncertain parameters (as in the uncertain signal in Chapter 3) and non-deterministic adversarial disturbance (as it is treated in this research).

3.1.2 Summary and Contributions

This chapter focuses on the study of the robust mean-field game. The collective decision-making problem investigated in Chapter 2 is extended to the mean-field game framework. The resulting mean-field game is a generalisation of the original problem, which can be obtained from the studied mean-field game when the players' control and adversarial disturbance are assumed to be of a certain kind. Specifically, this means that the control and disturbance are linked to the parameters of the consensus problem, such as the cross-inhibitory stop signal. The macroscopic dynamics are introduced and then the problem of a reference player is tackled, which corresponds to the microscopic dynamics. The initial-terminal value problem (ITVP) is introduced by combining the macroscopic and microscopic dynamics. Then, the corresponding stationary solutions are studied with emphasis on the stability property of the system. Finally, a basin of attraction for the stationary solutions is found.

The main contributions of this chapter can be summarised in the following. First, the existence of a mean-field Nash equilibrium is given. The proposed model is a particular case of the framework developed in [40], but it has been extended to the robust case, where the adversarial disturbance is assumed to be a form of the worst-case deterministic signal. To prove stability of the robust mean-field game, the main argument is to derive stability properties for the stationary solutions when the Kolmogorov equations in the population distribution is already at an equilibrium point. The stability of the corresponding Kolmogorov equations are the focus of Chapter 2. Finally, the stability properties are extended to periodic solutions and a region of convergence for the system

is found.

3.1.3 Structure

Chapter 3 is organised as follows. In Section 3.2, the macroscopic dynamics in the form of Kolmogorov backward equations are introduced first. Then the microscopic dynamics in the form of Hamilton-Jacobi-Bellman forward equations are presented. Both equations together constitute the initial-terminal value problem (ITVP) and are investigated in two cases, namely when the optimisation depend on the reference player's control or when it depends on the control of any other player. In Section 3.3 the ITVP is studied and the corresponding stationary solutions are analysed. Specifically, the stationary solutions are studied under the hypothesis that the population distribution is at an equilibrium and thus stability properties are derived for the value function. Periodic solutions are investigated and a basin of attraction is given. Two applications are proposed, namely honeybee swarms and virus propagation in smart grids. Finally, two sets of simulations are provided to corroborate the theoretical results.

3.2 Terminal Value Problem

This section includes the formulation of the mean-field game model for a three-choice decision-making problem where a large population of players has to find consensus on one of two options across three possible states. The problem is formulated first in its macroscopic dynamics and then the perspective of a reference player is tackled. Finally, after studying the optimal control problem, the mean-field response for the reference player is given.

3.2.1 Dependance on the Reference Player's Control

Given a continuous time dynamic game framework and a large population of players, the problem of finding consensus on one of two options is considered. In the same way as the rest of this research, state 3 represents the uncommitted players, while the two options correspond to states 1 and 2, respectively. All players are homogeneous, i.e. they behave in the same way in the same circumstances. The game is symmetric with respect to any permutation of players, which means that each player's decisions do not

take into account individual players but rather the distribution of players in each state. Each player controls his/her states according to some optimality criteria. In detail, the controls of each player depend on the state in which he/she is and on the distribution of the population across the three states.

In the following, the problem from the perspective of a player, hereafter referred to as the *reference player*, is tackled. Let the probability vector modelling the distribution of the population across the three states be $\mathbf{x}(t) = [x_1, x_2, x_3]^T \in \mathcal{S}^3$, where $\mathcal{S}^3$ is the probability simplex in $\mathbb{R}^3$ and $t \geq 0$ is the time index. Players change state according to a continuous time Markov process with transition rate matrix $\beta(t) \in \mathbb{R}^{3\times 3}$. Matrix β depends on the state, and therefore the system that is presented later in this chapter is nonlinear. This is the analogous model of the system of equations in (2.5), where the number of players tend to infinity, in the mean-field case. Each element of matrix β, i.e. β_{ij}, denotes the transition rate from state i to state j and consists of two components ρ_{ij} and w_{ij}. Analogously, the same holds for each column, namely $\beta_i = \rho_i + w_i$. The component $\rho_i \in (\mathbb{R}_0^+)^3$ is the player's control, whereas $w_i \in (\mathbb{R}_0^+)^3$ is controlled by an adversarial disturbance.

In the mean-field limit when the number of players tends to infinity, the model is described by the following Kolmogorov equations:

$$\begin{aligned} \dot{x}_1 &= x_3\beta_{31} - x_1\beta_{13}, \\ \dot{x}_2 &= x_3\beta_{32} - x_2\beta_{23}, \\ \dot{x}_3 &= x_1\beta_{13} + x_2\beta_{23} - x_3\beta_{31} - x_3\beta_{32}, \end{aligned} \tag{3.1}$$

which, as in the previous chapter, are equivalent to the following nonlinear bidimensional system by considering the conservation of mass $\dot{x}_3 = -\dot{x}_1 - \dot{x}_2$, which implies $x_3 = 1 - x_1 - x_2$, as in the following:

$$\begin{aligned} \dot{x}_1 &= (1 - x_1 - x_2)\beta_{31} - x_1\beta_{13}, \\ \dot{x}_2 &= (1 - x_1 - x_2)\beta_{32} - x_2\beta_{23}. \end{aligned} \tag{3.2}$$

The above set of nonlinear ODEs in the bidimensional state space x_1-x_2 represents the macroscopic dynamics with initial condition on the distribution $\hat{\mathbf{x}} := \mathbf{x}(0)$, i.e. $\hat{\mathbf{x}} = (\hat{x}_1, \hat{x}_2)$. The initial condition corresponding to the 3-dimensional model in (3.1) can be derived from the conservation of mass.

To develop the microscopic dynamics, consider a reference player, given that the distribution of the rest of the population is fixed over the time horizon. The reference

player can either be committed to option 1, option 2 or be uncommitted, thus his/her state takes value in a finite discrete set with cardinality 3. Let the state of the player be denoted by $i \in \mathcal{I}^3$, where $\mathcal{I}^3$ is the set of the three possible states. The evolution of the state is described by a continuous time Markov chain, whose transition rates are chosen to minimise a total cost which consists of a running cost and a terminal cost.

The running cost accounts for a penalty incurred by the player during the time horizon and it depends on the player's state, on the population distribution and on the transition rates. Therefore, the running cost $g(i, x_i, \rho_i) : \mathcal{I}^3 \times \mathcal{S}^3 \times (\mathbb{R}_0^+)^3 \to \mathbb{R}$ is defined as in the following:

$$g(i, x_i, \rho_i) = \frac{1}{2}\|\rho_i\|^2_{R_i} + f_i(x_i(t)), \tag{3.3}$$

where $\rho_i = [\rho_{i1}, \rho_{i2}, \rho_{i3}]^T \in (\mathbb{R}_0^+)^3$ is the transition rate for the reference player, the term $\|\rho_i\|^2_{R_i}$ indicates the 2-norm weighted on matrix R_i, and $R_i \in \mathbb{R}^{3\times 3}$ is a 3×3 positive-definite diagonal matrix, defined as:

$$R_i = \begin{bmatrix} R_{i1} & & \\ & R_{i2} & \\ & & R_{i3} \end{bmatrix}. \tag{3.4}$$

In equation (3.3), the function $f_i(x_i(t)) : \mathcal{S}^3 \to \mathbb{R}$ depends on the state of the reference player and represents an additional cost or a discount. Both scenarios can be modelled depending on the aim. The two main scenarios are crowd-seeking or crowd-averse dynamics.

Assumption 2. *We suppose that the following holds for $g(\cdot)$, see [40]:*

(i) $g(\cdot)$ is Lipschitz continuous in x_i, with the Lipschitz constant w.r.t. x_i bounded independently of ρ_i;

(ii) $g(\cdot)$ is differentiable w.r.t. ρ_i and the derivative of $g(\cdot)$ w.r.t. ρ_i is Lipschitz w.r.t. x_i, $\forall i \in \mathbb{I}^3$, uniformly in ρ_i;

(iii) and $g(\cdot)$ does not depend on ρ_{ii}, is uniformly convex on the remaining coordinates and is superlinear on ρ_{ij}, $j \neq i$.

Remark 5. *The above assumption is in accordance with the definition of the running cost, given the following considerations. The Lipschitz continuity as in point (i) is preserved by the boundedness of $f_i(x_i(t))$. To ensure that the running cost does not depend on ρ_{ii}, one could set $\rho_{ii} = 0$, but this is in contrast with the definition of transition rates for discrete state Markov processes. Then, $\rho_{ii} \neq 0$ due to the exponential waiting*

time. Therefore, in order to prove that the running cost does not depend on ρ_{ii}, the values R_{ii} must be equal to zero.

Assume that the game has a finite horizon formulation and let $[0, T]$ indicate the horizon window. As anticipated before, the reference player incurs in a terminal cost which depends on the objective that he/she seeks to minimise. The terminal cost $\psi(i, x_i) : \mathcal{I}^3 \times \mathcal{S}^3 \to \mathbb{R}$ is defined as:

$$\psi(i, x_i) = f_i(x_i(T)). \tag{3.5}$$

Assumption 3. *We suppose that $\psi(\cdot)$ is Lipschitz continuous in x_i.*

Remark 6. *As for the running cost, the above assumption is in accordance with the definition of the terminal cost due to the boundedness of $f_i(x_i(t))$. This in turn implies that the value $f_i(x_i(T))$ at the end of the time horizon is also bounded.*

Each player minimises the following cost functional:

$$J^i_{x_i}(\rho_i, w_i, t) = \mathbb{E}^{\rho_i, w_i}_{i_t=i}\left[\int_t^T \left[g(i_\tau, x_{i_\tau}(\tau), \rho_{i_\tau}(\tau)) - \tfrac{1}{2}\|w_{i_\tau}\|^2_{\Gamma_{i_\tau}}\right] d\tau + \psi(i_T, x_{i_T})\right], \tag{3.6}$$

where $\Gamma_i \in \mathbb{R}^{3\times 3}$ is a 3×3 positive-definite diagonal matrix defined as:

$$\Gamma_i = \begin{bmatrix} \Gamma_{i1} & & \\ & \Gamma_{i2} & \\ & & \Gamma_{i3} \end{bmatrix}, \tag{3.7}$$

and $\mathbb{E}^{\rho_i, w_i}_{i_t=i}$ is the expectation for the event $i_t = i$.

The term in $w_i = [w_{i1}, w_{i2}, w_{i3}]^T \in (\mathbb{R}^+_0)^3$ represents a penalty on the energy of the disturbance signal. The cost functional in equation (3.6) has the structure of a robust mean-field game in spirit with H_∞-optimal control, see [11]. To provide a physical understanding, when the elements of matrix Γ_i increase, the values of the disturbance vector in the second norm become smaller.

Problem 1. *Let $\mathbf{x}(t) : [0, T] \to \mathcal{S}^3$ be given. Find the optimal control of the reference player which minimises the cost functional as in the following:*

$$v_i(x_i, t) = \inf_{\rho_i(\cdot)} \sup_{w_i(\cdot)} J^i_{x_i}(\rho_i, w_i, t), \tag{3.8}$$

where $v_i(x_i, t)$ is the value function. The minimisation is performed over the Markovian controls for the reference player control problem, i.e. $\beta_{ij_\tau}(\tau) = \rho_{ij_\tau}(\tau) + w_{ij_\tau}(\tau)$. For each time instant t, the measurable functions $\rho_{ij}(\cdot)$ and $w_{ij}(\cdot)$ yield a transition rate and a penalty for the disturbance, respectively.

In the following, the value function can also be denoted as $v_i(t)$ or v_i for simplicity. The Markov chain for a single player is defined as:

$$\mathbb{P}[i_{\tau+h} = j | i_\tau = i] = [\rho_{ij}(\tau) + w_{ij}(\tau)]h + o(h). \tag{3.9}$$

The generalised Legendre transform of the cost function is defined as:

$$h(x_i, \Delta_i v, i) = \min_{\rho_i(\cdot)} g(i, x_i, \rho_i) + \rho_i^T \cdot \Delta_i v, \tag{3.10}$$

where $\Delta_i : \mathbb{R}^3 \to \mathbb{R}^3$ is the difference operator on i given by

$$\Delta_i v = (v^1 - v^i, v^2 - v^i, v^3 - v^i)^T. \tag{3.11}$$

The Hamiltonian function $\mathcal{H}(\cdot)$ is obtained when in the above equation v is exactly the value function. The Hamiltonian is therefore:

$$\mathcal{H}(x_i, \Delta_i v, i) = \inf_{\rho_i(\cdot)} \sup_{w_i(\cdot)} g(\cdot) - \frac{1}{2}\|w_i\|^2_{\Gamma_i} + (\rho_i + w_i)^T \Delta_i v. \tag{3.12}$$

The optimal transition rates are given by the following equation:

$$\rho_i^*(x_i, \Delta_i v, i) = \operatorname*{argmin}_{\rho_i(\cdot)} \sup_{w_i(\cdot)} \Big[g(\cdot) - \frac{1}{2}\|w_i\|^2_{\Gamma_i} + (\rho_i + w_i)^T \Delta_i v \Big]. \tag{3.13}$$

Because of the superlinearity and uniform convexity of the cost function g, the above function is well defined except for its ith coordinate, namely ρ_{ii}, for which the following assumption holds:

$$\rho_{ii}^*(x, \Delta_i v, i) = -\sum_{j \neq i} \rho_{ij}^{*T}(x_j, \Delta_j v, j). \tag{3.14}$$

The microscopic dynamics are described by the following Hamilton-Jacobi-Bellman set of ODEs:

$$\begin{cases} -\dot{v}_i = \mathcal{H}(x_i, \Delta_i v, t), \\ v_i(T) = \psi(i, x_i). \end{cases} \tag{3.15}$$

The above system is referred to as *terminal value problem* due to the presence of the terminal condition on the value function. Before introducing the next result, it is worth

noting the nature of the adversarial disturbance w_i^*. The nature of the adversarial disturbance is not arbitrary: it is the worst-case deterministic time varying signal which depends on the aggregate behaviour of players choosing symmetrically opposite options, namely those committed to state 1 versus those committed to state 2. The next result establishes that the solution of (3.15) is the value function itself, which is in accordance with [40]. The major novelty about this result consists in the fact that the dynamics studied here include an adversarial disturbance, which is deterministic. Finally, assume that the running cost is concave in the disturbance w, which is in accordance with the coercivity condition, see [11].

Theorem 7. *Let $\mathbf{x}(t) : [0,T] \to \mathcal{S}^3$ be given over the time horizon. Assume that $v : \mathcal{S}^3 \times [0,T] \to \mathbb{R}$ is a solution of the terminal value problem in (3.15). Further assume w_i^* is the worst-case deterministic time varying signal depending on the players having made a choice distinct from that of the reference player. Then v is the value function associated with the distribution $\mathbf{x}$, and the optimal Markovian control is $\beta_i^* = \rho_i^* + w_i^*$ as in the following:*

$$\rho_i^* = -R_i^{-1}\Big[\Delta_i v\Big]^- = -\begin{bmatrix} R_{i1}^{-1}(v_1 - v_i)^- \\ R_{i2}^{-1}(v_2 - v_i)^- \\ R_{i3}^{-1}(v_3 - v_i)^- \end{bmatrix}, \tag{3.16}$$

$$w_i^* = \Gamma_i^{-1}\Big[\Delta_i v\Big]^+ = \begin{bmatrix} \Gamma_{i1}^{-1}(v_1 - v_i)^+ \\ \Gamma_{i2}^{-1}(v_2 - v_i)^+ \\ \Gamma_{i3}^{-1}(v_3 - v_i)^+ \end{bmatrix}. \tag{3.17}$$

Proof. See Section 3.5. □

Remark 7. *The above result states that the optimal Markovian control for the robust mean-field game can be achieved in the specific case where the adversarial disturbance is the worst-case deterministic time varying signal that depends on the players choosing the option different from the one chosen by the reference player.*

3.2.2 Dependance on other Players' Controls

As before, given a large population of players which can be in any of three possible states in a continuous time dynamic game framework, the problem tackled in the previous subsection is extended to the case where the strategy played by the reference player takes into account other players' controls. Again, assume that players are homogeneous

and that each player does not affect the evolution of the game, but his/her choice is added to the dynamics of the mass.

In order to study this scenario, the definition of the difference operator is given first, i.e. $\Delta_i : \mathbb{R}^3 \to \mathbb{R}^3$:

$$\Delta_i z = (z_1 - z_i, z_2 - z_i, z_3 - z_i)^T, \tag{3.18}$$

where $z_i(x_i, t) : \mathcal{S}^3 \times \mathbb{R}_0^+ \to \mathbb{R}$ is a generic function. The difference of function $z_i(x_i, t)$ at two nodes can be interpreted as the resistance of transitioning from one node to the other. To see this, recall that players change their state according to a continuous time Markov chain in order to minimise a running cost and a terminal cost. As before, the running cost is determined by the distribution $\mathbf{x}$ and the transition rates $\rho_i \in (\mathbb{R}_0^+)^3$, i.e. $g(i, x_i, \rho_i) : \mathcal{I}^3 \times \mathcal{S}^3 \times (\mathbb{R}_0^+)^3 \times \to \mathbb{R}$. The running cost is defined by the following equation:

$$g(i, x_i, \rho_i, t) = \frac{1}{2}\|\rho_i\|^2_{R_i(\Delta_i z)} + f_i(x_i(t)), \tag{3.19}$$

where $\|\rho_i\|^2_{R_i(\Delta_i z)}$ is the second maximum norm weighted on matrix $R_i(\Delta_i z) \in \mathbb{R}^{3\times 3}$ which is a 3×3 diagonal matrix, defined as

$$R_i(\Delta_i z) = \begin{bmatrix} R_{i1}(\Delta_i z) & & \\ & R_{i2}(\Delta_i z) & \\ & & R_{i3}(\Delta_i z) \end{bmatrix}. \tag{3.20}$$

The resistance to transitions is captured by the dependance of the penalty matrix $R_i(\Delta_i z)$ on $\Delta_i z$. Note that, as before, $g(\cdot)$ is Lipschitz continuous in x_i, with the Lipschitz constant w.r.t. x_i bounded independently of ρ_i and it is differentiable w.r.t. ρ_i, and the derivative w.r.t. ρ_i is Lipschitz continuous w.r.t x_i, $\forall i \in \mathcal{I}^3$. Moreover, $g(\cdot)$ is uniformly convex and is superlinear on ρ_j, $j \neq i$ and independent of ρ_i. The terminal cost is defined as in equation (3.5).

The cost functional is defined over the finite horizon $[0, T]$ as

$$J^i_{x_i}(\rho_i, w_i, t, \Delta_i z) = \mathbb{E}^{\rho_i, w_i}_{i_t=i}\left[\int_t^T \left[g(i_\tau, x_{i_\tau}(\tau), \rho_{i_\tau}(\tau)) - \tfrac{1}{2}\|w_{i_\tau}\|^2_{\Gamma_{i_\tau}(\Delta_i z)}\right] d\tau + \psi(i_T, x_{i_T})\right], \tag{3.21}$$

where $\mathbb{E}^{\rho_i, w_i}_{i_t=i}$ is the expectation for the event $i_t = i$, w_{i_τ} models the energy of the adversarial disturbance in terms of penalty and $\|w_{i_\tau}\|^2_{\Gamma_{i_\tau}(\Delta_i z)}$ is the second maximum norm

weighted on matrix $\Gamma_i(\Delta_i z) \in \mathbb{R}^{3\times 3}$, which is a 3×3 diagonal matrix defined as:

$$\Gamma_i(\Delta_i z) = \begin{bmatrix} \Gamma_{i1}(\Delta_i z) & & \\ & \Gamma_{i2}(\Delta_i z) & \\ & & \Gamma_{i3}(\Delta_i z) \end{bmatrix}. \tag{3.22}$$

Problem 2. *Let $\mathbf{x}(t) : [0,T] \to \mathcal{S}^3$ be given over the time horizon. Let $\Delta_i z$ be the difference operator on function $z_i(x_i, i)$ that captures the resistance to transition from a state to another. Find the optimal control for the reference player which minimises the cost functional that depends on the distribution and on the control of the other players:*

$$v_i(x_i, t) = \inf_{\rho_i(\cdot)} \sup_{w_i(\cdot)} J^i_{x_i}(\rho_i, w_i, t, \Delta_i z), \tag{3.23}$$

where $v_i(x_i, t)$ is the value function and the minimisation is performed over the Markovian controls for the single player control problem, i.e. $\beta_{ij_\tau}(\tau) = \rho_{ij_\tau}(\tau) + w_{ij_\tau}(\tau)$.

The corresponding Hamiltonian function $\mathcal{H}(\cdot)$ for the above problem can be obtained as:

$$\mathcal{H}_{\Delta_i z}(x_i, \Delta_i v, i) = \inf_{\rho_i(\cdot)} \sup_{w_i(\cdot)} [g(\cdot) - \tfrac{1}{2}||w_i||^2_{\Gamma_i(\Delta_i z)} + (\rho_i + w_i)^T \Delta_i v]. \tag{3.24}$$

Finally, the corresponding Hamilton-Jacobi-Bellman ODEs are the following:

$$\begin{cases} -\dot{v}_i = \mathcal{H}_{\Delta_i z}(x_i, \Delta_i v, t), \\ v_i(T) = \psi(i, x_i), \end{cases} \tag{3.25}$$

where the robust Hamiltonian is described by equation (3.24), for which the weight matrices depend on the difference operator $\Delta_i z$. The solution of the above equations is the value function derived under the optimal Markovian Control $\beta_i^* = \rho_i^* + w_i^*$ as stated in the following theorem.

Theorem 8. *Let $\mathbf{x}(t) : [0,T] \to \mathcal{S}^3$ be given over the time horizon. Assume that $v : \mathcal{S}^3 \times [0,T] \to \mathbb{R}$ is a solution of the terminal value problem in (3.25). Further assume that w_i^* is the worst-case deterministic time varying signal depending on the players' opposite strategies between the two options. Then v is the value function associated with the distribution $\mathbf{x}$, and the optimal Markovian control is $\beta_i^* = \rho_i^* + w_i^*$ as in the following:*

$$\rho_i^* = -R_i^{-1}(\Delta_i z)\Big[\Delta_i v\Big]^- = -\begin{bmatrix} R_{i1}^{-1}(\Delta_i z)(v_1 - v_i)^- \\ R_{i2}^{-1}(\Delta_i z)(v_2 - v_i)^- \\ R_{i3}^{-1}(\Delta_i z)(v_3 - v_i)^- \end{bmatrix}, \tag{3.26}$$

$$w_i^* = \Gamma_i^{-1}(\Delta_i z)\Big[\Delta_i v\Big]^+ = \begin{bmatrix} \Gamma_{i1}^{-1}(\Delta_i z)(v_1 - v_i)^+ \\ \Gamma_{i2}^{-1}(\Delta_i z)(v_2 - v_i)^+ \\ \Gamma_{i3}^{-1}(\Delta_i z)(v_3 - v_i)^+ \end{bmatrix}. \tag{3.27}$$

Proof. It follows from the proof of Theorem 7, see Section 3.5. □

Remark 8. *The main difference between Theorem 7 and Theorem 8 is that the latter is a more general result: in fact in Theorem 8 the strategy of the reference player takes into account the other players' controls through the difference operator. The adversarial disturbance is treated again as the worst-case deterministic time varying signal. The choice of modelling the signal in this way is motivated by the context in which the problem originates, i.e. collective decision-making in honeybee swarms.*

3.3 Stationary Solutions

In this section, firstly the mean-field Nash equilibrium is presented in the form of initial-terminal value problem (ITVP), see [40]. The corresponding value function is calculated and the stationary solutions are given as the difference in value function between the uncommitted state and committed states. When an equilibrium point in the population distribution is fixed, the existence of the corresponding stationary solution is proved and the stability of this solution depends on the stability of the fixed equilibrium point. For certain conditions, a basin of attraction can be found and its stability can be proved. Finally, applications in the specific contexts of honeybee swarms and virus propagation are presented as a link to the general model. A numerical analysis is given to corroborate the theoretical results.

3.3.1 Existence and Stability

In the situation where the reference player uses strategy ρ in response to the rest of the population playing strategy ρ as well, the current solution is therefore called a mean-field Nash equilibrium. Such a solution brings together the Kolmogorov equations and the

Hamilton-Jacobi-Bellman equations as in the following:

$$\begin{cases} \dot{x}_i(t) = (1 - x_1 - x_2)\beta_{3i} - x_i\beta_{i3}, & i = 1, 2 \\ -\dot{v}_i(t) = \mathcal{H}(x_i, \Delta_i v, t), & \forall i \in \mathcal{I}^3 \\ \mathbf{x}(0) = \hat{\mathbf{x}}, & \\ v_{i_T}(T) = \psi(i_T, x_{i_T}). & \end{cases} \tag{3.28}$$

The set of equations (3.2) and equation (3.13) are combined to form the above system. Both equations (3.2) and (3.13) describe one aspect of the game. The first equations describe the macroscopic interactions among players, thus showing how the population evolves as a whole when assuming that all players follow (3.13). The second equation models the microscopic dynamics for individual players, and it characterises their behaviour in response to the macroscopic behaviour described by (3.2). Due to the presence of an initial condition for the population distribution in the Kolmogorov equations, and because of the presence of a terminal condition for the value function in the Hamilton-Jacobi-Bellman equations, this system is referred to as *initial-terminal value problem (ITVP)* for the mean-field game.

The value function can be calculated by expanding the Hamiltonian according to (3.12). As for the control and disturbance, the optimal control and disturbance from (3.16) and (3.17) are used. The calculation is as in the following:

$$\begin{aligned} -\dot{v}_i &= \tfrac{1}{2}\|\rho_i^*\|_{R_i}^2 - \tfrac{1}{2}\|w_i^*\|_{\Gamma_i}^2 + (\rho_i^* + w_i^*)^T \Delta_i v + f_i(x_i) \\ &= -\tfrac{1}{2}\Big[R_{ij}^{-1}[(v_j - v_i)^-]^2 + R_{ik}^{-1}[(v_k - v_i)^-]^2\Big] \\ &\quad + \tfrac{1}{2}\Big[\Gamma_{ij}^{-1}[(v_j - v_i)^-]^2 + \Gamma_{ik}^{-1}[(v_k - v_i)^-]^2\Big] + f_i(x_i) \\ &= -\tfrac{1}{2}(\Delta_i v)^{-^T} R_i^{-1}(\Delta_i v)^- + \tfrac{1}{2}(\Delta_i v)^{+^T} \Gamma_i^{-1}(\Delta_i v)^+ + f_i(x_i). \end{aligned} \tag{3.29}$$

Due to the original formulation of the model, the following assumptions hold: let $R_{12}, R_{21}, \Gamma_{12}, \Gamma_{21} > 0$ be sufficiently large, such that the cost to transition from state 1 to state 2 and vice versa is large enough. This can be explained from the fact that players cannot move directly between the committed states but have to move in the uncommitted state first. Further, assume that $v_1, v_2 < v_3$. The value function is specialised for each state i as in the following:

$$\begin{cases} -\dot{v}_1 = \tfrac{1}{2}\Gamma_{13}^{-1}(v_3 - v_1)^2 + f_1(x_1), \\ -\dot{v}_2 = \tfrac{1}{2}\Gamma_{23}^{-1}(v_3 - v_2)^2 + f_2(x_2), \\ -\dot{v}_3 = -\tfrac{1}{2}[R_{31}^{-1}(v_1 - v_3)^2 + R_{32}^{-1}(v_2 - v_3)^2] + f_3(x_3). \end{cases} \tag{3.30}$$

In order to investigate the transitions from the two committed states to the uncommitted state and vice versa, in the following the first and the second equations are subtracted to the third equation in the above system. This yields:

$$\begin{cases} \dot{v}_3 - \dot{v}_1 = \frac{1}{2}\left[\Gamma_{13}^{-1}(v_3 - v_1)^2 + R_{31}^{-1}(v_1 - v_3)^2 + R_{32}^{-1}(v_2 - v_3)^2\right] + f_1(x_1) - f_3(x_3), \\ \dot{v}_3 - \dot{v}_2 = \frac{1}{2}\left[\Gamma_{23}^{-1}(v_3 - v_2)^2 + R_{31}^{-1}(v_1 - v_3)^2 + R_{32}^{-1}(v_2 - v_3)^2\right] + f_2(x_2) - f_3(x_3). \end{cases} \tag{3.31}$$

To simplify the notation, let $y_1 := v_3 - v_1$ and $y_2 := v_3 - v_2$. In light of this notation, the above system can be rewritten as:

$$\begin{cases} \dot{y}_1 = \frac{1}{2}(\Gamma_{13}^{-1} + R_{31}^{-1})y_1^2 + \frac{1}{2}R_{32}^{-1}y_2^2 + f_1(x_1) - f_3(x_3), \\ \dot{y}_2 = \frac{1}{2}R_{31}^{-1}y_1^2 + \frac{1}{2}(\Gamma_{23}^{-1} + R_{32}^{-1})y_2^2 + f_2(x_2) - f_3(x_3). \end{cases} \tag{3.32}$$

The above system is used to establish existence of a stationary solution. For the game under consideration, stationary solutions, also called stationary mean-field equilibrium points, are defined as:

$$\begin{cases} \sum_k x_k \beta_{ki}^* - \sum_j x_i \beta_{ij}^* = 0, \qquad \forall i \in \mathcal{I}^3, \\ \mathcal{H}(\mathbf{x}, \Delta_i v, t) = \kappa, \end{cases} \tag{3.33}$$

where κ is a constant. It is worth noting that in a stationary mean-field equilibrium functions $f_i(x_i)$ are fixed and constant. This is due to the fact that the population distribution $\mathbf{x}$ is at an equilibrium of (3.2) and thus constant. The existence and stability property of the first equation of (3.33), namely stationary distributions $\mathbf{x}(t)$, are studied in Chapter 2. The aim of the rest of this section is to investigate the solutions of the second equation of (3.33). The next result establishes the existence of stationary value functions, namely value functions that satisfy the second equation of (3.33).

Theorem 9. *Let a stationary distribution be given $t \mapsto \mathbf{x}(t) := \hat{\mathbf{x}} \in \mathcal{S}^3$. Then a stationary value function exists and is given by the mean-field game described by equations (3.32) for the stationary problem (3.33):*

$$y_1^* = -\sqrt{\Gamma_{23}^{-1}\Gamma_{13}y_2^{*2} + 2\Gamma_{13}(f_2(x_2) - f_1(x_1))}. \tag{3.34}$$

Proof. See Section 3.5. □

Remark 9. *The system of equations in (3.32) shares similarities to the equation of the ellipse, provided that the difference in $f_i(x_i)$ is negative in both equations, namely*

$f_i(x_i) - f_3(x_3) < 0$, for $i = 1, 2$. The equilibrium points can be found at the intersection of the two ellipses centred at the origin corresponding to the equations in (3.32). Among the four intersections, the equilibrium point in the third quadrant is the one of interest and this explains the negative sign in equation (3.34). The latter equation provides the conditions of existence for a stationary solution in terms of the difference in value functions. The difference in value functions can also be seen as the potential energy required to move from the uncommitted state to the committed states or vice versa.

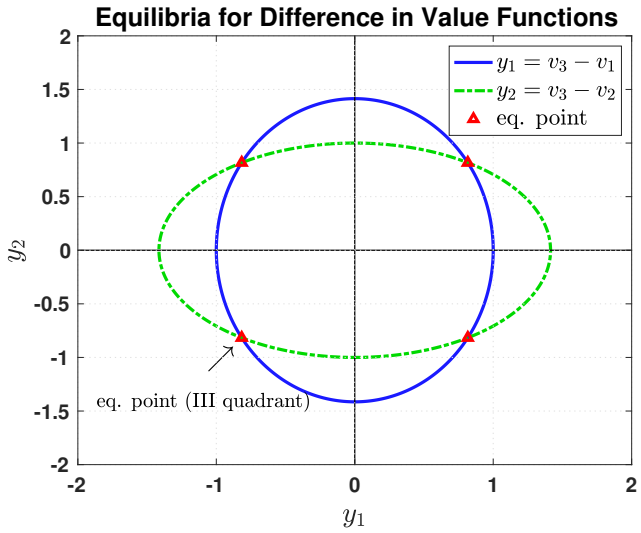

Figure 3.1: Graphical representation of the system of equations (3.32) as ellipses. The intersections between the ellipses represent the equilibrium points of the difference in value functions for the stationary solution in (3.33).

The ellipses corresponding to the equations in (3.32) are depicted in Fig. 3.1. Different values of Γ_{13}^{-1} and Γ_{23}^{-1} change the shape of the ellipses. In other terms, when one term decreases, the corresponding distance between the focal points of the corresponding ellipse becomes larger along its major axis, namely y and x axes for increasing Γ_{13}^{-1} and Γ_{23}^{-1}, respectively. When the cost of the disturbance is lower, the equilibrium point shifts towards the axes, y_2 and y_1, respectively. As anticipated in the above remark, if the difference in value functions between two nodes is seen as a difference of potentials, the latter can be considered constant, i.e. the potential at the nodes is the same. Therefore, it can also be seen that the disturbance can easily make the players go back to the node where their gain is lower. In this scenario, the difference in $f_i(x_i)$ affects the distance of the ellipses from the centre of the axes, which can be thought of as the equivalent of the

radius in a circle.

The next result establishes that, for a fixed $\tilde{\mathbf{x}}$, a stationary solution exists and this solution is robust to variations in the value function.

Theorem 10. *Given $T > 0$, an initial condition in the distribution, namely $\mathbf{x}(0) = \hat{\mathbf{x}}$, and a terminal condition in the value function, namely $v_{i_T}(T) = \psi(i_T, x_{i_T})$, let $(\mathbf{x}, v)$ be the solution of (3.28) with initial-terminal conditions $\mathbf{x}(-T) = \hat{\mathbf{x}}$ and $v_{i_T}(T) = \psi(i_T, x_{i_T})$. There exists a solution $(\bar{\mathbf{x}}, \bar{v})$ of the stationary problem (3.33), and this solution is robust to variations of $\bar{v}$. Furthermore, being $\tilde{\mathbf{x}}$ a stable equilibrium point, then the stationary solution in v is also stable.*

Proof. See Section 3.5. □

Remark 10. *The above theorem investigates the conditions for asymptotic stability of the system of stationary solutions under a deterministic adversarial disturbance. Thanks to the study of the equilibrium points in the population distribution for system (3.28), the evolution of the difference in value functions can be studied under the following condition: by fixing the equilibrium points for the population distribution and by checking the stability on the value functions.*

3.3.2 Limit Cycles and Basin of Attraction

The problem of oscillations and periodic solutions is investigated in the following. The ITVP corresponding to the robust Hamiltonian in (3.24) is the following:

$$\begin{cases} \dot{x}_i(t) = (1 - x_1 - x_2)\beta_{3i} - x_i\beta_{i3}, & i = 1, 2 \\ -\dot{v}_i(t) = \mathcal{H}_{\Delta_i z}(x_i, \Delta_i v, t), & \forall i \in \mathcal{I}^3 \\ \mathbf{x}(0) = \hat{\mathbf{x}}, \\ v_{i_T}(T) = \psi(i_T, x_{i_T}). \end{cases} \tag{3.35}$$

By expanding the Hamiltonian function in (3.24), the value function can be calculated from the optimal control and disturbance in (3.26)-(3.27) as:

$$\begin{aligned} -\dot{v}_i &= \tfrac{1}{2}||\rho_i^*||^2_{R_i(\Delta_i z)} - \tfrac{1}{2}||w_i^*||^2_{\Gamma_i(\Delta_i z)} + (\rho_i^* + w_i^*)^T \Delta_i v + f_i(x_i) \\ &= -\tfrac{1}{2}\left[R_{ij}^{-1}(\Delta_i z)(v_j - v_i)^2 + R_{ik}^{-1}(\Delta_i z)(v_k - v_i)^2\right] \\ &\quad + \tfrac{1}{2}\left[\Gamma_{ij}^{-1}(\Delta_i z)(v_j - v_i)^2 + \Gamma_{ik}^{-1}(\Delta_i z)(v_k - v_i)^2\right] + f_i(x_i) \\ &= -\tfrac{1}{2}(\Delta_i v)^{-^T} R_i^{-1}(\Delta_i z)(\Delta_i v)^- + \tfrac{1}{2}(\Delta_i v)^{+^T} \Gamma_i^{-1}(\Delta_i z)(\Delta_i v)^+ + f_i(x_i). \end{aligned} \tag{3.36}$$

The same assumption as in the previous subsection holds, namely the cost of transition rates from state 1 to state 2 and vice versa is large enough. Formally, assume that the penalty coefficients $R_{12}(\Delta_i z), R_{21}(\Delta_i z), \Gamma_{12}(\Delta_i z), \Gamma_{21}(\Delta_i z)$ are sufficiently large. Consider the y_1-y_2 plane, similarly as in the previous subsection. Due to the different evolution in each quadrant of the y_1-y_2 plane, the system is investigated in each quadrant. Symmetric arguments apply to the first and third quadrants, and to the second and fourth quadrants, and therefore they are presented in this order. In order to simplify the notation, the compact notation R_{ij}^{-1} and Γ_{ij}^{-1} is used in state of $R_{ij}^{-1}(\Delta_i z)$ and $\Gamma_{ij}^{-1}(\Delta_i z)$, respectively.

[**Quadrant I**]. In this quadrant the value function in the uncommitted state is greater than in committed states, namely $v_3 > v_1, v_2$. The corresponding value function for each $i \in \mathcal{I}^3$ can be calculated from (3.36) as:

$$\begin{cases} -\dot{v}_1 = \frac{1}{2}\Gamma_{13}^{-1}(v_3 - v_1)^2 + f_1(x_1), \\ -\dot{v}_2 = \frac{1}{2}\Gamma_{23}^{-1}(v_3 - v_2)^2 + f_2(x_2), \\ -\dot{v}_3 = -\frac{1}{2}[R_{31}^{-1}(v_1 - v_3)^2 + R_{32}^{-1}(v_2 - v_3)^2] + f_3(x_3). \end{cases} \tag{3.37}$$

It is worth noting that in the first quadrant players control the transitions from the uncommitted state 3 to states 1 and 2. The adversarial disturbance forces the players to move back to the uncommitted state 3, instead. In the y_1-y_2 plane, the above system can be rewritten in terms of y_1 and y_2 as:

$$\textit{Quadrant I} \begin{cases} \dot{y}_1 = \frac{1}{2}[(\Gamma_{13}^{-1} + R_{31}^{-1})y_1^2 + R_{32}^{-1}y_2^2] + f_1(x_1) - f_3(x_3), \\ \dot{y}_2 = \frac{1}{2}[R_{31}^{-1}y_1^2 + (\Gamma_{23}^{-1} + R_{32}^{-1})y_2^2] + f_2(x_2) - f_3(x_3). \end{cases} \tag{3.38}$$

[**Quadrant III**]. In the third quadrant, the situation is symmetric to the first quadrant. Therefore, the condition $v_3 < v_1, v_2$ holds. From (3.36), the calculation for the value function is the following:

$$\begin{cases} -\dot{v}_1 = -\frac{1}{2}R_{13}^{-1}(v_3 - v_1)^2 + f_1(x_1), \\ -\dot{v}_2 = -\frac{1}{2}R_{23}^{-1}(v_3 - v_2)^2 + f_2(x_2), \\ -\dot{v}_3 = \frac{1}{2}[\Gamma_{31}^{-1}(v_1 - v_3)^2 + \Gamma_{32}^{-1}(v_2 - v_3)^2] + f_3(x_3). \end{cases} \tag{3.39}$$

In the third quadrant, players control transitions from the committed states 1 and 2 to the uncommitted state 3. Analogously to the first quadrant, the disturbance forces

players back to the original states, therefore it pushes players from state 3 to states 1 and 2. The system in the y_1-y_2 plane is the following:

$$\textit{Quadrant III} \begin{cases} \dot{y}_1 = -\frac{1}{2}[(R_{13}^{-1} + \Gamma_{31}^{-1})y_1^2 + \Gamma_{32}^{-1}y_2^2] + f_1(x_1) - f_3(x_3), \\ \dot{y}_2 = -\frac{1}{2}[\Gamma_{31}^{-1}y_1^2 + (R_{23}^{-1} + \Gamma_{32}^{-1})y_2^2] + f_2(x_2) - f_3(x_3). \end{cases} \tag{3.40}$$

[**Quadrant II**]. In the second quadrant, the value function satisfies the following inequalities: $v_1 > v_3 > v_2$. Therefore, the calculation is obtained from (3.36) as:

$$\begin{cases} -\dot{v}_1 = -\frac{1}{2}R_{13}^{-1}(v_3 - v_1)^2 + f_1(x_1), \\ -\dot{v}_2 = -\frac{1}{2}R_{23}^{-1}(v_3 - v_2)^2 + f_2(x_2), \\ -\dot{v}_3 = \frac{1}{2}[\Gamma_{31}^{-1}(v_1 - v_3)^2 + \Gamma_{32}^{-1}(v_2 - v_3)^2] + f_3(x_3). \end{cases} \tag{3.41}$$

As for the second quadrant, players control the transitions from state 1 to state 3 and from state 3 to state 2. On the other hand, the adversarial disturbance controls the transitions from state 2 to state 3 and from state 3 to state 1. The above system can be rewritten in terms of y_1 and y_2 as in the following:

$$\textit{Quadrant II} \begin{cases} \dot{y}_1 = -\frac{1}{2}[(R_{13}^{-1} + \Gamma_{31}^{-1})y_1^2 + \Gamma_{32}^{-1}y_2^2] + f_1(x_1) - f_3(x_3), \\ \dot{y}_2 = \frac{1}{2}[\Gamma_{31}^{-1}y_1^2 + (R_{23}^{-1} + \Gamma_{32}^{-1})y_2^2] + f_2(x_2) - f_3(x_3). \end{cases} \tag{3.42}$$

[**Quadrant IV**]. In the last quadrant to be considered, the condition $v_2 > v_3 > v_1$ holds. Thus, equation (3.36) yields the following value function:

$$\begin{cases} -\dot{v}_1 = \frac{1}{2}\Gamma_{13}^{-1}(v_3 - v_1)^2 + f_1(x_1), \\ -\dot{v}_2 = -\frac{1}{2}R_{23}^{-1}(v_3 - v_2)^2 + f_2(x_2), \\ -\dot{v}_3 = -\frac{1}{2}R_{31}^{-1}(v_1 - v_3)^2 + \frac{1}{2}\Gamma_{32}^{-1}(v_2 - v_3)^2 + f_3(x_3). \end{cases} \tag{3.43}$$

In this last case, players control transitions from state 2 to state 3 and from state 3 to state 1. The disturbance, instead, forces players back from state 1 to state 3 and from state 3 to state 2. System (3.43) can be rewritten in the form of difference in value function as:

$$\textit{Quadrant IV} \begin{cases} \dot{y}_1 = \frac{1}{2}[(R_{13}^{-1} + \Gamma_{31}^{-1})y_1^2 - \Gamma_{32}^{-1}y_2^2] + f_1(x_1) - f_3(x_3), \\ \dot{y}_2 = -\frac{1}{2}[-R_{31}^{-1}y_1^2 + (R_{23}^{-1} + \Gamma_{32}^{-1})y_2^2] + f_2(x_2) - f_3(x_3). \end{cases} \tag{3.44}$$

The corresponding Markov chain for all the systems investigated in each specific quadrant is depicted in Fig. 3.2. The control actions for the players and for the adversarial disturbances as given in the former analysis are represented by the direction of the arrows. So, for instance, in the first quadrant, players control the transition rates from the uncommitted state 3 to the commited states 1 and 2. This is represented by the arrows in the top half of the Markov chain in Fig. 3.2 (top-left). In the following, the analogies between the system for each region of the y_1-y_2 plane are explored in order to find the conditions for existence of limit cycles.

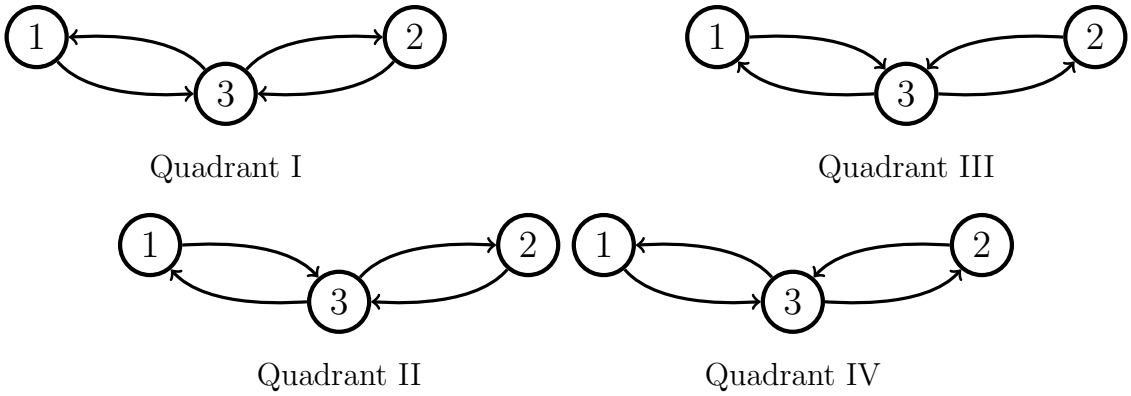

Figure 3.2: Markov chain representations corresponding to system (3.38) in the top-left corner, system (3.40) in the top-right, system (3.42) in the bottom-left and system (3.44) in the bottom-right. The arrow directions in the top half of each Markov chain describe the control of the players, while the directions in the bottom half describe the effect of the adversarial disturbance.

In order to show the main result of this part, which involves the nonexistence of stationary solutions for the mean-field equilibrium under certain boundary conditions, the corresponding stationary solutions must be given first. Similarly to the stationary solutions in the case of the dependance on the reference player's control, they are defined as:

$$\begin{cases} \sum_k x_k \beta^*_{ki} - \sum_j x_i \beta^*_{ij} = 0, \forall i \in \mathcal{I}^3 \\ \mathcal{H}_{\Delta_i z}(\mathbf{x}, \Delta_i v, t) = \kappa, \end{cases} \tag{3.45}$$

where κ is, again, a constant. The following result proves that there exists a basin of attraction under certain conditions.

Theorem 11. *Given $T > 0$, an initial condition in the distribution, namely $\mathbf{x}(0) = \hat{\mathbf{x}}$, and a terminal condition in the value function, namely $v_{i_T}(T) = \psi(i_T, x_{i_T})$, let $\mu < 0$ and $|\mu| < 1$. Let $(\mathbf{x}, v)$ be the solution of (3.35) with initial-terminal conditions $\mathbf{x}(-T) = \hat{\mathbf{x}}$ and $v_{i_T}(T) = \psi(i_T, x_{i_T})$. Moreover, let $f_1(x_1) - f_3(x_3) = \mu y_1 + y_2$ and $f_2(x_2) - f_3(x_3) = -y_1 + \mu y_2$. Then, the following statements hold true:*

- ***Case 1.*** *If $\hat{\mathbf{x}} \in \mathcal{B} := \{\bar{r} \in \mathbb{R}^2 : \|\bar{r}\|_2 < \sqrt{-2\mu}\}$, then the orbit intersects the y_1-axis in points internal to $\mathcal{B}$. Therefore $\mathcal{B}$ is a* basin of attraction *for the origin of the space defined by y_1 and y_2.*
- ***Case 2.*** *If $\hat{\mathbf{x}} \notin \mathcal{B} := \{\bar{r} \in \mathbb{R}^2 : \|\bar{r}\|_2 < \sqrt{-2\mu}\}$, then no stationary solutions exist.*

Proof. See Section 3.5. □

Remark 11. *It is worth noting that simulations provide useful information on the borderline conditions in the proximity of the closed orbit, specifically in the proximity of quadrants II and IV. In fact, as it can be seen from the simulations, the region of convergence is larger, accounting for the absence of the limit cycle in quadrants II and IV.*

3.3.3 Applications

In the following, two models are introduced to link the general mean-field game to real applications, namely honeybee swarms and virus propagation in smart grids. The first application describes the context of honeybee swarms and the corresponding consensus problem. The second application extends the mean-field model to the smart grid scenario where a virus is propagating in the network. For the analysis of the structured counterpart of both applications, the reader is referred to Chapter 4.

Swarm of Honeybees. The model originated from this application, which motivates this study. The original scenario involves the biological study of the collective decision-making problem that a swarm of honeybee faces when selecting a nest for the next season. In short, the swarm has to find consensus on one of two possible nest places (or next boxes, as these were used for the experiments in [91]), while sharing information about the quality and position of the found nests. During the collective decision-making process, they use two main behaviours: the so-called *waggle dance*, in order to convey information about the nests, and the *cross-inhibitory stop signals*, in order to disrupt the dance of scout bees committed to the other option. Additionally to being recruited by

the scouts (through the waggle dance) and becoming uncommitted through the signals, bees can spontaneously choose to commit or to abandon any of the options.

The above behaviours are captured by four parameters: r and σ for the waggle dance and the cross-inhibitory signal, respectively; γ and α for the actions of spontaneously committing to an option and of rejecting the option they are committed to, respectively. Given the equilibrium point calculated in (3.34), when the equilibrium point involves the transition rates from the uncommitted state 3 to state 1 and state 2, it follows:

$$y^* = \begin{bmatrix} y_1^* \\ y_2^* \end{bmatrix} = \begin{bmatrix} v_1 - v_3 \\ v_2 - v_3 \end{bmatrix} = \begin{bmatrix} -\gamma_1 - rx_1 \\ -\gamma_2 - rx_2 \end{bmatrix}. \tag{3.46}$$

The above equation links the difference in value functions between state 3 and states 1 and 2 to the transition rates presented in Chapter 2, bridging the gap between the general mean-field game model and the evolutionary game model. As an example, consider the case where $R_{31}, R_{32} = 1$; from Theorem 7, it follows:

$$\rho_3^* = -\begin{bmatrix} v_1 - v_3 \\ v_2 - v_3 \\ 0 \end{bmatrix} = \begin{bmatrix} \gamma_1 + rx_1 \\ \gamma_2 + rx_2 \\ 0 \end{bmatrix}. \tag{3.47}$$

Likewise, for the disturbance:

$$w_1^* = \begin{bmatrix} 0 \\ 0 \\ \Gamma_{13}^{-1}(v_3 - v_1)^+ \end{bmatrix} = \begin{bmatrix} 0 \\ 0 \\ \frac{\alpha+\sigma x_2}{\gamma_1+rx_1}(\gamma_1 + rx_1) \end{bmatrix} = \begin{bmatrix} 0 \\ 0 \\ \alpha + \sigma x_2 \end{bmatrix}, \tag{3.48}$$

where the second equality is obtained by setting

$$\Gamma_{13} = (\gamma_1 + rx_1)/(\alpha + \sigma x_2).$$

Thus, when the values are set as the parameters of the honeybee swarm consensus problem, the mean-field game model introduced in the above sections yields the evolutionary game model for the collective decision-making problem of honeybee swarms. The cross-inhibitory signal in the evolutionary game model takes the form of a disturbance in the general formulation of the robust mean-field game model.

Virus Propagation. When the parameter defining the behaviour of the cross-inhibitory signal is negligible, the corresponding system can be used to model a virus propagation

scenario. As introduced in the previous chapter, the compartmental SIS and SIR models captures the dynamics used to describe the context of a virus propagating, see [21]. In the SIS model, individuals can either be susceptible, or infected. After being infected by the virus, a portion of infected individuals can heal from the virus and move back to the susceptible state. The *SIR* model describes the case where the individuals who recover from the virus cannot be infected again.

Assume that the equilibrium point calculated in (3.34) is given by:

$$y^* = \begin{bmatrix} y_1^* \\ y_2^* \end{bmatrix} = \begin{bmatrix} v_1 - v_3 \\ v_2 - v_3 \end{bmatrix} = \begin{bmatrix} -\beta_{31} \\ -\beta_{32} \end{bmatrix}. \tag{3.49}$$

Assuming that $R_{31}, R_{32} = 1$, from Theorem 7, it can be seen that:

$$\rho_3^* = - \begin{bmatrix} v_1 - v_3 \\ v_2 - v_3 \\ 0 \end{bmatrix} = \begin{bmatrix} \beta_{31} \\ \beta_{32} \\ 0 \end{bmatrix}. \tag{3.50}$$

Likewise, as for the disturbance, the following holds true:

$$\begin{aligned} w_1^* = \begin{bmatrix} 0 \\ 0 \\ \Gamma_{13}^{-1}(v_3 - v_1)^+ \end{bmatrix} := \begin{bmatrix} 0 \\ 0 \\ \frac{\beta_{13}x_3}{\beta_{31}}\beta_{31} \end{bmatrix} = \\ = \begin{bmatrix} 0 \\ 0 \\ \beta_{13}x_3 \end{bmatrix}. \end{aligned} \tag{3.51}$$

In the above, the value of Γ_{13} is set as:

$$\Gamma_{13} = \frac{\beta_{13}x_3}{\beta_{31}}.$$

The mean-field game studied in its general form reduces to a virus propagation model, when the cross-inhibitory coefficient are assumed negligible. In this context, the infection rate can thus be linked to the matrix Γ which is the cost matrix for the adversarial disturbance.

3.3.4 Numerical Analysis

In this section, two sets of simulations are provided to corroborate the theoretical results presented in this chapter. The first set involves the study of the intersection of the

difference in value functions in the form of y_1 and y_2. The equilibrium point at the intersection of the two ellipses in the third quadrant is the one of interest. In the second set of simulations, the limit cycles and the corresponding basin of attraction are simulated to show how trajectories evolve in the cases reported in Theorem 11.

In the first set of simulations, the mean-field response is investigated. Two cases are proposed. The first case involves the scenario where the equilibrium point at the intersection is asymptotically stable and parameters are symmetric, similarly to previous symmetric models in Chapter 2. In practice, this means that the components of the matrix for the adversarial disturbance are identical, namely $\Gamma_{13}^{-1} = \Gamma_{23}^{-1}$, which leads to $\Gamma_{13} = \Gamma_{23}$. In this symmetric scenario, the functions present in the running and terminal costs on the distribution $\mathbf{x}$ are identical, too, namely $f_1(x_1) = f_2(x_2)$. The second and last case simulate the scenario where parameters are no longer symmetric, namely $\Gamma_{13}^{-1} > \Gamma_{23}^{-1}$ and $f_1(x_1) > f_2(x_2)$. In addition, parameters are chosen in such a way that the two ellipses do not intersect, thus the previous asymptotically stable node is no longer present. In this set, $N = 20$ trajectories are simulated in each case and $R_{31}^{-1} = R_{32}^{-1} = 1$. Parameter c_i denotes the difference as in the following: $f_i(x_i) - f_3(x_3)$. The varying parameters are shown in Table 3.1 and the algorithm is shown below.

Table 3.1: Varying parameters for the two sets of simulations.

Parameter \ Case	I	II
c_1	-1	-0.65
c_2	-1	-1.4
Γ_{13}^{-1}	1	1.2
Γ_{23}^{-1}	1	1

In the first case, i.e. the scenario with a stable equilibrium and symmetric parameters, trajectories converge when in a neighbourhood of the equilibrium point, which led to the hypothesis of a basin of attraction as in Theorem 11. All trajectories starting within the region of convergence, which is simulated in the second set of simulations, are drawn in green and converge to the equilibrium point, while the other trajectories simply diverge, and are depicted in red. Finally, the second case deals with the scenario

Algorithm

Input: Parameters set as in Table 3.1, and $R_{31}^{-1} = R_{32}^{-1} = 1$

Output: Difference in value function in terms of $\dot{y}_1, \dot{y}_2$

1 : **Initialize:** Set initial values as in Input
2 : **for** time $t = T-1, T-2, \ldots, 0$ **do**
3 : **for** $n = 1, 2, \ldots, N$ **do**
4 : compute the dynamics as in (3.32):
$$\dot{y}_i = \tfrac{1}{2} a_{i1} y_1^2 + \tfrac{1}{2} a_{i2} y_2^2 + c_i, \text{ for } i = 1, 2$$
5 : **end for**
6 : **end for**
7 : **STOP**

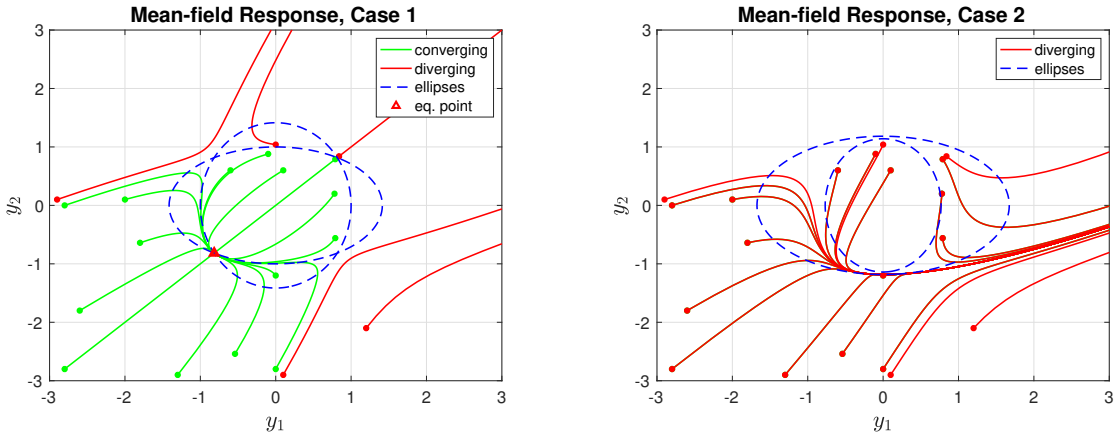

(a) In the case of symmetric parameters and stable equilibrium point: trajectories in green converge.

(b) For asymmetric parameters (no intersections between ellipses) and no stable equilibria: all trajectories diverge.

Figure 3.3: Behaviour of the system in the presence of a stable equilibrium (left) or no stable equilibria (right). The presence of a basin of attraction can be seen from trajectories diverging even in the presence of a stable node.

without an asymptotically stable node, since there are no intersections between the ellipses. In this case, all trajectories diverge. Figure 3.3 shows the case of asymptotically stable equilibrium on the left and no equilibria on the right.

The second set of simulations investigates the results coming from Theorem 11. The evolution of system (3.64) is presented, in the cases of $\mu \in \{-0.5, -0.3\}$. Both cases are depicted in Fig. 3.4. In general, trajectories starting outside the closed orbit of radius $r = \sqrt{-2\mu}$ diverge, while those starting inside converge. So, the system presents an unstable limit cycle, with asymptotically stable spirals within and unstable spirals outside, in accordance with Theorem 11. When μ is sufficiently small, two phenomena can be observed: the speed of convergence decreases and the trajectories within a neighbourhood of the limit cycle becomes stable, due to the fact that in quadrants II and IV there are no closed orbits and the speed of convergence is quadratic. So, if a trajectory enters this region very close to it, it converges to the origin. This can be seen from Fig. 3.4 (right).

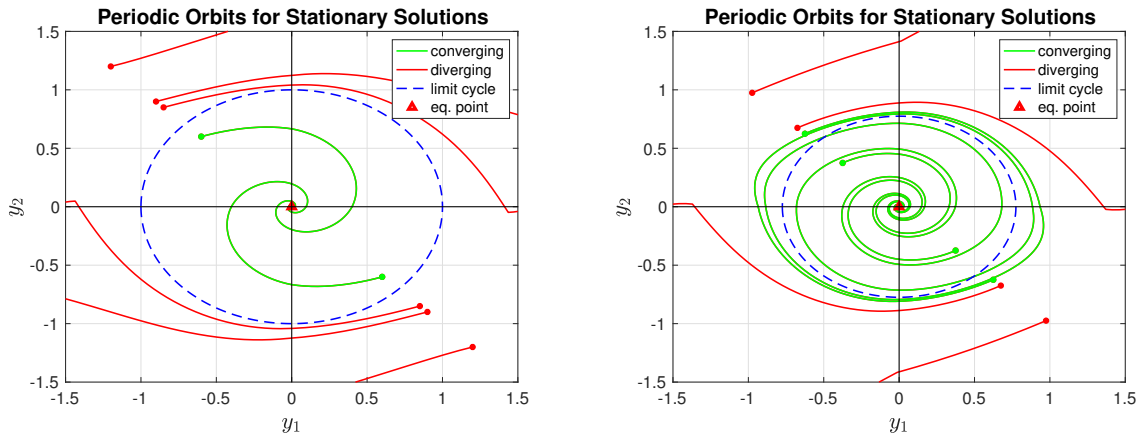

(a) Evolution for $\mu = -0.5$.

(b) Evolution for $\mu = -0.3$.

Figure 3.4: Behaviour of system (3.64), for $\mu = -0.5$ (left) and $\mu = -0.3$ (right). Simulations suggest that due to the different behaviours in each quadrant, and given different values of μ, the region of convergence can be slightly larger.

3.4 Summary and Discussion

This chapter extends the evolutionary game model presented in Chapter 2 to a mean-field game formulation. In the mean-field game, the perspective of a reference player is taken into account. The reference player can control his/her state in presence of an adversarial disturbance. When the controls β_{ij} take the same values as the parameters in

the honeybee swarm model, the proposed mean-field game is a more general formulation of the honeybee swarm consensus problem. When β_{ij} take the other values, the game model can be reframed in the context of virus propagation. Both are a result of Theorem 7. After formulating the corresponding initial-terminal value problem, the stationary solutions are studied in terms of the difference in value function between the committed states, namely 1 and 2 and the uncommitted state 3. These results are reported in Theorem 9 and Theorem 10.

An additional generalisation is given, in which the reference player's controls do not depend only on the controls of the reference player himself/herself, but also on the controls of other players. This is achieved by generalising the difference operator with a function z which represents the resistance to transitions between two states. When this scenario is explored in terms of the stationary solutions, the optimal controls for the reference player and adversarial disturbance can be found, analogously to the former case. Furthermore, the stationary solutions are studied for periodic solutions at each quadrant of the y_1-y_2 plane, and the corresponding basin of attraction is found. These results are reported in Theorem 11.

In both Chapter 2 and this chapter, the game models under analysis do not include any interaction topology nor any consideration on how players come in contact. The assumption is that the population is fully connected, and the results depend on this assumption. In a more realistic scenario, each player would interact with a portion of the population. This situation is captured by an interaction topology, where the players' connectivity is taken into account in terms of the interactions with other players. This is the goal of Chapter 4, where a different network topology is used to model different scenarios.

3.5 Proofs

The tools used in this section include the ones presented in Chapter 2. Additionally, Lypunov stability theory limit cycles and periodic orbits is used. Moreover, the Dynkin's formula is used to find the optimal control and disturbance for the mean-field response. The Dynkin's formula is used to obtain the expected value of a stochastic process at a given stopping time, see [40].

The existence of limit cycles and periodic orbits in a nonlinear system is of signifi-

cance for their impact on the behaviour of the system itself. A system is said to have a periodic solution when, for some $T > 0$, $\dot{x}(t+T) = x(t), \forall t \geq 0$. The closed trajectory in the phase portrait is called *periodic orbit* or *closed orbit*. For a small perturbation of the system, a limit cycle can either be stable, if the behaviour of the system approaches the limit cycle, or unstable, when the trajectories diverge. The *Pointcaré-Bendixson criterion* is a corollary of the Pointcaré-Bendixon theorem and is a powerful tool as a condition for the existence of periodic orbits. For a second-order autonomous system, the Pointcaré-Bendixson criterion states the following: given a closed bounded subset of the plane M, if M contains either no equilibrium points or only one whose eigenvalues have positive real part and every trajectory that starts in M stays in M for all time, then M contains a periodic orbit, see [58]. Likewise, the *Bendixson criterion* is a tool to rule out the existence of periodic orbits: it states that, given a simply connected region D, if the sum of partial derivatives $\partial f_1/\partial x_1 + \partial f_2/\partial x_2$ is non-zero and does not change sign, then D does not contain periodic orbits.

When studying the structural stability properties of a system, small perturbations can change equilibrium points or periodic orbits. The change in the qualitative behaviour, as a parameter is varied, of a system is called *bifurcation*. Depending on the bifurcation parameter, the system can exhibit several behaviours. As an example, a saddle-node bifurcation is the result of the presence of a saddle and a stable node when the bifurcation parameter is varied. In the case of subcritical and supercritical Hopf bifurcations, the corresponding limit cycle is stable and unstable, respectively, and is often represented in elliptical form. Since all these bifurcations occur in the proximity of an equilibrium point, they are called *local bifurcation*. When they involve larger regions of the state plane, they are called *global bifurcations*.

Proof of Theorem 7

Let ρ_i be any control and let also w_i^* be the optimal disturbance obtained from the robust hamiltonian in (3.12), for given ρ_i. Due to the nature of w_i^*, the disturbance can

be considered as a constant value. Therefore, the following can be established:

$$\begin{aligned} J^i_{x_i}(\rho_i, w_i, t) &= \mathbb{E}^{\rho_i, w_i^*}_{i_t=i}\left[\psi(i_T, x_{i_T}) + \int_t^T g(\cdot) - \tfrac{1}{2}\|w^*_{i_\tau}\|^2_{\Gamma_{i_\tau}}\right] d\tau\Bigg] \\ &= v_i(t) + \mathbb{E}^{\rho_i, w_i^*}_{i_t=i}\Bigg[\int_t^T \left[\tfrac{dv_{i_\tau}}{dt}(\tau) + (A^\rho v)^{i_\tau}(\tau) + g(i_\tau, x_{i_\tau}(\tau), \rho_{i_\tau}(\tau)) - \tfrac{1}{2}\|w^*_{i_\tau}\|^2_{\Gamma_{i_\tau}}\right] d\tau\Bigg]. \end{aligned} \tag{3.52}$$

In the above, the second equality is obtained from the Dynkin's formula as:

$$\mathbb{E}^{\rho_i, w_i^*}_{i_t=i}\left[v_{i_T}(T) - v_i(t)\right] = \mathbb{E}^{\rho_i, w_i^*}_{i_t=i}\left[\int_t^T \left[\tfrac{dv_{i_\tau}}{dt}(\tau) + (A^\rho v)^{i_\tau}(\tau)\right] d\tau\right], \tag{3.53}$$

where the terminal condition is $v_{i_T}(T) = \psi(i_T, x_{i_T})$ and $(A^\rho v)^{i_\tau}(\tau) = \sum_j \rho_{ij}(\tau)[v_j(\tau) - v_{i_\tau}(\tau)]$ is the infinitesimal generator of process i_τ. It follows:

$$\begin{aligned} J^i_{x_i}(\rho_i, w_i, t) \geq v_i(t) + \mathbb{E}^{\rho_i, w_i^*}_{i_t=i}\Bigg[\int_t^T \Big[\tfrac{dv_{i_\tau}}{dt}(\tau) + \min_{\mu(\cdot)} \textstyle\sum_j \mu_j \Big[v_j(\tau) - v_{i_\tau}(\tau)\Big] \\ + g(i_\tau, x_{i_\tau}(\tau), \rho_{i_\tau}(\tau)) - \tfrac{1}{2}\|w^*_{i_\tau}\|^2_{\Gamma_{i_\tau}}\Big] d\tau\Bigg]. \end{aligned} \tag{3.54}$$

The above inequality follows from the fact that the minimisation is performed over any control $\mu(\cdot) \in (\mathbb{R}^+_0)^3$. Given that the running cost is concave in the disturbance and given the boundedness of the coefficients, the RHS of the previous equation can be written as:

$$\begin{aligned} J^i_{x_i}(\rho_i, w_i, t) \geq v_i(t) + \mathbb{E}^{\rho_i, w_i}_{i_t=i}\Bigg[\int_t^T \Big[\tfrac{dv_{i_\tau}}{dt}(\tau) + \min_{\mu(\cdot)} \max_{w(\cdot)} \textstyle\sum_j \mu_j \Big[v_j(\tau) - v_{i_\tau}(\tau)\Big] \\ + g(i_\tau, x_{i_\tau}(\tau), \rho_{i_\tau}(\tau)) - \tfrac{1}{2}\|w_{i_\tau}\|^2_{\Gamma_{i_\tau}}\Big] d\tau\Bigg]. \end{aligned} \tag{3.55}$$

The above equation is obtained from the definition of w_i^*, by maximising over any possible disturbance. The next step involves replacing the minimax term by the robust Hamiltonian in (3.12) as:

$$\begin{aligned} J^i_{x_i}(\rho_i, w_i, t) &= v_i(t) + \mathbb{E}^{\rho_i, w_i^*}_{i_t=i}\left[\int_t^T \left[\tfrac{dv_{i_\tau}}{dt}(\tau) + \mathcal{H}(x_{i_\tau}(\tau), \Delta_{i_\tau} v(\tau), i_\tau)\right] d\tau\right] \\ &= v_i(t). \end{aligned} \tag{3.56}$$

The last part of the proof deals with the existence of a solution to the mean-field response as in (3.15). The solution is indeed the value function of the optimal control

problem. This can be seen by differentiating (3.12) with respect to ρ_i and taking the gradient equal to zero, as in the following:

$$R_i\rho_i + \Delta_i v = 0,$$

from which the optimal control in (3.16) is obtained, in the general case for any R_{ij}. For consistency with the assumptions on the initial and terminal cost functions and the way R_{ii} are defined, the controls corresponding to R_{ii}^{-1} are set to zero, since they are not used in the control problem. Similarly, by differentiating (3.12) with respect to w_i and taking the gradient equal to zero, it follows:

$$-\Gamma_i w_i + \Delta_i v = 0,$$

which yields the optimal adversarial disturbance in (3.17), in the general case for Γ_{ij}. Analogously to R_{ii}^{-1}, Γ_{ii}^{-1} are set to zero, for the same reasons as before. This concludes the proof.

Proof of Theorem 9

First, by equating $\dot{y}_1$ and $\dot{y}_2$, the following is obtained:

$$\tfrac{1}{2}(\Gamma_{13}^{-1} + R_{31}^{-1})y_1^2 + \tfrac{1}{2}R_{32}^{-1}y_2^2 + c_1 = \tfrac{1}{2}R_{31}^{-1}y_1^2 + \tfrac{1}{2}(\Gamma_{23}^{-1} + R_{32}^{-1})y_2^2 + c_2, \tag{3.57}$$

where $c_1 = f_1(x_1) - f_3(x_3)$ and $c_2 = f_2(x_2) - f_3(x_3)$. The above can be simplified as in the following:

$$\frac{1}{2}\Gamma_{13}^{-1}y_1^2 + c_1 = \frac{1}{2}\Gamma_{23}^{-1}y_2^2 + c_2. \tag{3.58}$$

By substituting c_1 and c_2 back in the above equation and after rearranging the equation, the equilibrium point as in (3.34) is obtained by taking the square root of the following:

$$y_1^2 = \Gamma_{23}^{-1}\Gamma_{13}y_2^2 + 2\Gamma_{13}(f_2(x_2) - f_1(x_1)). \tag{3.59}$$

Due to need for the negative values for stability, only the negative value of the square root is taken into consideration, which yields the equilibrium point as in (3.34). This concludes the proof.

Proof of Theorem 10

The distribution is given and is constant over the horizon, namely $\mathbf{x}(t) = \hat{\mathbf{x}} : [0, T] \to \mathcal{S}^3$. To study the system around an equilibrium point, the Jacobian for system (3.32) is

calculated as:

$$J = \begin{bmatrix} (\Gamma_{13}^{-1} + R_{31}^{-1})y_1 & R_{32}^{-1}y_2 \\ R_{31}^{-1}y_1 & (\Gamma_{23}^{-1} + R_{32}^{-1})y_2 \end{bmatrix}. \tag{3.60}$$

System (3.32) admits four equilibrium points, which can be found at the intersections between the ellipses in the y_1-y_2 plane. Recall that $y_1 = v_3 - v_1$ and $y_2 = v_3 - v_2$. The equilibrium point at the intersection in the third quadrant is the only asymptotically stable equilibrium point. This can be seen by calculating the determinant and trace of the above Jacobian matrix point as:

$$\begin{aligned} T &= (\Gamma_{13}^{-1} + R_{31}^{-1})y_1 + (\Gamma_{23}^{-1} + R_{32}^{-1})y_2, \\ \Delta &= (\Gamma_{13}^{-1} + R_{31}^{-1})(\Gamma_{23}^{-1} + R_{32}^{-1})y_1y_2 - R_{31}^{-1}R_{32}^{-1}y_1y_2, \end{aligned} \tag{3.61}$$

where the determinant Δ is expanded as in the following:

$$\Delta = (\Gamma_{13}^{-1}\Gamma_{23}^{-1} + \Gamma_{13}^{-1}R_{23}^{-1}R_{32}^{-1} + R_{31}^{-1}\Gamma_{23}^{-1})y_1y_2 > 0, \tag{3.62}$$

and analogously the square of the trace as:

$$T^2 = (\Gamma_{13}^{-1} + R_{31}^{-1})^2y_1^2 + (\Gamma_{23}^{-1} + R_{32}^{-1})^2y_2^2 + 2(\Gamma_{13}^{-1} + R_{31}^{-1})(\Gamma_{23}^{-1} + R_{32}^{-1})^2y_1y_2. \tag{3.63}$$

By comparing the square of the trace and the determinant from the above equations, it is easy to see that $T^2 > 4\Delta$ holds for the third quadrant. Therefore, a solution in the value function exists and this solution is asymptotically stable when the equilibrium point in the distribution is stable as well. Thus the distribution is constant over the time horizon due to the fact that it is at an equilibrium. This concludes the proof.

Proof of Theorem 11

Each of the four regions at the intersection of two quadrants of the y_1-y_2 plane is considered, since the system behaves differently in each quadrant. Recall that $y_1 = v_3 - v_1$ and $y_2 = v_3 - v_1$. Assume that function z is the value function v, so the notation R_{ij}^{-1} and Γ_{ij}^{-1} has the following meaning: $R_{ij}^{-1}(\Delta_i v)$ and $\Gamma_{ij}^{-1}(\Delta_i v)$, respectively.

[**Quadrants I-III**]. In quadrant I and III, the system can be written as:

$$\begin{cases} \dot{y}_1 = \frac{1}{2}y_1(y_1^2 + y_2^2) + \mu y_1 + y_2, \\ \dot{y}_2 = \frac{1}{2}y_2(y_1^2 + y_2^2) - y_1 + \mu y_2. \end{cases} \tag{3.64}$$

For quadrant I the following hypotheses are made: $\Gamma_{13}^{-1} + R_{31}^{-1} = R_{32}^{-1} = y_1$, $R_{31}^{-1} = \Gamma_{23}^{-1} + R_{32}^{-1} = y_2$, which are true when $\Gamma_{13}^{-1}, \Gamma_{23}^{-1} \approx 0$. Analogously, for quadrant III the following assumptions are made: $\Gamma_{31}^{-1} + R_{13}^{-1} = \Gamma_{32}^{-1} = y_1$, $\Gamma_{31}^{-1} = \Gamma_{32}^{-1} + R_{23}^{-1} = y_2$, implying that $R_{13}^{-1}, R_{23}^{-1} \approx 0$.

By turning into polar coordinates, i.e. r and θ, recall that $x = rcos\theta$ and $y = rsin\theta$, $r^2 = x^2 + y^2$ and $\theta = tan^{-1}(y/x)$. System (3.64) can be rewritten as:

$$\begin{cases} \dot{r} = \frac{1}{2}r(r^2 + 2\mu), \\ \dot{\theta} = -1, \end{cases} \tag{3.65}$$

whose expression for $\dot{r}$ is derived from:

$$r\dot{r} = x\dot{x} + y\dot{y} = \mu r^2 + \frac{1}{2}r^4 = \frac{1}{2}r^2(2\mu + r^2).$$

Similarly, by differentiation, the expression for θ, which follows from $\theta = tan^{-1}(y/x)$, is derived as:

$$\dot{\theta} = \frac{1}{1 + (\frac{y^2}{x^2})}\Big(\frac{\dot{y}}{x} - \frac{y\dot{x}}{x^2}\Big) = \frac{x\dot{y} - y\dot{x}}{x^2 + y^2} = -1.$$

For $\mu < 0$, the above system has an asymptotically stable spiral in $(0, 0)$ and an unstable limit cycle for $r = \sqrt{-2\mu}$. Thus, trajectories starting inside the limit cycle converge to the equilibrium point, while those starting outside the limit cycle diverge.

[**Quadrant II-IV**]. For quadrant II and IV, the system can be written in the form:

$$\begin{cases} \dot{y}_1 = \frac{1}{2}(y_1^3 + y_2^3) + \mu y_1 + y_2, \\ \dot{y}_2 = \frac{1}{2}(y_1^3 + y_2^3) - y_1 + \mu y_2. \end{cases} \tag{3.66}$$

The following hypotheses are made for quadrant II: $\Gamma_{31}^{-1} + R_{13}^{-1} = \Gamma_{31}^{-1} = y_1$, $R_{32}^{-1} = \Gamma_{23}^{-1} + R_{32}^{-1} = y_2$, which are true when $R_{13}^{-1}, \Gamma_{23}^{-1} \approx 0$. Similarly, for quadrant IV, let $R_{31}^{-1} + \Gamma_{13}^{-1} = R_{31}^{-1} = y_1$, $\Gamma_{32}^{-1} = \Gamma_{32}^{-1} + R_{23}^{-1} = y_2$, which comes from the condition $\Gamma_{13}^{-1}, R_{23}^{-1} \approx 0$.

When system (3.66) is studied in the neighbourhood of the bisector, the system can be rewritten in polar coordinates as in the following:

$$\begin{cases} \dot{r} = r\mu, \\ \dot{\theta} = -1. \end{cases} \tag{3.67}$$

The above expressions for $\dot{r}$ and $\dot{\theta}$ can be derived as in the following:

$$\begin{aligned} &r\dot{r} = x\dot{x} + y\dot{y} = r^2\mu \quad \Rightarrow \quad \dot{r} = r\mu, \\ &\dot{\theta} = \tfrac{1}{1+(\frac{y^2}{x^2})}\Big(\tfrac{\dot{y}}{x} - \tfrac{y\dot{x}}{x^2}\Big) = \tfrac{x\dot{y}-y\dot{x}}{x^2+y^2} = -1. \end{aligned}$$

For system (3.67), nothing can be said about the limit cycle, but for $\mu < 0$, it is straightforward to see that trajectories converge to the equilibrium point (clockwise rotation), thus the origin is an asymptotically stable spiral. For $\mu > 0$, instead, the trajectories diverge, and therefore an unstable spiral with clockwise rotation is present at the origin.

[**Quadrant I-IV**]. This case investigates the behaviour of the trajectories not in the neighbourhood of the bisector. In this case, the intersection between quadrant I and IV is considered, thus the space in the neighbourhood of the y_1 axis. From the study in the first quadrant, the system can be written in polar coordinates as:

$$\begin{cases} \dot{r} = \frac{1}{2}r(r + 2\mu), \\ \dot{\theta} = -1, \end{cases} \tag{3.68}$$

whereas in quadrant IV the following holds true:

$$\begin{cases} \dot{r} = \frac{1}{2}r(r + 2\mu), \\ \dot{\theta} = -\mu - 1, \end{cases} \tag{3.69}$$

which holds true when trajectories are close to the limit cycle, otherwise the derivative of θ is $\dot{\theta} = 1/2y_1^2 - 1$. When trajectories approximate the limit cycle and μ is sufficiently small, the direction of rotation does not change, namely for $-1 < \mu < 0$. When the latter condition is met, there is no discontinuity between the two systems.

Finally, the two cases can be proved. As for **Case 1**, from systems (3.65)-(3.67), all trajectories starting within the limit cycle converge to $(0, 0)$. This is due to the radius of the systems in polar coordinates being strictly negative in both regions. More specifically, in the region of quadrants I-III, μ dominates the quadratic term in r. This comes from the premises of the theorem, since $|\mu| < 1$. Similarly, for the quadrants II-IV, the same behaviour can be seen. Therefore, $\mathcal{B}$ is a basin of attraction for the origin of the y_1-y_2 plane. For $\mu > 0$, the system is unstable.

As for **Case 2**, systems (3.65)-(3.67) provide the conditions to prove that all trajectories starting outside the closed orbit of radius $\sqrt{-2\mu} + \epsilon$ diverge. This happens regardless of the starting region and for a given $\epsilon > 0$. This behaviour can be explained by the fact that, for the region of quadrants I-III, the quadratic term in r dominates μ. Therefore the trajectories will move further away from the cycle, which is unstable. In

the borders of quadrants II and IV, the behaviour is analogous. It is worth noting that, when trajectories approximate the bisector, they exhibit a convergence behaviour. This can be the subject of future study. This concludes the proof.

CHAPTER 4

Evolutionary Dynamics via Structured and Stochastic Interactions

4.1 Introduction

In Chaper 2, the problem originating in the context of swarm of honeybees was reframed in the context of evolutionary game theory. The evolutionary game dynamics were generalised in the form of a mean-field game, when the population is composed by an infinite number of players. In both cases, however, the results are general and difficult to apply in realistic contexts due to the assumption that the population is fully connected. Despite being a common assumption for these kinds of models, the need to explore the connectivity in terms of the agents' interactions is crucial and it is the main aim of this chapter. This leads to results in terms of speed of convergence towards the equilibrium point and higher number of uncommitted agents.

Another important aspect is to explore the situation where the states are no longer 3. Instead, later in this chapter, each agent can choose among n different options. The structure of the model remains unaltered, namely the transition rates are such that no transitions are allowed between states i and $i+1$ where $i \neq n$, and the uncommitted state is labelled state $n+1$. Also, a form of noise is considered, and when this noise is assumed to be of a certain kind, the corresponding model can be reframed in the context of nudge theory.

Two variations of the model discussed so far are presented in this chapter. The first variation deals with a structured environment, where a network topology is introduced in the model in order to capture the agents' interactions. The term agent or player can

be used interchangeably in this context due to the fact that the proposed model can be interpreted in a game setting or in a multi-agent modelling context. As far as it concerns the structure, the network topology can provide information about the connectivity of the population and the impact on the decision-making problem. Different thresholds for consensus can therefore be analysed. In terms of the actual design, the structure can be modelled in a variety of ways: complex networks and undirected graph are both studied with the aim to consider two scenarios, i.e. an infinite number of agents and a finite number of agents. In the scenario of an infinite, or very large, population, complex networks capture the interactions through a probability distribution of the node degrees. Applications include honeybee swarms, duopolistic competition and opinion dynamics. In the other scenario, a fixed number of nodes form an undirected network, and each node can be in one of three possible states in probability. This means that every agent has an infinite number of possible combinations in terms of the distributions among the three states. In this second scenario, two applications are given, one tackling a different perspective for honeybee swarms and another on smart grids.

The second variation includes the extension of the original model to the case of n possible choices, whereby the uncommitted players are considered to be in the $n+1$ state. Additionally, this n-option model aims at capturing the stochastic interactions that arise due to noise, e.g. imperfect information, noisy channel of communication, etc. This leads to the investigation of the stability properties in the context of Lyapunov stochastic analysis. When the noise is assumed to be of a certain kind, the model can be linked to nudge theory and buffer networks. In the first case, the noise can model a set of phenomena, such as personal preference or the learning process, which are crucial in the case of a nudge theoretic approach. In the second case, the noise can represent the noisy channel in the communication network between two robots or servers. Finally, an initial study on a robot network is given, and each agent in the network represents the memory buffer a robot. The problem to find consensus on n different options is investigated via a probabilistic graphical model and a message passing approach.

4.1.1 Literature Review

When dealing with real systems, a crucial aspect to be taken into account is the consideration that many interconnected elements constitute the elementary parts that compose these systems, see [97]. To model these complex interactions, complex networks have

recently developed, specifically since 2000, in the field of graph networks, with the difference that a complex network includes non-trivial topological features such as lattices or random graphs. Complex networks find inspiring examples in real systems such as the Internet, social communities, power grids, social animals, e.g. see [16]. The last category includes bird flocks, fish schoolings, and can also be applied in the case of social insects, namely the discussed honeybee swarms, but also ant or termite colonies. Moreover, this framework can be used to study consensus in the case of multi-agent systems, see [68].

Depending on the connectivity distribution, complex networks can be divided into two main classes: scale-free (SF) networks and small-world networks. SF networks are characterised by a power-law degree distribution, where the vast majority of nodes have low connectivity and only few nodes have a large number of connections, see [4]. Additionally, SF networks are inhomogeneous networks, whose most notable examples can be found in the World-Wide Web (WWW) and the Internet. Small-world networks are characterised by a degree distribution with a peak at the average value and exponential decay, see [104]. Moreover, small-world networks are homogeneous and have a diameter which is usually smaller than SF networks, therefore showing a higher level of clustering, e.g. social networks. The diameter d of a complex network is the average distance between any two given nodes in the network.

The authors in [97] provide a comprehensive study on the evolutionary dynamics over complex networks. The authors motivate the use of complex networks by outlining the importance of the underlying structure for the evolutionary dynamics, in order to investigate collective behaviours in a realistic context. One of the most important concept is the *fitness*, i.e. a function $f(s)$, which assigns a *fitness value* to each state of the network. This function can be of different kinds, e.g. *random drift*, when all states in the evolution are equally likely in probability, *constant selection*, when the function is constant during the entire process but not equal at all states, or *networked game*, when the states can be associated to strategies in a game theoretic framework and the fitness is the result of this game played among neighbours. Finally, the *fixation probability* is the probability of convergence when all states are mutated. However, the binary-state evolutionary dynamics analysed in [97] define a finite state discrete time Markov chain, whereas the system studied in the present work is in continuous time.

A continuous time system where the interactions are modelled via complex networks can be found in [72]. The main focus of this article is to investigate SF networks in

the context of compartmental models. The authors motivate this study by stressing the fact that SF networks are extremely prone to infections, much more than small-world networks, and no threshold can be found to contain the disease due to the nature of this kind of networks. The study of an epidemic model is carried out in the case of a Watts-Strogatz model (small-world) and Barabási-Albert model (SF) in the context of the SIR model. Recall that the SIR acronym stands for Susceptible-Infected-Recovered. The results provide confirmation on the critical importance of the topology studied, in which higher connectivity enhances the epidemic spreading. The work presented here follows this path to stress how susceptibility to infections is linked to the heterogeneity of the network, especially in the case of SF networks. For a study of the error and attack tolerance of SF networks, see [2].

Each node of the network acts as an agent in the context of multi-agent systems. Each agent can be seen as an autonomous entity, whose role is twofold: it can act as part of the network of the interconnected nodes or as a whole. This duality can also be linked to the framework of complex networks. As for the first aspect, the agent is part of a bigger system and is able to communicate with other agents and interact with the environment. As for the second aspect, the agent is able to tackle a problem autonomously without the need to depend on the bigger system. To convey both aspects in a single word, the word *holon* was coined by Koestler in 1967, see [61]. The term holon (from ὅλος, holos, which means whole, in Greek) takes inspiration from the principle stated by Aristotle in the Metaphysics, Book 8, "The whole is greater than the sum of its parts". A similar concept is the *monad* by philosopher Leibniz, but with the difference that the whole described in the latter term is intended as the most elementary part of a system.

Examples of holonic systems can be found in a variety of disciplines. For instance, fractals in mathematics and tree structures in informatics are examples of holons. Fractals can be seen as a whole in the bigger picture, but each part of the whole is a stable sub-structure of the whole. The same applies to trees in informatics, where a tree is a collection of nodes that can be considered as sub-trees of the original tree. Hierarchical structures can be found in holons as well, and it is called holarchy. An example of holarchy is the one that exists between atoms and molecules in biology. In short, a holon is seen as a single entity from the outside but it consists of simpler sub-parts with a coherent structure on their own. For further reading, see [22], [38], and plenty of references therein.

Holons, holarchy and the relative terminology are useful to introduce the extension to smart grids and virus propagation that is proposed later in the present chapter. A smart grid differs from a traditional energy network in that it integrates smarter technologies for increased observability, communication and distributed control across all users, be they producers, consumers or both, for which the term *prosumers* is used, see [73], [74]. A major drawback connected to the deployment of more advanced smart grids is found in the vulnerability of the interconnected parts of the network. This vulnerability can be exploited through several kinds of cyber-attacks. The impact of such attacks can be evaluated by assessing the vulnerabilities first and then the strength of the attacks, see [69]. Another perspective on an integrated cyber-physical framework can be found in [100].

The motivations that justify the inclusion of smart grids and their cyber-related vulnerabilities in this research can be found in the direct extension of compartmental models in the case of cyber-attacks. Additionally, the popularity of smart grids and the corresponding multi-agent representation is well suited for a game theoretic approach of the topic, see [59], [87], [103], and plenty of references therein. The authors in [102] propose a game model with the aim to calculate and prevent system total losses, by regulating the distribution generation at each generator. Reducing the system losses is modelled as a reward in this framework, thus providing benefits to achieve a more effective power system. For the formulation of the corresponding robust mean-field game model in the context of cyber-physical systems, see [10]. To mitigate the impact of different cyber-attacks that belong to the family of Denial-of-Service (DoS) attacks, an integrated control approach through interdependency can be used, see [24]. The notorious Kuramoto model of coupled oscillators, see [21] for a general survey, was used to analyse power grids, [36]. The model proposed in this chapter extends the Kuramoto oscillators to study cyber-attacks in the context of smart grids.

In order to capture aspects of the decision-making process such as personal tastes or biased/misleading information, a concept that is worth considering is the concept of *nudge*. A *nudge* is a small incentive, often in the form of a slight change in the environment, that does not involve coercion or other ways to achieve compliance. The term was coined for the first time by James Wilk, see [107], in the context of cybernetics and used sometimes in the form of "micronudge". It was only later that it was applied to behavioural sciences. Recently, the term gained popularity thanks to Richard Thaler, who was awarded the Nobel Memorial Prize in Economic Sciences in 2017 for his con-

tributions to the field of behavioural economics. In [99], Thaler and Sunstein describe the crucial aspects of nudges in real life scenarios. When dealing with real problems, individuals' choices are modelled without taking into account biased information, incomplete or misleading knowledge and personal taste. In reality, however, decision makers take into account one or a combination of the mentioned aspects. Due to the strong link between game theory and economics, it is worth mentioning the terms *econ* and *human*. The first is used to describe the individuals (or players) whose behaviour takes into account all the above and the second those who don't.

Nudges are sometimes paired with the concept of default option. The default option is the one taken when an individual does nothing, i.e. does not actively choose. For instance, customers are more willing to choose the renewable energy when it is given as the default option, see [83]. However, the solution provided by the default option has found opposition due to the fact that those who should choose which one has to be the default option do not necessarily promote the more ethical or better option. Putting a product at eye level to attract customers is another example of nudge, see [99]. A quantitative analysis on the impact of nudges in various cases and when they can be determinant in changing the behaviour of decision-makers, see [26].

The concept of nudge was also applied to standard game theory with the aim of taking into account the information received as part of learning, the limits in strategic reasoning and the impact on specific contexts, see [23]. A work that combines prospect theory and nudge in mean-field game can be found in [67]. Prospect theory characterises more accurately decision making problems under risk and uncertainty, see [57]. The main characteristics include the following observations about real decision makers, see [67]: they are willing to avoiding losses more than having a certain gain, i.e. concave value function for gains and convex for losses; they are more concerned with scenarios that would unlikely happen and less with frequently happening scenarios, i.e. nonlinear transformation of probability scale; they consider their gains and loss in a way relative to a reference point instead of a final or terminal condition, namely the framing effect.

When number of states is no longer 3, but the agents can choose among many different options, the need of a master model is due. In [17], the master model is studied within the framework of opinion dynamics. In this framework, the decision-making process of an agent that wants to change opinion i in favour of opinion j includes a parameter λ_j. This parameter represents the attractive force of the neighbouring

agents which have already chosen opinion j. In order to derive the master model, the assumption is that the parameter λ_j does not depend on the opinion anymore, and therefore the equations can be marginalised. The model exhibits a crowd-seeking mechanism, or an emulative interaction mechanism to use other words present in the literature. The main difference with the model presented in this thesis is the fact that the authors study the Markov chain for each individual agent first, and then marginalise to obtain the master model. Analogously in this dissertation, except for Chapter 3 where the system can as well be used to model crowd-seeking and crowd-averse dynamics, the systems show a crowd-seeking mechanism. The waggle dance, where the main system in this work takes inspiration from, corresponds to the attraction force for a given option i. When this force does not depend on the agents that have already chosen that option, the master model can be marginalised and the system can be studied in the form of a linearised uncertain second order system. The formulation of the corresponding master model is not the focus of this work, but it is already been taken into account as a possible future direction of research.

4.1.2 Summary and Contributions

This chapter extends the original model in order to study the impact of the structure to the system equilibria and how noise influences the corresponding dynamics. The structure can be modelled in a variety of ways: in the following, complex networks and undirected graphs are investigated. In the case of complex networks, an infinite population of players is considered, where each player belongs to a class of a specified connectivity. However, this does not restrict the interactions only for players belonging to the same class. When a network topology is considered, a finite set of players is taken into account, but each player can be in one of the three states in probability. Therefore, this scenario models a finite number of infinite populations, where each player represents one of those populations. Furthermore, a case study on smart grids and virus propagation is proposed in the context of a UK energy grid. Another extension is to the n-state model via noisy dynamics, where the value n represents the number of options and thus does not include the uncommitted state. Finally, a probabilistic approach is taken to study the consensus problem in the context of robot networks where each agent represents a robot buffer.

The main results are summarised in the following. The first contribution involves

the presence of an interaction topology in the form of a complex network and the corresponding study of its impact. The second contribution includes the extension to a finite network graph. Also in this case, the importance of the topology is investigated and the analysis is specialised in two separate models. The third contribution takes into account the effects of a noisy environment when the number of possible choices increases to n. In this context, the noise can be considered as a nudge, capturing the uncertainty coming from, for instance, biased information or personal taste. Finally, an initial study on buffer networks is carried out, where the stochastic dynamics are investigated through a probabilistic graphical model.

4.1.3 Structure

Chapter 4 is organised as follows. In Section 4.2, the scenario where the structure is modelled by means of a complex network is presented. The corresponding general interaction model is studied in both symmetric and asymmetric cases. Some applications are also provided to link the above system to three different contexts: honeybee swarms, where the model originates, duopolistic competition and opinion dynamics. Then, the stability analysis is carried out and results in terms of the impact of the topology are given, corroborated by several numerical studies. In Section 4.3, the interactions are captured by an indirected network graph where the each node represents a player and the edges are modelled through an adjacency matrix. Two scenarios are presented: the first involving the honeybee swarm problem and the second describing a virus propagation scenario in the context of smart grids. In Section 4.4, the original 2-state model is extended to the case of n possible choices in a noisy environment. The noise is modelled as a Weiner process with weight given by matrix G. When further assumptions are given for this matrix, a nudge model is proposed. Finally, a probabilistic graphical model is used to study the consensus problem on a robot network.

4.2 Complex Networks

This section includes an extension to structured environment for the system in Chapter 2, where players can interact by means of a network topology. The structure is captured by a complex network, with given degree distribution. Fig. 4.1 shows a graphical representation of the Barabási-Albert complex network used for the numerical analysis. The

different link colours have the sole purpose of better visualising them, whereas the size of the nodes, represented by red circles, depends on the number of connections of each node, i.e. it represents the node degree.

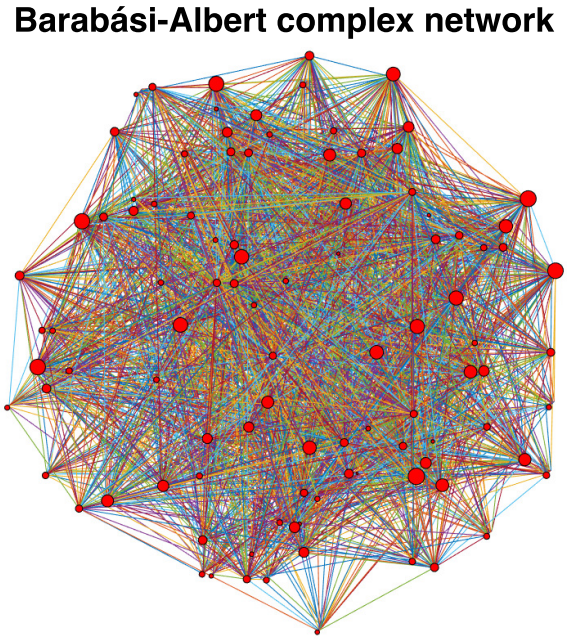

Figure 4.1: Graphical representation of the Barabási-Albert complex network used in this section.

Formally, a large population of players is considered. Let a complex network be given, where $P(k)$ is the probability distribution of the node degrees. The degree of a node is defined as the number of connections of that node. Due to the structured environment, the population of players is no longer homogeneous. Heterogeneity in the population is described by a set of classes which represent the different connectivity of the players in the population. Let x_i^k be the portion of the population with k connections (class k in short) using strategy i. For instance, x_1^1 and x_1^2 represent the portion of players choosing strategy 1 for classes $k = 1$ and $k = 2$, respectively.

The following parameters are used to describe the interactions among players. Let $\psi_k = \frac{k}{k_{max}}$ be the parameter capturing the connections of the players in the network, where k_{max} is the value corresponding to a fully connected network. When $k = k_{max}$ for all classes, the structured case is described by the same equations of the unstructured case. Furthermore, let $\langle k \rangle$ be the mean value of all parameters k in the network. Let

$\theta_i := \frac{1}{\langle k \rangle} \sum_k kP(k)x_i^k$ be the probability that a link, chosen at random, will point to an agent using strategy i. Therefore, the model considered is a general interaction model where any player of class k interacts with players of other classes through θ_i. The proposed model is not state dependent, e.g. as in [50], but, through θ_i, it does not include selective interaction, whereby each player can interact only with the other players in the same class.

In the following, two cases are taken into account. The first case deals with same-valued options, thus it can be linked to the symmetric parameters in Chapter 2. The second case is the one arising from the link to epidemiology and compartmental models, i.e. the SIS and SIR as discussed in Chapter 2. In the latter case, the system of equation can be associated with the asymmetric structure studied in Chapter 2 for uncertain cross-inhibitory coefficient.

4.2.1 Symmetric and Asymmetric Models

The corresponding structured model of (2.9) in the symmetric case is the following:

$$\begin{cases} \dot{x}_1^k = (1 - x_1^k - x_2^k)(\psi_k r\theta_1 + \gamma) - x_1^k(\alpha + \psi_k \sigma\theta_2), \\ \dot{x}_2^k = (1 - x_1^k - x_2^k)(\psi_k r\theta_2 + \gamma) - x_2^k(\alpha + \psi_k \sigma\theta_1), \end{cases} \tag{4.1}$$

where parameters γ, α and σ describe, as before, the act of spontaneously commit to an option, the act of spontaneously abandon the commitment and cross-inhibitory signal sent to players who chose the other option, respectively. System (4.1) models the dynamics of the players for every class $k \in \mathbb{Z}^+$ and can be viewed as a microscopic model of the players in class k parametrised by the macroscopic parameters θ_1 and θ_2.

The corresponding structured model of (2.19) in the asymmetric case, i.e. both for structure and parameters, is the following:

$$\begin{cases} \dot{x}_1^k = \gamma_1 x_3^k, \\ \dot{x}_2^k = -\psi_k \sigma x_2^k \Theta_1 + \gamma_2 x_3^k, \\ \dot{x}_3^k = -\gamma_1 x_3^k - \gamma_2 x_3^k + \psi_k \sigma x_2^k \Theta_1, \end{cases} \tag{4.2}$$

where the parameters used, i.e. γ_i and σ, have the usual meaning. To stress that the interaction between classes are limited to the players in state 1 and that they are related to the cross-inhibitory signal, Θ_1 is used in this form in place of θ_1, but the meaning is unchanged. Therefore, Θ_1 is defined as:

$$\Theta_1 := \frac{\sum_k kP(k)x_1^k}{\sum_j jP(j)} = \frac{\sum_k kP(k)x_1^k}{\langle k \rangle}, \tag{4.3}$$

and its first derivative Ψ is defined as:

$$\Psi := \dot{\Theta}_1 = \frac{\sum_k kP(k)\dot{x}_1^k}{\langle k \rangle} = \frac{\sum_k kP(k)\gamma_1 x_3^k}{\langle k \rangle}. \tag{4.4}$$

Example 2. *Consider the second derivative of x_2^k:*

$$\ddot{x}_2^k = -\psi_k \sigma \dot{x}_2^k \Theta_1 - \psi_k \sigma x_2^k \dot{\Theta}_1 + \gamma_2 \dot{x}_3^k.$$

The above second-order differential equation corresponds to the following bidimensional first-order system:

$$\begin{bmatrix} \dot{x}_2^k \\ \ddot{x}_2^k \end{bmatrix} = \begin{bmatrix} 0 & 1 \\ -\sigma\Psi\frac{k}{k_{max}} & -\sigma\Theta_1\frac{k}{k_{max}} \end{bmatrix} \begin{bmatrix} x_2^k \\ \dot{x}_2^k \end{bmatrix} + \begin{bmatrix} 0 \\ \gamma_2 \dot{x}_3^k \end{bmatrix}.$$

The above system presents analogies with a mass-spring-damper, where Θ_1 plays the role of a viscous term, while the eigenvalues determine the amplitude of the oscillations.

The above models, in the symmetric case presented at the beginning and in the asymmetric case which follows, admit the Markov chain representations displayed in Fig. 4.2 (left) and in Fig. 4.2 (right), respectively. The structured system presented here shares similarities with the 3-valued logical network in [25], but differs in that two aspects: the 3-valued logical network does not include a complex network to model the interaction topology and its analysis is carried out in discrete time.

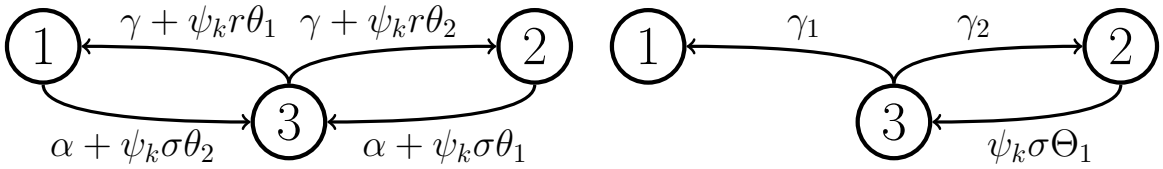

Figure 4.2: Markov chain representations of the structured environment which correspond to the set of equations in (4.1) (left) for the symmetric case, and to the set of equations in (4.2) (right) for the asymmetric case.

4.2.2 Applications

In this section, three applications of the game models discussed so far are presented. A different interpretation of the parameters and impact of the network topology is provided in each case. The first application, where this model originates from, describes

the decision-making problem that honeybees face when choosing a nest. The second one involves duopolistic competition in marketing, where two manufacturers produce the same product. The last one relates to opinion dynamics in a voting campaign, where two political parties aim at winning the elections.

Swarm of honeybees. The original formulation of the model comes from the biological studies of honeybee swarms. The problem under analysis involves the collective decision-making process to choose the future nest for the swarm, see [81], [82], [101]. Consider the situation in which the swarm has two possible choices, nest-box 1 and nest-box 2. In the examples conducted to study this problem, the nest-boxes can either be identical, namely the two options have the same value, which would link this case to the symmetric scenario, or they can be different, i.e. the first is better than the second or vice versa, which links to the asymmetric case. The undecided portion of the swarm is called uncommitted, as in the models discussed so far.

The swarm has two main behaviours to convey information and make a decision: the so-called *waggle dance* and *the cross-inhibitory stop signal*. The waggle dance, described by parameters r_1 and r_2 (or r when the options have the same value), is performed by scout bees who had previously discovered one of the nests. Scouts dance in front of the swarm to convey information about the direction and distance (location in short), and most importantly the quality of the nest. The cross-inhibitory stop signal, denoted by σ in its forms (constant and time varying), is a way in which bees stop the waggle dance of scouts committed to the other option. Parameters γ and α represents the spontaneous commitment to the nest just discovered and spontaneous rejection of their commitment, respectively.

In technical terms, variables x_1, x_2 and x_3 can be interpreted as the portion of the swarm selecting option 1, 2 or 3, respectively. In the transition from option 3 to 1, γ_1 weighs those bees that spontaneously choose to commit to option 1 and $r_1 x_1$ accounts for the bees attracted by those already in 1 through the waggle dance. Similarly, in the case where bees move from strategy 1 to 3, α_1 is the quantity of bees that spontaneously abandon their commitment and $\sigma_2 x_2$ is the amount of bees influenced by the cross-inhibitory signal sent by bees committed to option 2. Note that in the unstructured case, the players are not clustered in groups with same connectivity and therefore the index k used in the structured scenario is dropped. Analogously, ψ_k, which represents

the portion of population that a player in each class interact with, can be dropped in the unstructured scenario due to $\psi_k = 1$.

It is worth explaining the sophistication of the waggle dance, which is noteworthy for such small social insects. A scout bee, after finding a nest and returning to the swarm, inform the other bees about the position and quality of the findings. Two main parts can be distinguished: the waggle run and the return run. The waggle run is an oscillatory dance behaviour around the main axis, while the return run is a semicircular flight from the ending position to the starting position of the waggle run. One second of the dance corresponds roughly to 1000 meters in terms of distance from the swarm position to the found nest box. When dancing, the orientation of the waggle run is such that the angle of the nest relative to the sun in the outbound flight corresponds to the same angle relative to the straight up in the comb. Finally, the quality of the findings depends on the number of circuits, i.e. the product between the return runs and the duration of the dance.

Duopolistic competition in marketing. Another application of the model in unstructured and structured forms can be found in the context of duopolistic competition in marketing, for instance see Example 9, p. 27 in [18]. The classical scenario is captured by the notorious *Lanchester* model: two manufacturers produce the same good and thus have a share of the same market, namely x_1 and x_2. The variable x_3 represent the share of the market of potential customers. Parameters r and σ represent different advertising efforts, which enter the problem as either fixed parameters or controlled inputs in the analysis or design of the advertising campaign. In particular, r portrays the advertisements aimed at convincing the potential customers which are still undecided to choose one product. The other parameter, i.e. σ, models the effort of disrupting the campaign of the other manufacturer. The rest of the population plays an active role when contributing to the advertising effort, e.g. word of mouth to advice others which product to buy or not to buy. Finally, γ and α describe the situation in which players willingly get convinced to buy one of the two products or change their minds, respectively.

As underlined before, the proposed framework builds on concepts similar to the Lanchester model. However, the major difference is that the effort is not necessarily constant in the general formulation of the Lanchester model, while this is the case for the problem studied here, and this is captured by the offset. It is no longer the case when

parameter σ is used as an uncertain time varying coefficient, which therefore captures the advertising effort over time. A novel aspect of this research is attributable to the interaction topology, which models the *social influence* of the advertisement campaigns of both manufacturers. A stronger cross-inhibitory signal can be used to model the capability of reaching out to a larger number of potential clients.

Opinion dynamics. In this last example, a link to opinion dynamics is given, see [50]. The voting campaign of two political parties is modelled through the portion of the population choosing each party, namely states 1 and 2, which represent the *left* and *right* wing parties, respectively. People can also be undecided and do not vote for either party, which is described by state 3. Individuals can choose to vote for one party after being persuaded by politicians belonging to that party or by other people already voting for it, which is captured by r. At the same time, through parameter σ, voters for one party can change their mind due to the influence of people voting for the other party, or due to their propaganda. Lastly, people can be persuaded to vote or to stop voting for either party for their own personal beliefs, which is represented by γ and α, respectively.

Therefore, the above parameters describe the ways in which political parties invest in campaigning efforts and the impact on the voters' choices. The *political influence* on society is even stronger when modelled through an interaction topology, so that a higher social influence corresponds to a more effective persuasive strength to attract more people away from the competing party. At the same time, undecided individuals select one of the two parties proportionally to the level of popularity of that party. Finally, it is worth mentioning that the above example can be linked to case where people cast their vote for the party that is already winning, instead of their current opinion. This behaviour is referred to as *bandwagon effect*, see [109].

4.2.3 Stability Analysis

Likewise in the unstructured scenario, the analysis of the stability properties is now carried out. The mean-field response is investigated first, and the impact of the connectivity is analysed with regards to each of the previous applications. When the output of the macroscopic dynamics constitute the input to the microscopic dynamics and vice versa, a micro-macro model is obtained. The study of such model provides a threshold

for consensus in the structured case, similarly to what was done in Chapter 2 for the unstructured case.

Mean-field Response. Given the game dynamics in (4.1), the mean-field response is obtained for a given class of players by assuming that the distribution of the rest of the population is fixed. Due to the symmetry of the options, let the assumption $\theta := \theta_1 = \theta_2$ be given. System (4.1) can be written in matrix form as:

$$\begin{bmatrix} \dot{x}_1^k \\ \dot{x}_2^k \end{bmatrix} = \overbrace{\begin{bmatrix} -(r+\sigma)\psi_k\theta - \alpha - \gamma & -\psi_k r\theta - \gamma \\ -\psi_k r\theta - \gamma & -(r+\sigma)\psi_k\theta - \alpha - \gamma \end{bmatrix}}^{A_k(\theta)} \begin{bmatrix} x_1^k \\ x_2^k \end{bmatrix} + \overbrace{\begin{bmatrix} \psi_k r\theta + \gamma \\ \psi_k r\theta + \gamma \end{bmatrix}}^{c_k(\theta)}, \tag{4.5}$$

which can be rewritten in compact form as

$$\begin{bmatrix} \dot{x}_1^k \\ \dot{x}_2^k \end{bmatrix} = A_k(\theta) \begin{bmatrix} x_1^k \\ x_2^k \end{bmatrix} + c_k(\theta). \tag{4.6}$$

It is worth noting that if $r = \sigma = 0$ the equilibrium does not depend on k.

Theorem 12. *Given an initial state $\hat{\mathbf{x}}^k = (\hat{x}_1^k, \hat{x}_2^k, \hat{x}_3^k)$, for each class k, system (4.6) is locally asymptotically stable and convergence is faster with increasing connectivity ψ_k. Furthermore, in the cases of no connectivity $\psi_k = 0$ and full connectivity $\psi_k = 1$, system (4.6) has eigenvalues*

$$\lambda_{1,2} = \begin{cases} (-\alpha - 2\gamma, -\alpha), & \text{if} \quad \psi_k = 0, \\ (-(2r+\sigma)\theta - \alpha - 2\gamma, -\sigma\theta - \alpha), & \text{if} \quad \psi_k = 1. \end{cases}$$

Proof. See Section 4.6. □

Remark 12. *In light of the above result, a higher connectivity can be linked in terms of the discussed applications as: i) speeds up convergence to one of the nest-boxes in the case of the bees, ii) accelerates the clients' choices to one of the products, which then become dominant in the market in the case of duopolistic competition in marketing, iii) facilitates a quicker convergence to one of the two political parties in the case of opinion dynamics in a voting campaign. As it can be seen in Fig. 4.3, the connectivity shifts the eigenvalues further away from the origin (the ones for the case of no connectivity are labelled above the x-axis, while the ones for the case of full connectivity are below).*

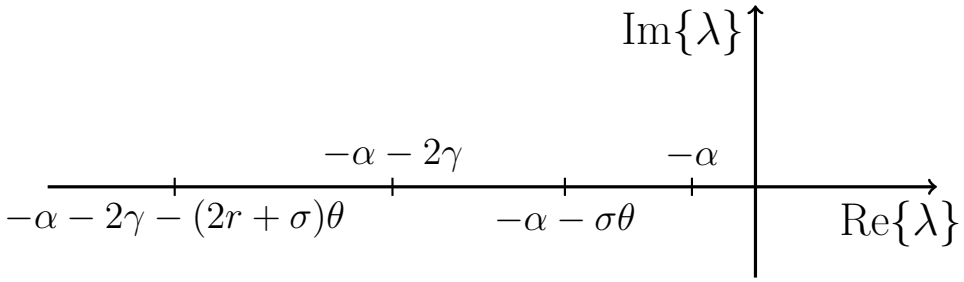

Figure 4.3: Diagram showing the change of the eigenvalues for system (4.6), where the ones above the x-axis refer to the case with no connectivity and the ones below to the case with full connectivity.

Theorem 13. *Given an initial state* $\hat{\mathbf{x}}^k = (\hat{x}_1^k, \hat{x}_2^k, \hat{x}_3^k)$*, for each class* k*, the equilibrium points are* $[\tilde{x}_1^k, \tilde{x}_2^k]^T = -A_k^{-1}(\theta)c_k(\theta)$*. Furthermore, at the equilibrium, the distribution of uncommitted players increases with connectivity* ψ_k*.*

Proof. See Section 4.6. □

Remark 13. *The above results states that, an increase in connectivity would correspond a proportional increase in the steady-state percentage of uncommitted bees, undecided clients in duopolistic competition or undecided voters in opinion dynamics.*

Micro-macro model. The macroscopic dynamics, which refers to the evolution of the whole population over time, and the microscopic dynamics, namely the evolution of the single classes of players when the strategies of the rest of the population are given as a parameter, can be combined in the following model:

$$\begin{cases} \dot{\theta}_1 = \frac{r\theta_1}{k_{max}}\left(\frac{V(k)}{\langle k\rangle} - \Psi_1 - \Psi_2\right) - \frac{\sigma\theta_2}{k_{max}}\Psi_1 - \theta_1\alpha + \gamma - \theta_1\gamma - \theta_2\gamma, \\ \dot{\theta}_2 = \frac{r\theta_2}{k_{max}}\left(\frac{V(k)}{\langle k\rangle} - \Psi_1 - \Psi_2\right) - \frac{\sigma\theta_1}{k_{max}}\Psi_2 - \theta_2\alpha + \gamma - \theta_1\gamma - \theta_2\gamma, \end{cases} \tag{4.7}$$

where $V(k) = \sum_k k^2 P(k) x^k$ and $\Psi_i = \frac{1}{\langle k\rangle}\sum_k k^2 P(k) x_i^k$. The above system is obtained from the equations in (4.5), by averaging on both sides using $\frac{1}{\langle k\rangle}\sum_k kP(k)$ and can be represented as a block system as in Fig. 4.4.

System (4.7) can be written in matrix form as:

$$\begin{bmatrix} \dot{\theta}_1 \\ \dot{\theta}_2 \end{bmatrix} = \begin{bmatrix} \frac{r}{k_{max}}\left(\frac{V(k)}{\langle k\rangle} - \Psi_1 - \Psi_2\right) - \alpha - \gamma & -\frac{\sigma}{k_{max}}\Psi_1 - \gamma \\ -\frac{\sigma}{k_{max}}\Psi_2 - \gamma & \frac{r}{k_{max}}\left(\frac{V(k)}{\langle k\rangle} - \Psi_1 - \Psi_2\right) - \alpha - \gamma \end{bmatrix} \begin{bmatrix} \theta_1 \\ \theta_2 \end{bmatrix} + \begin{bmatrix} \gamma \\ \gamma \end{bmatrix}. \tag{4.8}$$

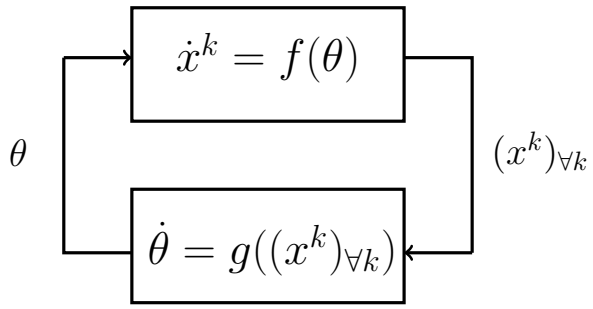

Figure 4.4: Scheme of micro-macro model, where $\dot{x}^k = f(\theta)$ and $\dot{\theta} = g((x^k)_{\forall k})$ represent the evolution of systems (4.6) and (4.7), respectively.

Theorem 14. *Given an initial state* $\hat{\mathbf{x}} = (\hat{x}_1, \hat{x}_2, \hat{x}_3)$ *on the population distribution, the symmetric equilibrium point in the case of structured environment is locally asymptotically stable if and only if*

$$\sigma \leq 2r - \frac{rV(k)}{\langle k \rangle \Psi} + \frac{\alpha k_{max}}{\Psi}. \tag{4.9}$$

Proof. See Section 4.6. □

Remark 14. *The above threshold for the cross-inhibitory signal generalises the results in the case of unstructured environment, namely equation (2.10). When* $k = k_{max}$*, i.e. in the case of full connectivity, the threshold in (4.9) coincides with the one found for the unstructured environment, see (2.10). In each of the examples provided, this result can be interpreted as a threshold on the strength of* σ*, which would prevent deadlocks in the case of honeybees when the nest-boxes are perceived as equal in value; in case of duopolistic competition when the products are of the same quality; and, finally, in case of opinion dynamics when similar political programs (in terms of political proposals) are given to voters.*

4.2.4 Numerical Analysis

In this section, the numerical analysis is carried out in the case of structured environment. The structure is modelled though the Barabási-Albert complex network, which can be physically interpreted as consisting of a few players only having high connectivity, whereas the majority of the population has very low connectivity. For the purpose of the simulations, a discretised version of the following power-law distribution is used, see [72]:

$$P(k) = \frac{2m^2}{k^3} \quad \text{for } k \geq m, \quad m = \langle k \rangle / 2. \tag{4.10}$$

To model the different classes of agents, the notation $k_i = N\%$ means that players in class $k = i$ are connected to $N\%$ of the population. The sum of all agents of all classes is in accordance with (4.10), i.e. $\sum_i k_i = 1$, for all i.

Three sets of simulations are presented. In the first one, the analogy of the asymmetric model with a mass-spring-damper model is shown. In the second set, the simulations corroborate the theoretical results in terms of faster steady-state response and distribution of population at steady-state in favour of the uncommitted state with increasing connectivity. Finally, the last set of simulations illustrates the link between the cross-inhibitory coefficient and the stability of the system.

Asymmetric Case. The system in the asymmetric case shares similarities with a mass-spring-damper model, as introduced in Example 2. Figure 4.5 shows the time evolution of the asymmetric system in the case of $\sigma = 3$ (top) and $\sigma = 10$ (bottom). The role of the cross-inhibitory parameter σ is investigated in a scenario where the population class into consideration is class $k = 8$, i.e. those players who are connected to only 5% of the population. The population represented by this class amounts to 30% of the total, thus it is highlighted with a dotted magenta line in the plots. The initial condition on the distributions for the class under consideration is $\hat{x}^8 = (0.03, 0.27, 0)$. It can be seen from the plots that a higher value of σ leads to a faster response of the first two state components, as expected. The system converge towards the only possible stable equilibrium, which is consensus on option 1.

Mean-field Response. The second set of simulations involves the mean-field response system in (4.6), given $\theta_1 = \theta_2 = 0.4$. In this scenario, two classes are considered, i.e. class $k = 1$ and $k = 9$. The first class has a connectivity $k_1 = 22\%$, while class $k_9 = 85\%$. The initial condition for each class is $\hat{x}^1 = (0.3, 0.7, 0)$ and $\hat{x}^9 = (0.3, 0.7, 0)$. The above initial conditions are normalised to ease readability. The case $\sigma = 3$ and $\sigma = 10$ are plotted in Figures 4.6-4.7, respectively. Two aspects can be observed from the plots. First, the class with higher connectivity, namely $k = 9$, has a faster transient response, which is in accordance with Theorem 12. The second aspect involves the number of uncommitted players at steady-state: the class with more connections reaches a higher value of the uncommitted players at steady-state, as stated in Theorem 13. Both aspects have a higher impact on the dynamics when the value of the cross-inhibitory parameter increases, as it can be seen by comparing Figures 4.6 and 4.7.

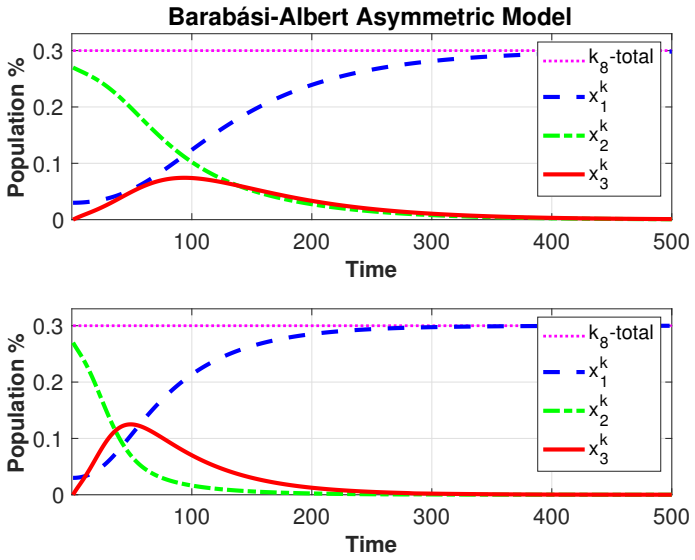

Figure 4.5: Behaviour of the structured asymmetric model for $\sigma = 3$ (top) and $\sigma = 10$ (bottom). The class $k = 8$ accounts for 30% of the total, shown in magenta.

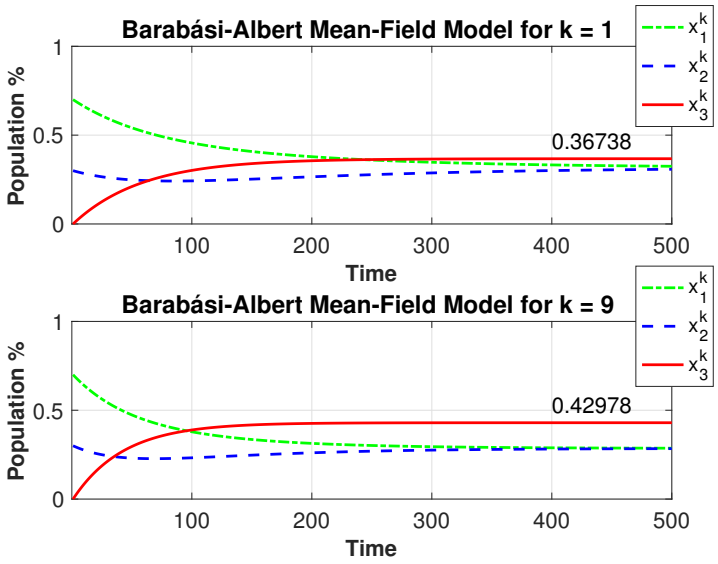

Figure 4.6: Time evolution of system (4.6) for $k_1 = 22\%$ (top) and $k_9 = 85\%$ (bottom). The cross-inhibitory signal is set to $\sigma = 3$.

Micro-macro Model. The last set of simulations includes the analysis of the micro-macro model which combines the evolution of the mean-field response with the evolution of the population as a whole. The classes used are the same as in the last set of simulations, namely $k_1 = 22\%$ and $k_9 = 85\%$. The starting condition is the same as well, i.e.

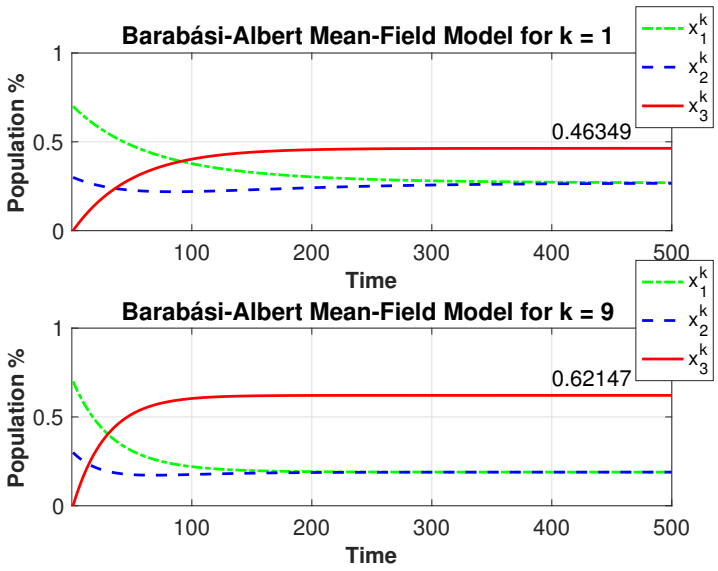

Figure 4.7: Time evolution of system (4.6) for $k_1 = 22\%$ (top) and $k_9 = 85\%$ (bottom). The cross-inhibitory signal is set to $\sigma = 10$.

$\hat{x}^1 = (0.3, 0.7, 0)$ and $\hat{x}^9 = (0.3, 0.7, 0)$. Figure 4.8 shows the dynamics in barycentric coordinates. As it can be seen from the plots, in the case of the population evolution as a whole, captured by θ, the connectivity affects the speed of convergence and the value of x_3 at the equilibrium, namely there are more uncommitted players at steady-state.

4.3 Network Topology

In this section, a network model is derived for two scenarios, namely the collective problem of choosing a nest for the swarm of honeybees and the security issues that a smart grid faces in presence of a virus. To study both scenarios, a finite number of players is considered. The mean-field game model in Chapter 3 can be seen as the asymptotic approximation when the number of players goes to infinity. Then, contrary to the mean-field game, where the population is infinite, the number of players is finite in this context. A clarification is due: in the two cases considered here, the number of agents is finite, but the state vector of each agent represents the probability of the agent to be in each of those states. Therefore, each agent represents an infinite population, modelled as the probability across the three states. In simple terms, it is more like a multi-population scenario, where each player represents a population itself and this population is infinite.

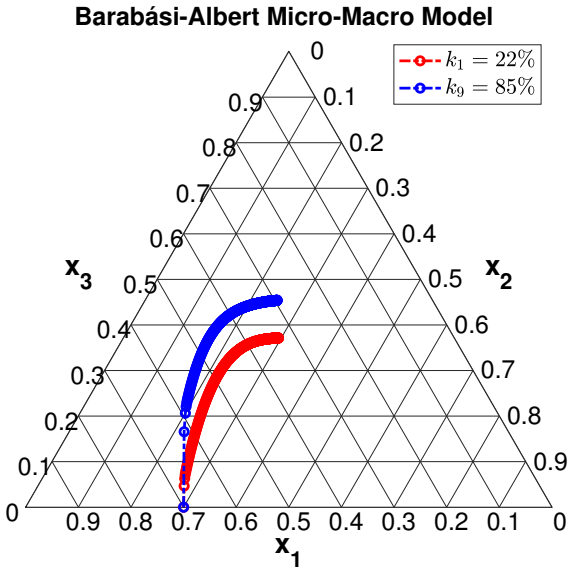

Figure 4.8: Behaviour of the micro-macro model in barycentric coordinates for $k_1 = 22\%$ (red) and $k_9 = 85\%$ (blue). The cross-inhibitory signal is set to $\sigma = 10$.

4.3.1 Network Topology in Honeybee Swarms

In this section, the model originating in the context of honeybee swarms is reframed to the case where two elemets coexist: a finite number of agents and an interaction topology. Agent i is represented by the probability across the three states r_i, s_i and x_i. To avoid confusion with the way number of each state and the number which refers to an agent, the variables r, s and x are used in place of x_1, x_2 and x_3 to indicate the states, while the subscript i, for example in r_i, represents the probability that agent i is in state r_i. Therefore, the microscopic dynamics for each agent i are the focus of this section.

The interaction network is described by a fully connected undirected graph G with adjacency matrix A. Let the network graph $G = (V, E)$, where V and E represent the set of vertices and the set of edges, respectively. The nodes of the network has cardinality $|V| = n$, and each node corresponds to an agent. Each edge in E has a corresponding weight in A, and the weights define the level of interactions between any pair of agents. The transitions rates to the committed states r and s and uncommitted state x are modelled by parameter β_{ij}, with the usual meaning from state i to state j. To keep the

same consistency with the previous chapter, numbers are used for the transition rates, i.e. β_{13} means from state r to state x. Additionally, in order to separate the linear and nonlinear terms, the linear ones are weighted by β_{ij}, while the nonlinear terms by β'_{ij}. To highlight the link with the SIR model, the word *infection* is used in the rest of this section, and the states in the model are presented in this order: s, x, r.

The model describing the time evolution of the infection probability for each agent is given by the following system of equations:

$$\begin{cases} \dot{s}_i(t) = -\beta'_{23} s_i(t) \sum_{j=1}^n a_{ij} r_j(t) + \beta'_{32} x_i(t) \sum_{j=1}^n a_{ij} s_j(t) - \beta_{23} s_i(t) + \beta_{32} x_i(t), \\ \dot{x}_i(t) = \beta'_{23} s_i(t) \sum_{j=1}^n a_{ij} r_j(t) - \beta'_{32} x_i(t) \sum_{j=1}^n a_{ij} s_j(t) + \beta'_{13} r_i(t) \sum_{j=1}^n a_{ij} s_j(t) \\ \qquad -\beta'_{31} x_i(t) \sum_{j=1}^n a_{ij} r_j(t) + \beta_{23} s_i(t) - \beta_{32} x_i(t) + \beta_{13} r_i(t) - \beta_{31} x_i(t), \\ \dot{r}_i(t) = -\beta'_{13} r_i(t) \sum_{j=1}^n a_{ij} s_j(t) + \beta'_{31} x_i(t) \sum_{j=1}^n a_{ij} r_j(t) - \beta_{13} r_i(t) + \beta_{31} x_i(t). \end{cases} \tag{4.11}$$

To link the above equations to the model for honeybees, in the equation for $\dot{s}_i$, the first term accounts for the cross-inhibitory signal, the second term describes the waggle dance and the last two terms accounts for the spontaneous rejection of the commitment and the spontaneous commitment itself, respectively. Similar comments apply to the equation for $\dot{r}_i$ and $\dot{z}_i$. The above system can be rewritten in vector form as

$$\begin{cases} \dot{s}(t) = -\beta'_{23} s(t) \mathbb{I}^n A r(t) + \beta'_{32} x(t) \mathbb{I}^n A s(t) - \beta_{23} s(t) + \beta_{32} x(t), \\ \dot{x}_i(t) = +\beta'_{23} s(t) \mathbb{I}^n A r(t) - \beta'_{32} x(t) \mathbb{I}^n A s(t) + \beta'_{13} r(t) \mathbb{I}^n A s(t) - \beta'_{31} x(t) \mathbb{I}^n A r(t) \\ \qquad +\beta_{23} s(t) - \beta_{32} x(t) + \beta_{13} r(t) - \beta_{31} x(t), \\ \dot{r}(t) = -\beta'_{13} r(t) \mathbb{I}^n A s(t) + \beta'_{31} x(t) \mathbb{I}^n A r(t) - \beta_{13} r(t) + \beta_{31} x(t), \end{cases} \tag{4.12}$$

where $\mathbb{I}^n$ indicates the $n \times n$ identity matrix, as before.

The results concerning the impact of the interaction topology to the collective decision-making process are presented next.

Theorem 15. *Given $\beta'_{ij} > 0$ for all i, j, $\beta_{23} \to 0$ and $\beta_{13} \to 0$, consider the network model in (4.12) in its bidimensional formulation over s and r, over a strongly connected graph with adjacency matrix A. The following statements hold:*

1. *If $s(0), r(0) \in [0,1]^n$, then $s(t), r(t) \in [0,1]^n$ for all $t > 0$.*
2. *The set of equilibrium points is the set of pairs $(\bar{1}^n, \bar{0}^n)$, $(\bar{0}^n, \bar{1}^n)$. The equilibrium points are asymptotically stable.*
3. *Let $\beta'_{23} = k\beta'_{32}$ and $\beta_{23} = k\beta_{32}$, where k is a parameter that corresponds to a measure of the connectivity. The set of equilibrium points includes the set of pairs*

$((1/(2+k))^n, (1/(2+k))^n)$. *These equilibrium points are asymptotically stable.*

Proof. See Section 4.6. □

Remark 15. *It is worth pointing out the similarities between the microscopic dynamics presented here and the study carried out under a complex network topology. In fact, in the case of complex networks, where the connectivity is parametrised by ψ_k, as the connectivity increases, so does the number of uncommitted players. The above result implies that, even in this case, the connectivity, which is defined by the adjacency matrix A and by parameter k, alters the value of infection at steady state. In other words, as the connectivity increases, the probability for an agent to be infected (or uncommitted) is higher.*

4.3.2 Network Topology in Smart Grids

The classical SIR model describes the common scenario of a virus infection in many possible contexts. In this section, the context of cyber-security is studied, with a particular emphasis on virus propagation in smart grids. In this scenario, a hacker tries to disrupt two holons. Recall that a *holon* is an intelligent entity which can be seen as a unit component of a larger system or as a whole. The latter happens when the holon autonomously makes a decision on its own after processing the gathered information. In this context, a holon is part of a power grid or information system, e.g. a bus or a database.

As in the case of honeybees, the microscopic dynamics of individual agents are studied. Let the number of agents be n, i.e. $|V| = n$, where V is the set of vertices in network. Each agent represents a component of the system and is connected to the other agents through a network topology. As anticipated before, the word agent is used in place of player but they are interchangeable. Variables r, s and x represent the probability of an individual of being in state 1, 2 and 3, respectively. Parameters β_{31}, β_{32} models the capability of the holons to recover from the infection or to mitigate the cyber-attacks. The model involves a cyber-attack at two kinds of holons, with the aim of disrupting the services or the data stored. The final values of s and r determine how far the corruption has propagated throughout the network. Three types of attacks are considered and can be modelled by different values of β_{ij}, see [24]:

- *sequential attack*: the hacker sends continuous burst attacks, disrupting the cus-

tomer layer and the information of control signals. In the simulations, the nodes under attack are characterised by high values of β_{13}, β_{23} for short periods of time;

- *continuous low rate attack*: usually aimed at disrupting voltage control at the holons; here smaller values of β_{13}, β_{23} endures for longer time in the simulations;
- *adaptive attack*: the hacker listens for any changes in the communication route and redirects the attack from one holon to the other. In the simulations this means that small and large values for β_{13} and β_{23} alternates in subsequent time instants.

The main difference with the honeybee model is the considerations about the cross-inhibitory coefficient, which is crucial in the case of honeybees, but it is marginal in the present case. Therefore, the focus is on the role of the connectivity at the equilibrium and on the stability properties of the system. Variables r and s represent the two kinds of holons, e.g. two different defence approaches, while x describes the infected state. Under no cross-inhibitory signal, the model reduces to the following system of ODEs:

$$\begin{cases} \dot{s}_i(t) = -\beta'_{23} s_i(t) \sum_{j=1}^{n} a_{ij} x_j(t) + \beta_{32} x_i(t), \\ \dot{x}_i(t) = \beta'_{23} s_i(t) \sum_{j=1}^{n} a_{ij} x_j(t) + \beta'_{13} r_i(t) \sum_{j=1}^{N} a_{ij} x_j(t) - \beta_{32} x_i(t) - \beta_{31} x_i(t), \\ \dot{r}_i(t) = -\beta'_{13} r_i(t) \sum_{j=1}^{n} a_{ij} x_j(t) + \beta_{31} x_i(t), \end{cases} \tag{4.13}$$

where the nonlinear rates (indicated as β'_{ij}) involves the interactions between a holon and a corrupted node, while the linear rates (in the form β_{ij}) can be seen as a curing rate from the remaining nodes that are still not infected. Given the conservation of mass, the above system can be rewritten in vector form as

$$\begin{cases} \dot{s}(t) = -\beta'_{23} s(t) \mathbb{I}^n A x(t) + \beta_{32} x(t), \\ \dot{r}(t) = -\beta'_{13} r(t) \mathbb{I}^n A x(t) + \beta_{31} x(t), \end{cases} \tag{4.14}$$

where $x(t) = 1 - s(t) - r(t)$. It is now time to establish the next result.

Theorem 16. *Consider the virus propagation network model (4.14), and let β'_{ij} and $\beta_{ij} > 0$ for all i and j, over a strongly connected graph with adjacency matrix A. The following statements hold:*

1. *If $s(0), r(0) \in [0,1]^n$, then $s(t), r(t) \in [0,1]^n$ for all $t > 0$.*
2. *The set of equilibrium points is the set of pairs $(s^*, \bar{1}^n - s^*)$, for any $s^* \in [0,1]^n$, and the linearisation of (4.14) about $(s^*, \bar{1}^n - s^*)$ is*

$$\begin{cases} \dot{s}(t) = -\beta'_{23} s^* \mathbb{I}^n A x(t) + \beta_{32} x(t), \\ \dot{r}(t) = -\beta'_{13} (\mathbb{I}^n - s^*) A x(t) + \beta_{31} x(t). \end{cases} \tag{4.15}$$

For the three-state system in (4.13), the set of equilibrium points is the set of tuples $(s^*, \bar{0}^n, \bar{1}^n - s^*)$. *Furthermore, the above equilibrium points are asymptotically stable if the following condition holds:*

$$\beta'_{23} s^* \mathbb{I}^n A \bar{1}^n + \beta'_{13} (\mathbb{I}^n - s^*) A \bar{1}^n < (\beta_{32} + \beta_{31}) \bar{1}^n. \tag{4.16}$$

3. *If* $\lim_{\beta_{32}, \beta'_{13} \to 0}$, *then system (4.13) can be approximated by the standard SIR model.*

Proof. See Section 4.6. □

Remark 16. *A physical understanding of the previous theorem can be given by considering inequality (4.16). For increasing connectivity, which in turn implies higher values of the entries of the adjacency matrix A, the left-hand side of the inequality increases, eventually becoming greater than the right-hand side. In the end, it means that the system turns unstable, due to the fact that a higher connectivity implies a higher chance of a virus spreading in the network and a cyber-attack infecting a holon. The last point of the above result links the model to the SIR model when two transition rates are set to zero, see [21]. Specifically, the two transition rates are the one between the infected state and the susceptible state and the one between the recovered state and the infected state, in this order.*

4.3.3 Case Study: Walpole GSP - Peterborough (EPN)

In this section, the virus propagation scenario is studied in the case of a real grid, namely the Walpole GSP - Peterborough (EPN), taken from the Regional Development Plan in [86, p. 18]. The line diagram is depicted in Fig. 4.9 (left) and the corresponding graph representation can be seen in Fig. 4.9 (right). For the purpose of the simulations, the cyber attack is assumed to happen at node 11. The attack is aimed at disrupting the frequency of the buses in the network, propagating according to one of the three mentioned kinds of attacks: continuous low-rate, sequential and adaptive. For each of the three attacks, a set of simulations is given. Each set is composed of three simulations. The first one describes the impact of the virus on the network topology, the second one presents the data corresponding to the probability of infection at each node in a histogram and the third one involves the frequency analysis of each node. Table 4.1 shows the infection rates in each set, while the curing rates are fixed for all simulations and set to $\beta_{31} = \beta_{32} = 0.1$.

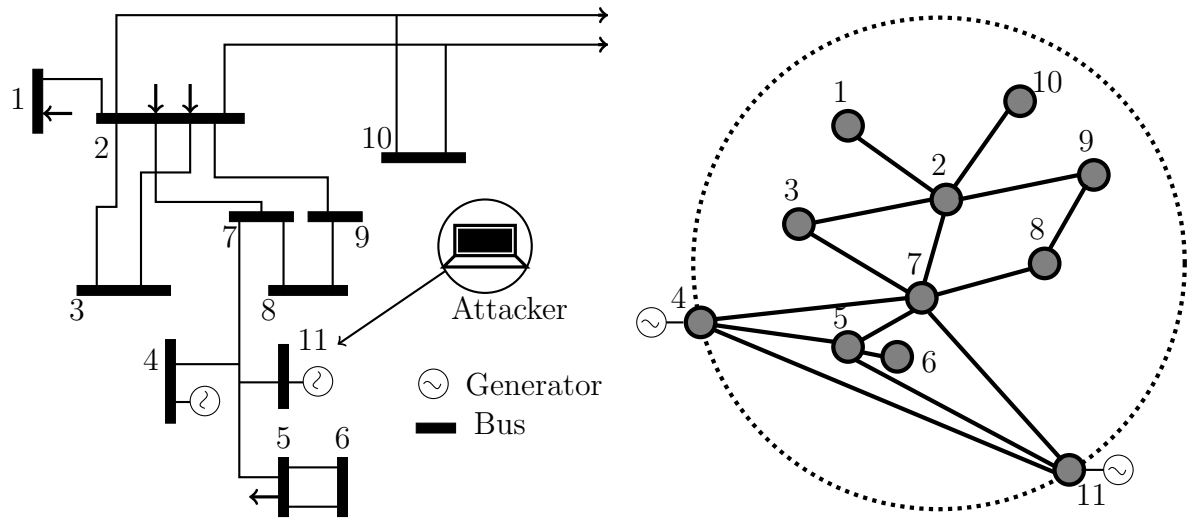

Figure 4.9: Line diagram representation (left) and graph representation (right) of the Walpole GSP - Peterborough (EPN), from the Regional Development Plan in [86, p. 18]. The infection starts spreading from bus 11, as depicted in the line diagram.

.

Table 4.1: Infection rates for each set of simulations.

Parameter	Set I	Set II	Set III
β_{13}	0.13	$\{0.13, 0.65\}$	$\{0.39, 0.13\}$
β_{23}	0.13	$\{0.13, 0.65\}$	$\{0.13, 0.39\}$

To show the impact of the infection on the network, the first simulation in each set describes the infection probability at each node. The nodes are coloured in greyscale to denote the difference in probability. In particular, a *black* node means that the probability of infection is high, namely it has a value greater than 0.75. When a node is depicted in *dark grey*, it indicates that the infection probability is moderate (or medium), i.e. between 0.5 and 0.75. If a node is *grey*, this denotes a low (or small) probability of being infected, with a value between 0.25 and 0.5. Finally, a node with a value less than 0.25 is coloured in *white*. The grid with the initial infection and the corresponding infection probability for each node are shown in Fig. 4.10. As previously stated, the infection starts at node 11, whose probability for each state is equal to $(0, 1, 0)$. The

rest of the nodes in the network are split in two subsets, each representing one holon. Therefore, the first five have an initial probability described by $(0, 0, 1)$, whereas the remaining five have an initial state vector as $(1, 0, 0)$.

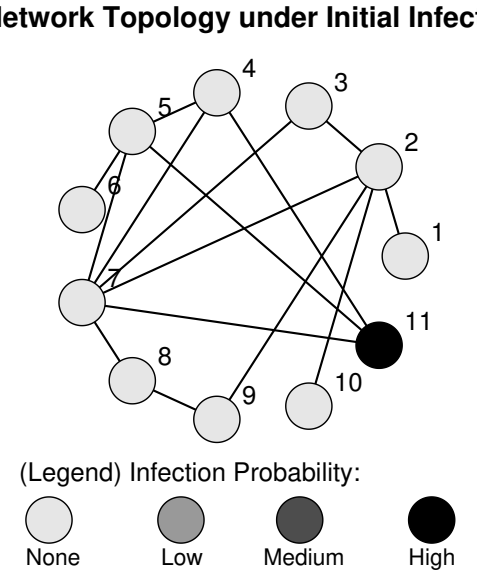

Figure 4.10: Initial configuration of the network for all sets of simulations. The infection spreads from node 11.

Each set of simulation comprises also a histogram, showing the number of nodes grouped by infection probability at two time instants, after few iterations from the beginning of the simulation and at the end. In more detail, the blue bars in every histogram represent the probabilities after a time interval $1/10$ of the total time T has elapsed. The red bars designate the probabilities at the end of the simulation, namely when $t = T$. It is worth noting that the histograms show an aggregate result across all nodes in the network, thus nodes are not distinguishable. But by cross-referencing the network topology plot and the histogram it is easy to see which nodes belong to which group. The histograms serve the purpose of showing the reader an immediate graphical representation of the evolution of the system for what it concerns the infection propagation.

The last simulation in each set includes the frequency analysis carried out at each node. The frequency is measured at each bus in the network while the attacks take place. To study the change in frequency, each bus is modelled as a coupled oscillator using the notorious Kuramoto coupled oscillator model, see [62], [95]. According to usual

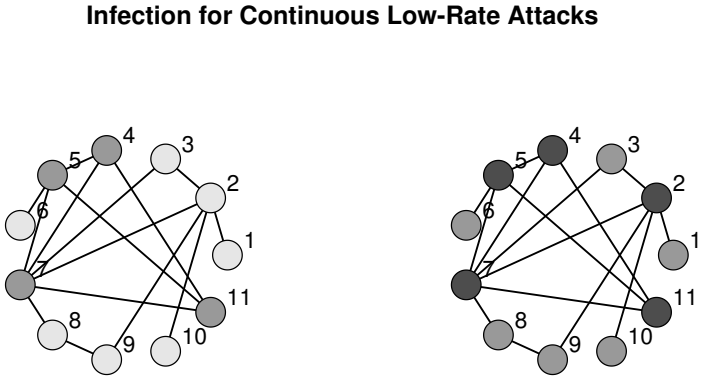

(a) Continuous low-rate attacks: after $T/10$ time instants (left) and at the end of the time horizon T (right).

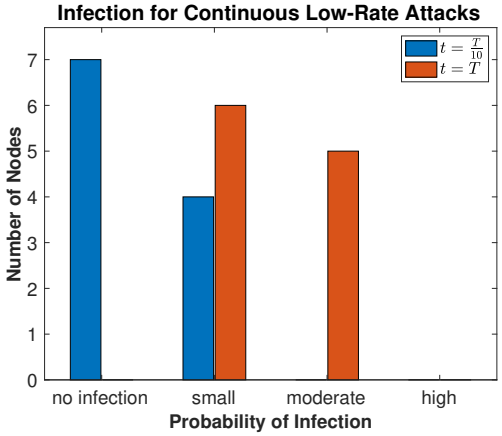

(b) Histogram showing the number of nodes and the corresponding infection probability for continuous low-rate attacks.

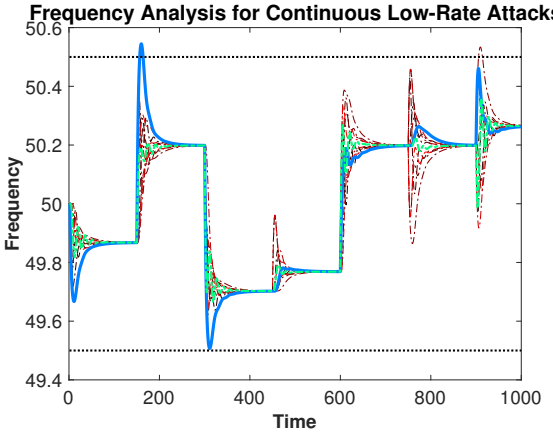

(c) Frequency analysis showing the impact of the attack, measured by the amplitude of the frequency of oscillations.

Figure 4.11: Behaviour of the system when the attacks are of the type continuous low-rate, in the order: network, histogram and frequency analysis.

frequency of a bus, as it is also reported in the Regional Development Plan, i.e. [86], the frequency is set at 50 hertz (Hz), with a given a tolerance of ± 0.5 Hz. The considered interval is therefore $[49.5, 50.5]$ Hz. Going above or lower these values can compromise the stability of the network, causing high damage to the provider and customers. In the original model, see [21], the frequency of each bus $\dot{\theta}_i$ evolves as in the following ODE:

$$\ddot{\theta}_i = \frac{\omega_i}{M_i} - \frac{K}{nM_i} \sum_{j=1}^{n} sin(\theta_i - \theta_j) - \frac{D_i}{M_i}\dot{\theta}_i, \tag{4.17}$$

where ω_i is the natural frequency, K parametrises the stiffness of the coupling strength, n

is the number of nodes in the network, M_i and D_i are the inertia and damping coefficients, respectively. The quotient K/n represents the coupling strength of the interconnected buses and it is equal for all the nodes.

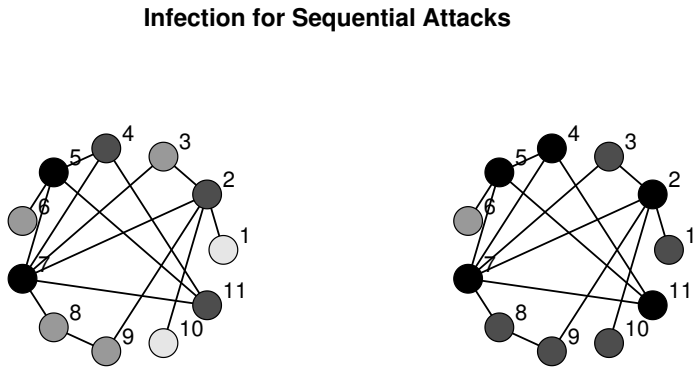

(a) Sequential attacks: as before, sampled after $T/10$ time instants (left) and at the end of the time horizon T (right).

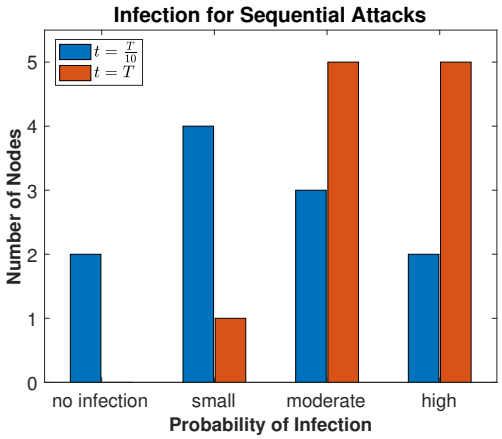

(b) Histogram showing the number of nodes and the corresponding infection probability for sequential attacks.

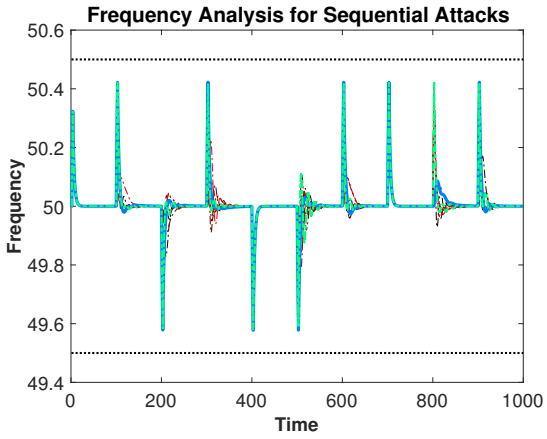

(c) Frequency analysis showing the impact of the sequential attacks. The amplitude is larger for lower connectivity (blue).

Figure 4.12: Behaviour of the system when the attacks are of the type sequential, in the order: network, histogram and frequency analysis.

The contribution to this model includes the extension to the case where an adversarial disturbance caused by the cyber-attacks is included. For simplicity, it is assumed that all buses have the same natural frequency. The extended model is therefore:

$$\ddot{\theta}_i = \frac{\omega}{M} - \frac{K}{nM}\sum_{j=1}^{n} sin(\theta_i - \theta_j) - \frac{D}{M}\dot{\theta}_i + \zeta_i, \tag{4.18}$$

where ζ_i is the added disturbance. The disturbance describes the probability that a node is being threatened by a cyber-attack at given time instant. The probabilities of such an event are obtained from the equations in 4.14 at steady-state, which constitutes the input to the extended coupled oscillator model. The attack is modelled through a disturbance of the type

$$\zeta_i = \pm \hat{k}\hat{\omega}, \tag{4.19}$$

where $\hat{\omega}$ represents the frequency of the disturbance and $\hat{k}$ is a parameter that depends on the infection rates of system 4.14. The added disturbance can be tuned to model the strength of the attack. To see how the connectivity impacts on the virus propagation in the network, two nodes are highlighted in the simulations, namely node 1 and node 7. The first one is connected to only one node and it is denoted by the thick blue line. The other one is the node with the highest connectivity and is represented by the thick green line. The rest are indicated by thin dashed lines. Finally, the probability of an attack is sampled every 150 iterations for the first and last type of attacks, while every 100 for the sequential attacks.

Continuous Low-Rate Attacks. In the first set of simulations, small values of the infection rates β_{13} and β_{23} endure for the entire duration, and so are the values for the curing rates β_{31} and β_{32}, such that the probability of infection at nodes remains under control. In detail, the infection rates are set to $\beta_{13} = \beta_{23} = 0.13$ while the curing rates are set to $\beta_{31} = \beta_{32} = 0.1$. In accordance with Theorem 16, a higher connectivity increases the probability that a node can be infected. Figure 4.11 shows the network topology (a), the corresponding histogram (b) and the frequency analysis (c). As is can be seen from the histogram, the infection is higher at the end of the time horizon, which is confirmed by the network topology as well. It turns out that 5 nodes have a moderate probability of being infected, while the other 6 have a low infection probability. As is can be seen from the network graph, the nodes with higher connectivity, or those linked to them, are the ones with a higher probability of infection. For the frequency analysis, it is true the opposite. Thanks to the coupling strength, nodes with higher connectivity, e.g. node 7 (green line), have smaller oscillations than nodes with low connectivity, e.g. node 1 (blue line).

Sequential Attacks. This set of simulations describes the context of a virus which is

modelled as sequential burst attacks. To simulate the behaviour of these attacks, the infection rates β_{13} and β_{23} are set to a value which is five times greater than the normal value every five iterations while the attacks are happening. Figure 4.12 illustrates the outcome of this scenario. Due to the burst nature of the attacks, the higher values of the infection rates make the network more unstable compared to the continuous low-rate counterpart. This can be seen from a microscopic perspective or a macroscopic perspective: from the network topology, one can see how each node is impacted (microscopic view). From the histogram, the focus is on the total number of nodes for each probability of infection (macroscopic view). From the frequency analysis, the role of the connectivity can be explored. Recall that the attacks happen every 100 iterations in this context, as it can be seen from the plot. By comparing the peak of the green (high connectivity, node 7) and blue (low connectivity, node 1) lines, it can be concluded that a high connectivity attenuates the amplitude of the oscillations. A final consideration can be made about the similarities of this scenario with the common denial of service (DOS) attacks. DOS attacks aim at disrupting the customer layer or the information of control signals, in order to make a service unavailable, e.g. a server that does not respond to requests from users.

Adaptive Attacks. In the last set of simulations, the impact of adaptive attacks is examined. The hacker's purpose is to attack the more vulnerable nodes, so the hacker redirects the attacks to the most convenient holon, which is represented by the probability of states s and r. As an example, the two holons might correspond to different defence strategies against the attacks. At the start of the simulations, the infection rates are set such that the value of β_{13} is three times larger than the one for β_{23}. By evaluating the speed of the propagation, the hacker swaps the values of the infection rates. Figure 4.13 presents the network topology, the histogram and the frequency analysis for this scenario. As it can be seen from the network, the first five nodes have a higher probability after few iterations, while the second five are impacted more at the end. This is due to the different values of the infection rates and the initial state vector for each node. Finally, the frequency analysis shows that highly connected nodes are more likely to be attacked. Therefore, even though attacking these nodes is more advantageous to compromise the whole network, the coupling strength reduces the amplitude of oscillations, as before. This can be seen from a larger displacement of ω for nodes with low connectivity. For instance, node 1 (blue line, low connectivity) is attacked less often than the other nodes but has larger displacements.

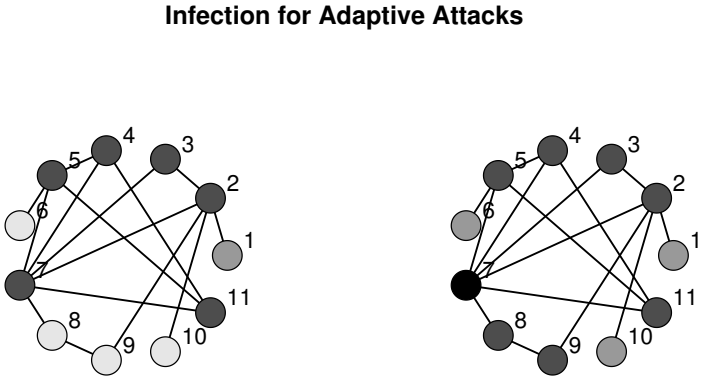

(a) Adaptive attacks: again, the network is shown after $T/10$ time instants (left) and at the end of the time horizon T (right).

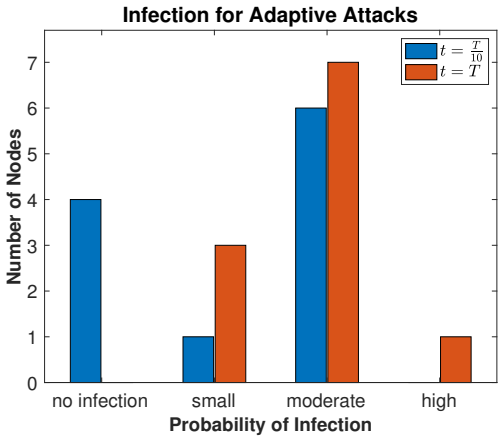

(b) Histogram showing the number of nodes and the corresponding infection probability for adaptive attacks.

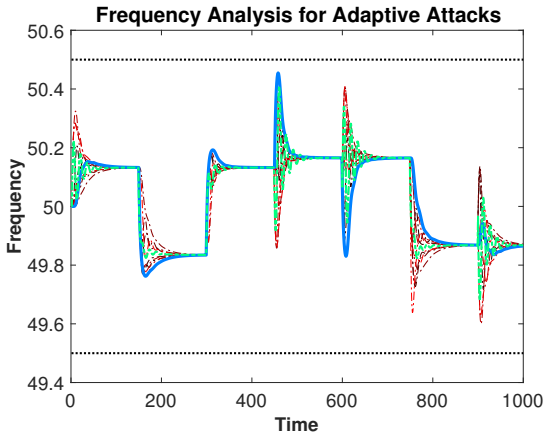

(c) Frequency analysis showing the impact of the adaptive attacks. Highly connected nodes are attacked more often by the virus.

Figure 4.13: Behaviour of the system when the attacks are of the type adaptive, in the order: network, histogram and frequency analysis.

4.4 Stochastic n-State Model

In this section, the 2-option case is extended to the n-state problem, i.e. the decision-making process where the players can choose to commit to one of n possible options or stay uncommitted. The term n-state model refers to the n possible options that the players can choose to commit to, while one additional state represents the uncommitted, i.e. $n+1$. Additionally, the model presented here is stochastic, and the noise is modelled

as a Weiner process. Due to the stochastic nature of the resulting system, the stability analysis is carried out within the framework of Lyapunov stochastic stability theory, see [70]. To depict the scenario where the options have equal value, it is assumed that the parameters are symmetric and the cross-inhibitory signals sent from all states have equal strength towards every other state. The corresponding stochastic n-state model is the following:

$$\begin{cases} \dot{x}_i = [x_{n+1}(\gamma + rx_i) - x_i(\alpha + \sigma \sum_{j\neq i}^{n} x_j)]dt + \sum_{k=1}^{n} g_k d\mathcal{B}_k, \\ x_{n+1} = 1 - \sum_{i=1}^{n} x_i, \end{cases} \tag{4.20}$$

where g_k is a weighting coefficient and $\mathcal{B}_k(t)$ is a Weiner process. In the above, the vector $\mathbf{x}(t) = [x_1(t), x_2(t), ..., x_{n+1}(t)]^T \in \mathcal{S}^{n+1}$, where $\mathcal{S}^{n+1}$ is the $n+1$ simplex and $\sum_{j\neq i}^{n} x_j$ is the sum of the population distribution at nodes $1, ..., n$ except j. In order to simplify the system, the effort of the players when sending the cross-inhibitory signal is assumed to be an average across the population distribution, which is motivated by the symmetry of all options.

Assumption 4. *Let the constant value $\bar{x}$ denote the average across the population distribution vector $\mathbf{x} = [x_1(t), x_2(t), ..., x_n(t)]^T$, for all states except the uncommitted state. The cross-inhibitory signal is directed at the average population $\bar{x}$ and its strength is weighted by the parameter $\bar{\sigma} := n\sigma$, whose value is appropriately tuned to reflect the n states involved.*

In light of Assumption 4, system (4.20) can be rewritten in vector form as:

$$\dot{x} = [A(x)x + c]dt + Gd\mathcal{B}, \tag{4.21}$$

where $A(x) \in \mathbb{R}^{n\times n}$ is defined as

$$A(x) = \begin{bmatrix} -\gamma - r - rx_1 - \alpha - \bar{\sigma}\bar{x} & -\gamma - rx_1 & \cdots & -\gamma - rx_1 \\ & -\gamma - rx_2 & \ddots & \\ & \vdots & & \\ & -\gamma - rx_n & \cdots & -\gamma - r - rx_n - \alpha - \bar{\sigma}\bar{x} \end{bmatrix}, \tag{4.22}$$

and $c = [\gamma, \gamma, \cdots, \gamma]^T$ is an n-dimensional transposed vector. The noise $\mathcal{B}(t)$ is a vector of Weiner processes and $G(t) \in \mathbb{R}^{n\times n}$ is a $n\times n$ matrix, whose coefficients define the strength of the noise. Figure 4.14 shows the Markov chain representation of system (4.21).

In the following proposition, the stability analysis of the stochastic n-state model described by system (4.21) is carried out.

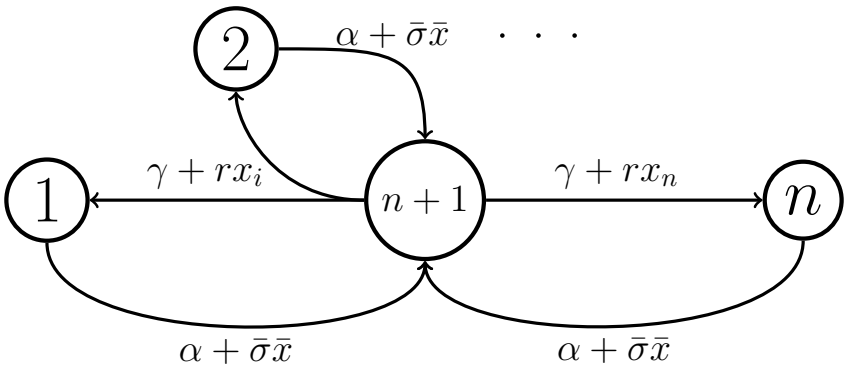

Figure 4.14: Markov chain representation of the n-state system (4.21). The transition rate from a committed state to the uncommitted state is weighted on the average across the population distribution, as in Assumption 4.

Proposition 1. *Given a positive-definite Lyapunov function $V(x) > 0$, if $\mathcal{L}V(x) \leq 0$, for $x \in Q_m \setminus \{0\}$, then the origin is stable "with probability one".*

Proof. Consider system (4.21). The corresponding stochastic processes can be studied in the framework of stochastic stability theory, see [70]. The Taylor expansion in

$$\dot{f}(t,x) \;\; = \tfrac{\partial f}{\partial t} + (\nabla_x f)^T \dot{x} + \tfrac{1}{2}(\dot{x})^T (\mathcal{H}_x f)\dot{x} + \ldots, \tag{4.23}$$

follows from *Itô's lemma* in higher dimensions. The notation $\nabla_x f$ represents the gradient of $f(\cdot)$ w.r.t. x and $\mathcal{H}_x f$ is the Hessian matrix of $f(\cdot)$ w.r.t. x. The corresponding infinitesimal generator can be computed as:

$$\begin{aligned} \mathcal{L} \;\; &= \left[\tfrac{\partial f}{\partial t} + (\nabla_x f)^T (Ax + c) + \tfrac{1}{2} Tr[G^T (\mathcal{H}_x f) G]\right] dt + (\nabla_x f)^T G d\mathcal{B}, \\ &= \tfrac{1}{2} Tr[G^T (\mathcal{H}_x f) G] + (\nabla_x f)^T (Ax + c), \end{aligned} \tag{4.24}$$

where Tr denotes the trace operator. The above is obtained in the limit for $dt \to 0$, for which the terms dt^2 and $dtd\mathcal{B}$ tend to zero faster than $d\mathcal{B}^2$ and thus are set to zero. Moreover, dt is replaced by $d\mathcal{B}^2$ since it is $O(dt)$ (due to the variance of a Wiener process). The terms $\partial f/\partial t$ and $d\mathcal{B}$ cancel out because $f(\cdot)$ does not depend on t and $\mathbb{E}[d\mathcal{B}] = 0$, respectively.

Consider the following positive-definite Lyapunov function: $V(x) = \sum_i x_i = x_1 +$

$x_2 + \cdots + x_n$. The defined Lyapunov function $V(x)$ can be substituted in (4.24) as:

$$\begin{aligned}\mathcal{L}V(x) &= \tfrac{1}{2}Tr[G^T(\mathcal{H}_x V(x))G] + (\nabla_x V(x))^T(Ax+c) \\ &= \tfrac{1}{2}Tr\left[G^T \begin{bmatrix} 2 & 2x_1+2x_2 & \cdots & 2x_1+2x_n \\ \vdots & & & \\ 2x_1+2x_n & \cdots & & 2 \end{bmatrix} G\right] \\ &+(2x_1+2x_2+\cdots+2x_n)^T(Ax+c).\end{aligned} \tag{4.25}$$

The components of the cross-state noise are assumed to be negligible and therefore $G = \xi\mathbb{I}^n$, where $\xi \in \mathbb{R}$. Thus, the system above simplifies as:

$$\begin{aligned}\mathcal{L}V(x) &= \tfrac{1}{2}Tr[2\xi\mathbb{I}^n] + (2x_1+2x_2+\cdots+2x_n)^T(Ax+c) \\ &= n\xi + [2x_1\bar{\partial}x_1 + 2x_2\bar{\partial}x_2 + \cdots + 2x_n\bar{\partial}x_n],\end{aligned} \tag{4.26}$$

where $\bar{\partial}x_i = x_{n+1}(\gamma + rx_i) - x_i(\alpha + n\bar{\sigma}\bar{x})$ and x_{n+1} is defined as in (4.20). By specialising the above equation at the origin, the condition $x_i = 0$ holds true. Therefore, the following can be derived:

$$\mathcal{L}V(x) = n\xi. \tag{4.27}$$

To ensure stability, the condition $\mathcal{L}V(x) < 0$ must hold true. Thus, $\xi < 0$. If $\mathcal{L}V(x) < 0$, given $Q_m = \{x : x^T\mathbb{I}^n x < m^2\}$, then the equilibrium point at the origin is stable "with probability one". This concludes the proof. □

To generalise the result of the above proposition, the stability of the n-dimensional space where the dynamics evolve according to (4.21) is now studied. To ensure stability of all equilibria residing in the convex hull $Co\{A(x)x + c\}$, the result is established in the following proposition.

Proposition 2. *Consider system (4.21) and let $G = \xi\mathbb{I}^n$. The equilibrium points residing in the convex hull $Co\{A(x)x + c\}$ are stable "with probability one" if $\xi < -2$.*

Proof. From Theorem **??**, the condition on the infinitesimal generator for the positive-definite Lyapunov function $V(x) = \sum_i x_i = x_1 + x_2 + \cdots + x_n$ is given by:

$$\mathcal{L}V(x) = n\xi + [2x_1\bar{\partial}x_1 + 2x_2\bar{\partial}x_2 + \cdots + 2x_n\bar{\partial}x_n]. \tag{4.28}$$

Due to $0 \leq \bar{\partial}x_i \leq 1$ and $0 \leq x_i \leq 1$, at most the above equation yields $[2x_1\bar{\partial}x_1 + 2x_2\bar{\partial}x_2 + \cdots + 2x_n\bar{\partial}x_n] \leq 2n$. By substituting it in the above, the following holds:

$$\mathcal{L}V(x) = n\xi + 2n. \tag{4.29}$$

Thus, the condition $\xi < -2$ follows. This concludes the proof. □

In the next subsections, two extensions are considered in their initial formulation. They are presented as possible developments of the current models.

4.4.1 Nudge

In this section, the concept of *nudge* is used to model how this form of incentives can impact the decision-making problem. Recall that a nudge is a predictable aspect of the players' decision-making process but not a mere incentive that changes the players' gain, see [99]. Therefore, enforcement or other means to achieve compliance are not to be considered nudges. A nudge, to be considered as such, must be easy to avoid. For instance, ordering the products in a supermarket such that a specific item is at eye level is a nudge, while removing all the competitor of a given product is not.

In light of the above clarifications, a nudge should not significantly change the values in the game, but rather slightly influence the players' behaviours. In order to do this, the role of the weight matrix G can be explored to achieve a nudge formulation of system (4.21). In particular, the initial study considering the nudge model starts from the following system:

$$\dot{x} = [A(x)x + c]dt + \hat{G}d\mathcal{B}, \tag{4.30}$$

where $A(x)$ is defined as in (4.22). The real question here is how to model $\hat{G}$ such that some of the values act as a nudge towards one specific option. This would solve the n-option consensus problem by shifting the agents' choices towards that specific option. This part is left as a possible extension of the n-state stochastic model.

4.4.2 Graphical Models for Buffer Networks

In this subsection, an initial study of a robot network is carried out with the final aim to achieve consensus in the corresponding multi-robot system. To model the data limit of each robot, buffer networks in the context of positive systems are used, see [85]. Buffer networks can be associated to positive systems where the actual values cannot be negative, but at most equal to zero. Then, a probabilistic approach is presented, where the network is captured by a probabilistic graphical model. An initial formulation of a message passing algorithm for this problem is proposed.

Positive systems are investigated to describe the evolution of a swarm of robots that need to share information via dynamical networks. The presented model is within

the context of buffer networks, where each node is represented by a buffer and each edge corresponds to the transmission link between any two given robots. This system aims at capturing real issues such as buffer limit, congestion, message propagation and flooding. While the structure models the connections among robots, the added noise captures the probability of error free transmission and the probability of message loss due to transmission or congestion.

Formally, given a graph network $\mathcal{G} = (\mathcal{V}, \mathcal{E})$, where $\mathcal{V}$ denotes the vertices and $\mathcal{E}$ the edges, let $\mathbf{x} = (x_1, ..., x_n)^T \in \mathbb{R}_0^n$ represent the content of all the buffers. The corresponding continuous time model is given by the following:

$$\dot{x}_i = a_i x_i + \sum_{(i,j)\in\mathcal{E}} (u_{ji} - u_{ij}) + w_i, \quad i \in \mathcal{V}, \tag{4.31}$$

where x_i is the buffer content, u_{ji} is the flow from buffer j to buffer i, $a_i x_i$ is the natural decay (or growth) and w_i is the local production or consumption. System (4.31) models the evolution of the buffer for robot i in terms of content. To model the propagation of a message in the robot network, an instance of the message passing algorithm on a probabilistic graphical model is investigated, see [110], [111].

Given an Erdós-Rényi graph G of N vertices, M edges and q options, consider a set of discrete variables, $\mathbf{x} = \{x_1, x_2, ..., x_N\}$, each corresponding to one node in the graph. Each node represents one robot. The state of each variable is represented by the discrete value associated to the option chosen by the robot in $\{0, 1, ..., q\}$, where $q \in \mathbb{Z}^+$ and 0 represents the uncommitted state. Given the assumption that the given graph has sparse connectivity, this in turn implies that the graph acts as a tree locally. The first step is to convert the graph into a factor graph $\hat{G}$. The assumption on sparse connectivity makes sure that the factor graph has a tree structure locally.

Before introducing the message passing algorithm for the graph consensus problem, a few definitions are due. The following is the definition of the factor $f_a(x_i, x_j)$ relating to the edge between nodes i and j, which assigns the joint probability for the two states for any arbitrary dummy index a:

$$f_a(x_i, x_j) = \begin{cases} 1, & x_i = x_j, \\ 0, & x_i \neq x_j. \end{cases} \tag{4.32}$$

The message passing algorithm for the graph consensus problem can be split in two parts: first, the messages are propagated forward from the leaf nodes to the root

node, and then propagated backward from the root node to the leaf nodes. The first part, namely leaves to root, can be expressed by the following set of equations:

$$\begin{cases} \mu_{x_i \to f_a}(x_i) = 1, & \forall x_i \in \mathcal{L}(\hat{G}), \\ \mu_{f_a \to x_j}(x_j) = \frac{1}{|ne(f_a)|-1} \sum_{x_i} f_a(x_i, x_j), & \forall x_j \in ne(x_i), \\ \mu_{x_k \to f_r}(x_k) = \prod_{l \in ne(x_k) \setminus f_r} (\mathbf{1} - \mu_{f_l \to x_k}(x_k)), & \forall x_k \notin \mathcal{L}(\hat{G}), \\ \mu_{f_r \to x_r}(x_r) = \frac{1}{|ne(f_r)|-1} \sum_{x_k} f_r(x_k, x_r) \mu_{x_k \to f_r}(x_k), & \forall x_r \in ne(x_k), \end{cases} \tag{4.33}$$

where $\mathcal{L}(\hat{G})$ denotes the set of leaf nodes in the factor graph $\hat{G}$, $ne(x)$ denotes the neighbour nodes of node x, and $\mathbf{1}$ denotes the q-sized vector of ones. In the above, the first two equations account for the propagation from the leaves to the corresponding factor nodes and from these factor nodes to the neighbouring nodes in the graph. The other two equations account for all the other nodes in the graph. To propagate the message back from the root node to the leaf nodes, the corresponding equations take the form:

$$\begin{cases} \mu_{x_r \to f_r}(x_r) = 1, & \forall x_r \in \mathcal{R}(\hat{G}), \\ \mu_{f_r \to x_k}(x_k) = \frac{1}{|ne(f_r)|-1} \sum_{x_r} f_r(x_k, x_r), & \forall x_k \in ne(x_r), \\ \mu_{x_j \to f_a}(x_j) = \prod_{l \in ne(x_j) \setminus f_a} (\mathbf{1} - \mu_{f_l \to x_j}(x_j)), & \forall x_k \notin \mathcal{R}(\hat{G}), \\ \mu_{f_a \to x_i}(x_i) = \frac{1}{|ne(f_a)|-1} \sum_{x_j} f_a(x_i, x_j) \mu_{x_j \to f_a}(x_j), & \forall x_r \in ne(x_k), \end{cases} \tag{4.34}$$

where $\mathcal{R}(\hat{G})$ denotes the root node of graph $\hat{G}$. For a sufficiently small ratio M/N, the algorithm will converge to a solution where any two adjacent nodes have chosen the same option. The entire network will therefore converge to the same option.

By running the algorithm from the node to the root and vice versa, we have now all the values to calculate the approximate marginal for each node. This process would allow convergence in $O(2M)$, where M is the number of links in the graph. The marginal can be calculated as:

$$p(x) = \tilde{p}(x)/Z, \tag{4.35}$$

where $1/Z$ is the unknown normalisation coefficient and $\tilde{p}(x)$ is defined as:

$$\tilde{p}(x) = \prod_{f_a \in ne(x)} \mu_{f_a \to x}(x). \tag{4.36}$$

A possible future extension of this model would include the consideration of a dynamical network structure which changes over time, namely $G(t)$. An initial framework has been given here to investigate the consensus problem in the context of swarm robotics, which can be linked to the initial consensus problem for honeybees.

4.5 Summary and Discussion

In this chapter, two main elements of novelty are considered with respect to the previous chapters. The first element is to introduce an interaction topology in the system. Two main cases are analysed, one where the topology is modelled via scale-free complex networks, and another where the connections are determined by an adjacency matrix. The second element is to consider stochastic dynamics, and a large number of options, namely n.

As for the structured cases, in the former case, the population is large and it is discretised in many different sub-populations, each with a given connectivity distribution that follows a discretised version of the Barabási-Albert complex network. Results are given in terms of the equilibrium points, their stability properties and a threshold for the cross-inhibitory signal similarly to the unstructured case. These results are given in Theorem 12, Theorem 13 and Theorem 14, respectively. In the latter case, the number of agents is finite, but each agent is in probability in one of the three possible states. Therefore, this case can be seen as a finite number of infinite sub-populations. The impact of the connectivity in the form of an adjacency matrix is investigated in this case and results are given for two models, one for honeybees in Theorem 15 and another for virus propagation in Theorem 16. An additional contribution is the proposed case study on virus propagation in smart grids.

As for the stochastic dynamics, the number of options is increased to n, and the uncommitted state is labelled state $n + 1$. When the noise is in a general form, a polytope is found to assess convergence. Additional assumptions can be made to link this stochastic model to nudge theory, where an option is favoured by the nudge, without changing the general dynamics for the system.

4.6 Proofs

As for the other chapters, Lyapunov's stability theory is used in most of the proofs that follow, see [58]. For the part dealing with complex networks, some assumptions on the parameters describing the network are taken into account in order to derive asymptotic stability. When the network topology is characterised by an undirected graph, further conditions on the adjacency matrix must be considered, see [21]. Moreover, one crucial

aspect is to prove that the set considered is an invariance set, see [13]. In the case of necessary and sufficient conditions, Nagumo's Theorem states that a set is invariant if and only if the inner product of any point in the set with any normal vector exterior to the set is nonpositive. Namely, at the boundaries of the manifold, the products of each point with a vector pointing outside the manifold remains inside the manifold itself. Lastly, the proofs relating to the stochastic system are not included here since they have not been previously peer-reviewed. Therefore, they are left in the body of the chapter and are to be found in the corresponding section below the result in the form of a proposition.

Proof of Theorem 12

The determinant Δ of matrix $A_k(\theta)$ is always positive. This follows from

$$(r+\sigma)\psi_k\theta + \alpha + \gamma \geq \psi_k r\theta + \gamma. \tag{4.37}$$

Also, the trace T of the same matrix is negative, as it can be seen from

$$T = -2(r+\sigma)\psi_k\theta - 2\alpha - 2\gamma < 0, \tag{4.38}$$

given that the parameters are nonnegative. Therefore the system is asymptotically stable. Additionally, the equilibrium point given by the set of equations in (4.6) is locally asymptotically stable as

$$T^2 - 4\Delta = T^2 - 4[(T/2)^2 - (\psi_k r\theta + \gamma)^2] = 4(\psi_k r\theta + \gamma)^2 > 0. \tag{4.39}$$

As for the speed of convergence, the eigenvalues of the Jacobian matrix can be found from the previous calculations as $\lambda_{1,2} = -(\sigma + r)\psi_k\theta - \alpha - \gamma \pm (\psi_k r\theta + \gamma)$. In the two extreme cases of no connectivity $\psi_k = 0$ and full connectivity $\psi_k = 1$:

$$\lambda_{1,2} = \begin{cases} (-\alpha - 2\gamma, -\alpha), & \psi_k = 0, \\ (-(2r+\sigma)\theta - \alpha - 2\gamma, -\sigma\theta - \alpha), & \psi_k = 1. \end{cases} \tag{4.40}$$

Proof of Theorem 13

To compute the equilibrium points, the following holds true:

$$\begin{aligned} x_k^* &= A_k^{-1}(\theta)c_k(\theta) \\ &= \tfrac{1}{-(2r+\sigma)\psi_k\theta - \alpha - 2\gamma}[-\psi_k r\theta - \gamma, \quad -\psi_k r\theta - \gamma]^T \\ &= \tfrac{1}{(2r+\sigma)\psi_k\theta + \alpha + 2\gamma}[\psi_k r\theta + \gamma, \quad \psi_k r\theta + \gamma]^T. \end{aligned} \tag{4.41}$$

In order to evaluate the impact of the connectivity, the cases of zero connectivity and full connectivity, namely $\psi_k = 0$ and $\psi_k = 1$, are considered. The equilibrium points in each case are:

$$\begin{aligned} x_k^* &= \tfrac{1}{\alpha+2\gamma}[\gamma \quad \gamma]^T, && \psi_k = 0, \\ x_k^* &= \tfrac{1}{(2r+\sigma)\theta+\alpha+2\gamma}[r\theta+\gamma \quad r\theta+\gamma]^T, && \psi_k = 1. \end{aligned} \tag{4.42}$$

Due to the smaller values of the equilibrium point for full connectivity, from the conservation of mass, the number of players in the uncommitted state is higher than in the case for zero connectivity. Therefore, a higher connectivity increases the number of uncommitted players at steady-state.

Proof of Theorem 14

In order to find a value for the threshold, the equilibrium points of micro-macro model are studied. To compute the equilibria, let $\dot{\theta}_1 = \dot{\theta}_2$:

$$(\theta_1 - \theta_2)(r/k_{max}\Psi_3 - \alpha) + \frac{\sigma\theta_1}{k_{max}}\Psi_2 - \frac{\sigma\theta_2}{k_{max}}\Psi_1 = 0. \tag{4.43}$$

Note that in a symmetric equilibrium where $\theta_1 = \theta_2$, the last two terms can be neglected. Saddle points are obtained when the determinant of the Jacobian is less than 0. Due to the symmetry of the equilibrium, let $\Psi_1 = \Psi_2$. By imposing that the right-hand side is greater than the left-hand side, it follows:

$$\Big(-\frac{\sigma}{k_{max}}\Psi - \gamma\Big)^2 > \Big(\frac{r}{k_{max}}(V(k)/\langle k\rangle - 2\Psi) - \alpha - \gamma\Big)^2. \tag{4.44}$$

By taking the square root on both sides, because of the fact that the left-hand side is strictly negative, the following holds:

$$-\frac{\sigma}{k_{max}}\Psi < -2\frac{r}{k_{max}}\Psi + \frac{rV(k)}{k_{max}\langle k\rangle} - \alpha, \tag{4.45}$$

from which the threshold in (4.9) is obtained after some basic algebra. The obtained threshold for the cross-inhibitory signal constitutes the counterpart of (2.10) in the case of structured environment.

Proof of Theorem 15

To prove the theorem, each statement must be proved individually. Therefore, the proof for each statement follows:

1. To prove that by assuming $s(0), r(0) \in [0,1]^n$, the condition $s(t), r(t) \in [0,1]^n$ holds for all $t > 0$, it means that $[0,1]^n$ must be an invariant set for the differential equation (4.12). To see that, the right-hand side of the equations in (4.12) can be specialised in 0 and 1 for the corresponding bidimensional system as:

$$\begin{cases} \dot{s}(t) = -\beta'_{23}\bar{0}^n\mathbb{I}^n A r(t) + \beta'_{32}x(t)\mathbb{I}^n A\bar{0}^n - \beta_{23}\bar{0}^n + \beta_{32}x(t) = \beta_{32}x(t), \\ \dot{r}(t) = -\beta'_{13}\bar{0}^n\mathbb{I}^n A s(t) + \beta'_{31}x(t)\mathbb{I}^n A\bar{0}^n - \beta_{13}\bar{0}^n + \beta_{31}x(t) = \beta_{31}x(t), \end{cases} \tag{4.46}$$

where both equation are positive definite. Analogously, in 1:

$$\begin{cases} \dot{s}(t) = -\beta'_{23}\mathbb{I}^n A\bar{0}^n + \beta'_{32}\bar{0}^n\mathbb{I}^n A\bar{1}^n - \beta_{23}\bar{1}^n + \beta_{32}\bar{0}^n = -\beta_{23}\bar{1}^n, \\ \dot{r}(t) = -\beta'_{13}\mathbb{I}^n A\bar{0}^n + \beta'_{31}\bar{0}^n\mathbb{I}^n A\bar{1}^n - \beta_{13}\bar{1}^n + \beta_{31}\bar{0}^n = -\beta_{13}\bar{1}^n, \end{cases} \tag{4.47}$$

which are both negative definite. By checking the above conditions, for the property of continuity of the equations, the set $[0,1]^n$ is therefore an invariant set for the differential equations in (4.12).

2. Given the notation where the dependence on time is not explicit, system (4.12) can be rewritten as a bidimensional system as:

$$\begin{cases} \dot{s} = -\beta'_{23}s\mathbb{I}^n Ar + \beta'_{32}(\bar{1}^n - s - r)\mathbb{I}^n As - \beta_{23}s + \beta_{32}(\bar{1}^n - s - r), \\ \dot{r} = -\beta'_{13}r\mathbb{I}^n As + \beta'_{31}(\bar{1}^n - s - r)\mathbb{I}^n Ar - \beta_{13}r + \beta_{31}(\bar{1}^n - s - r), \end{cases} \tag{4.48}$$

where, for the usual condition on the conservation of mass, $x = \bar{1}^n - s - r$. By inspection, it is straightforward to prove that the pairs $(\bar{1}^n, \bar{0}^n)$ and $(\bar{0}^n, \bar{1}^n)$ are equilibrium points of the above system. As regards stability, the Jacobian matrices for the above system linearised about each equilibrium point are:

$$J = \begin{bmatrix} -\beta_{23}\bar{1}^n - \beta_{32}\bar{1}^n & -\beta'_{23}A\bar{1}^n - \beta'_{32}A\bar{1}^n - \beta_{32}\bar{1}^n \\ -\beta_{31}\bar{1}^n & -\beta'_{13}A\bar{1}^n - \beta_{13}\bar{1}^n - \beta_{31}\bar{1}^n \end{bmatrix}, \tag{4.49}$$

for the equilibrium point $(\bar{1}^n, \bar{0}^n)$, while for the other one, i.e. $(\bar{0}^n, \bar{1}^n)$, it follows:

$$J = \begin{bmatrix} -\beta'_{23}A\bar{1}^n - \beta_{23}\bar{1}^n - \beta_{32}\bar{1}^n & -\beta_{32}\bar{1}^n \\ -\beta'_{13}A\bar{1}^n - \beta'_{31}A\bar{1}^n\beta_{31}\bar{1}^n & -\beta_{13}\bar{1}^n - \beta_{31}\bar{1}^n \end{bmatrix}. \tag{4.50}$$

For both matrices, the trace is negative. Asymptotic stability can be ensured when the coefficients of the main diagonal of the Jacobian matrix are, in absolute value, greater than those in the off-diagonal. When the opposite is true, the equilibria are saddle points.

3. To prove that the pair $((1/(2+k))^n, (1/(2+k))^n)$ for the bidimensional system presented above is a set of equilibrium points, the symmetry condition is explored, i.e. $s = r$. The first equation can be rewritten as:

$$\dot{s} = -(\beta'_{23} + 2\beta'_{32})s\mathbb{I}^n As + \beta'_{32}As - \beta_{23}s + \beta_{32}(\bar{1}^n - 2s). \tag{4.51}$$

The above equation is linearised about $((1/(2+k))^n, (1/(2+k))^n)$, and, by inspection, the following holds:

$$\begin{aligned} \dot{s} = \; & -(k\beta'_{32} + 2\beta'_{32})((1/(2+k))^n)\mathbb{I}^n A(1/(2+k))^n \\ & +\beta'_{32}A(1/(2+k))^n + \beta_{32}(\bar{1}^n - (2+k)(1/(2+k))^n), \end{aligned} \tag{4.52}$$

where the first two terms and the last one cancel out. Thus, $((1/(2+k))^n, (1/(2+k))^n)$ is an equilibrium point of the system. The corresponding set of equilibrium point for the 3-dimensional system (4.12) is $((1/(2+k))^n, \bar{1}^n - (2/(2+k))^n, (1/(2+k))^n)$. As for the stability property of this equilibrium point, the corresponding Jacobian matrix is

$$J = \begin{bmatrix} -\beta'_{32}A\bar{1}^n - \beta_{32}\bar{1}^n & -\beta'_{32}A\bar{1}^n - \beta_{32}\bar{1}^n \\ -\beta'_{31}A\bar{1}^n - \beta_{31}\bar{1}^n & -\beta'_{31}A\bar{1}^n - \beta_{31}\bar{1}^n \end{bmatrix}. \tag{4.53}$$

The determinant of the above Jacobian is $\Delta = 0$, while the trace is $T = -\beta'_{32}A\bar{1}^n - \beta_{32}\bar{1}^n - \beta'_{31}A\bar{1}^n - \beta_{31}\bar{1}^n$. It follows that the equilibrium point is asymptotically stable due to $T < 0$, since all the coefficients of the Jacobian matrix are negative. This conclude the proof.

Proof of Theorem 16

The proof of each statement is listed in the following:

1. As for the case of honeybees, the condition for this statement means that $[0,1]^n$ must be an invariant set for the differential equations in (4.14). Again, this can be checked by setting the right-hand side of the equations in (4.14) to 0 and to 1 and examine whether whether the derivatives are positive and negative definite, respectively.

$$\begin{cases} \dot{s}(t) = -\beta_{23}\bar{0}^n\mathbb{I}^n Ax(t) + \beta_{32}x(t) = \beta_{32}x(t), \\ \dot{r}(t) = -\beta_{13}\bar{0}^n\mathbb{I}^n Ax(t) + \beta_{31}x(t) = \beta_{31}x(t), \end{cases} \tag{4.54}$$

which are positive definite. Similarly, in 1:

$$\begin{cases} \dot{s}(t) = -\beta_{23}\mathbb{I}^n A\bar{0}^n + \beta_{32}\bar{0}^n = 0, \\ \dot{r}(t) = -\beta_{13}\mathbb{I}^n A\bar{0}^n + \beta_{31}\bar{0}^n = 0, \end{cases} \tag{4.55}$$

which are nonpositive definite. By using Nagumo's Theorem, see, e.g., [13], which gives necessary and sufficient conditions for invariance of a closed subset of a manifold, namely the inner product of each point with any exterior normal vector to the set must be nonpositive. In the present case, for any x belonging on the boundary of the set $[0,1]^n$, the corresponding vector $x\mathbb{I}^n Ax$ is either tangent or point inside the set $[0,1]^n$. Therefore $[0,1]^n$ is an invariant set for the set of differential equations (4.14).

2. System (4.14) can be rewritten by removing the explicit dependence on time as:

$$\begin{cases} \dot{s} = -\beta_{23} s^* \mathbb{I}^n A(\bar{1}^n - s - r) + \beta_{32}(\bar{1}^n - s - r), \\ \dot{r} = -\beta_{13}(\bar{1}^n - s^*)\mathbb{I}^n A(\bar{1}^n - s - r) + \beta_{31}(\bar{1}^n - s - r). \end{cases} \tag{4.56}$$

The corresponding Jacobian matrix can be calculated as:

$$J = \begin{bmatrix} \beta_{23} s^* \mathbb{I}^n A\bar{1}^n - \beta_{32}\bar{1}^n & \beta_{23} s^* \mathbb{I}^n A\bar{1}^n - \beta_{32}\bar{1}^n \\ \beta_{13}(\bar{1}^n - s^*)\mathbb{I}^n A\bar{1}^n - \beta_{31}\bar{1}^n & \beta_{13}(\bar{1}^n - s^*)\mathbb{I}^n A\bar{1}^n - \beta_{31}\bar{1}^n \end{bmatrix}. \tag{4.57}$$

The determinant of the above Jacobian is $\Delta = 0$, while the trace is $T = \beta_{23} s^* \mathbb{I}^n A\bar{1}^n - \beta_{32}\bar{1}^n + \beta_{13}(\bar{1}^n - s^*)\mathbb{I}^n A\bar{1}^n - \beta_{31}\bar{1}^n$. The equilibrium point is asymptotically stable if $Tr(J) < 0$, which holds true when the condition in (4.16) holds.

3. When $\lim_{\beta_{32},\beta_{13}\to 0}$, system (4.14) can be rewritten in vector form as

$$\begin{cases} \dot{s}(t) = -\beta_{23} s(t)\mathbb{I}^n Ax(t), \\ \dot{x}(t) = \beta_{23} s(t)\mathbb{I}^n Ax(t) - \beta_{31} x(t), \\ \dot{r}(t) = \beta_{31} x(t), \end{cases} \tag{4.58}$$

which corresponds to the standard SIR network model. This conclude the proof.

CHAPTER 5

Conclusion

In this thesis, the study of the collective decision-making problem originating in the context of honeybee swarms is carried out.

In Chapter 2, the original problem is extended to a game theoretic framework, which highlights the strategic evolution of the population distribution across three possible states. Two of these states represent the possible alternatives (nest boxes in the original formulation of the model) while the last state is expression of the percentage of players not committed to either alternative. Three game settings are examined. First, a more general setting is considered, in which the payoffs are asymmetric and so are the corresponding transition rates. The second setting involves the study where the two options have equal intrinsic value, and thus all strategies are awarded symmetric payoffs. In the last setting, the case of certain strategies having payoff equal to zero is investigated, which corresponds to a different structure for the Markov chain. The latter case is also linked to compartmental models: the population is partitioned in compartments, where individuals share similar characteristics with other people of the same compartment. The model is also analysed in the case where one coefficient of the payoff matrix is treated as a time varying parameter.

As regards the analysis, the evolutionary dynamics is reframed in an evolutionary game theoretic setting first, and then the corresponding ODEs for the collective decision-making problem are derived. The fixed points are explicitly calculated in each context, i.e. symmetric and asymmetric cases, and the study of the stability properties is carried out for each scenario. Furthermore, the role of the cross-inhibitory signal is investigated and a more general formulation of the threshold present in the literature is found via a different perspective, namely Lyapunov stability theory. Although both scenarios could

be treated as separate systems, it is shown that they share a common ground and, as a result, that the conclusions can be linked from one context to the other. To this extent, the study of an uncertain cross-inhibitory coefficient is derived in both symmetric and asymmetric cases, and it is shown that absolute stability is achieved in the former, whereas the passivity of the system is ensured in the latter.

In terms of future directions, one can consider to extend the model to inhomogeneous players or in the presence of stubborn agents. In a similar game setting, the impact of stubborn agents or bandwagon effects has been studied, for instance see [30]. The role of the dynamics that attract players towards one option, such as the equivalent of the waggle dance, could constitute another direction of research, in which committed players can adjust their effort in order to collaboratively attract uncommitted players. Although changing this parameter to a time varying coefficient would make the system much more complex, it would also make it more realistic in many of the applications proposed throughout this thesis, such as opinion dynamics. The case of collaborating agents in a cooperative setting can also be a possible extension to the model.

Chapter 3 includes the formulation of the mean-field game model corresponding to the original collective decision-making problem, where the interactions of a large population of small players are considered. The macroscopic dynamics, that regulate how the population distribution evolves across the three states, and the microscopic dynamics, which instead define the strategic response of a reference player, constitute together the mean-field game model. The corresponding stationary solutions are derived and then studied by considering the difference between the uncommitted state and the committed states in terms of the value function calculated at each state. This is motivated by the fact that the problem of reaching consensus depends in fact on the dynamics involving the players that have no commitment. When a large number of players remains uncommitted, this situation can be interpreted as a deadlock, in which the population remains undecided between the two proposed alternatives.

The analysis of the mean-field game is achieved by bringing together the macroscopic and microscopic dynamics in the form of the Kolmogorov and Hamilton-Jacobi-Bellman equations, respectively. The resulting mean-field Nash equilibrium is studied in the form of initial-terminal value problem. Under the assumption that the adversarial disturbance is the worst-case deterministic time varying signal sent by the players who chose the option opposite to the one chosen by the reference player, the corresponding

optimal Markovian control is obtained. The asymptotic stability analysis is carried out for the derived stationary solutions, but not in terms of the three initial states, rather as the difference between the uncommitted state and each of the committed states. Due to the extensive analysis of the Kolmogorov equations in the corresponding macroscopic model from the previous chapter, the stability properties of the equilibrium points are derived for the value functions, thanks to the connection to the stability properties in the population distribution. Furthermore, the stability of periodic solutions is investigated and a basin of attraction for the stationary mean-field equilibrium points is found.

An important contribution to the field could come from a possible extension to the study of monotone and contractive MFGs under the scope of robustness. In short, this would implies to prove that the stationary solutions can be approximated to the nonstationary solutions in the presence of an adversarial disturbance. The monotone and contractive MFGs has been studied in [40], and under certain assumptions on the adversarial disturbance, such as the ones proposed in this chapter, this could lead to the extension in the case of robust MFGs.

In Chapter 4, an instance of the original problem is investigated as a multi-agent system, in the case of structured environment. First, the structure is modelled as a scale-free complex network, which captures the agents' interactions in the system. Within this context, both the symmetric and asymmetric cases are studied. Then, the agents are connected by means of an undirected graph. The corresponding model can take the form of a system in which the agents can either represent the bees and their communications or physical buses in a smart grid for a virus propagation scenario. Later, the case in which the agents can choose one of two options is extended to the n-option setting, under some stochastic disturbance. This disturbance can take the form of a nudge to push the agents towards consensus. Another proposed extension involves a swarm of robots and buffer networks, where a set of agents need to broadcast a piece of information in a stochastic dynamical network with limitations on the buffer size.

As for the analysis in this chapter, the structure is first modelled as a SF complex network, namely Barabási-Albert, for the symmetric and asymmetric cases. The impact of the connectivity on the equilibrium points is investigated from two points of view: a perspective on how fast the dynamics converge, namely the speed of the transient response; and a perspective on how many agents remain uncommitted at steady-state, causing a potential deadlock and no consensus. Additionally, a link to the unstructured

case is provided from each perspective and also in terms of the threshold on the cross-inhibitory coefficient. When the structure is modelled as an undirected graph through an adjacency matrix, a small number of agents is considered. However, each agent represent an infinite number of populations, because his/her distribution (the vector of the three states) denotes the probability of being in any of the three possible states. A case study is proposed for the Walpole GSP - Peterborough network. Furthermore, the 2-option case is extended to the stochastic n-option case and the link with nudge theory is provided through the stochastic disturbance. Finally, the interaction dynamics are linked to the context of swarm robotics through buffer networks and the corresponding problem of exchanging information among the agents in the network.

Future directions of research include the extension of the results to stochastic dynamics in the structured case, with births and deaths in the population. Additionally, the impact of curing rates for the virus propagation scenario can be investigated. Last but not least, a possible path could involve the study of similar models in chemistry and how the structure influences the reaction process. For an overview on this topic, the reader is referred to [32], [33]. For more recent developments, see [28], [29].

Bibliography

[1] Y. Achdou, F. Camilli and I. Capuzzo-Dolcetta, "Mean Field Games: Numerical Methods for the Planning Problem", *SIAM Journal of Control and Optimization*, vol. 50, pp. 77-109, 2012. Available: 10.1137/100790069.

[2] R. Albert, H. Jeong and A. Barabási, "Error and attack tolerance of complex networks", *Nature*, vol. 406, no. 6794, pp. 378-382, 2000. Available: 10.1038/35019019.

[3] F. Bagagiolo and D. Bauso, "Mean-Field Games and Dynamic Demand Management in Power Grids", *Dynamic Games and Applications*, vol. 4, pp. 155-176, 2014. Available: 10.1007/s13235-013-0097-4.

[4] A. Barabási and R. Albert, "Emergence of Scaling in Random Networks", *Science*, vol. 286, no. 5439, pp. 509-512, 1999. Available: 10.1126/science.286.5439.509.

[5] M. Bardi, "Explicit Solutions of Some Linear-Quadratic Mean-Field Games", *Network and Heterogeneous Media*, vol. 7, no. 2, pp. 243-261, 2012. Available: 10.3934/nhm.2012.7.243.

[6] A. Barron and J. Plath, "The evolution of honey bee dance communication: a mechanistic perspective", *The Journal of Experimental Biology*, vol. 220, no. 23, pp. 4339-4346, 2017. Available: 10.1242/jeb.142778.

[7] D. Bauso, "Consensus via Multi-population Robust Mean-Field Games", *Systems & Control Letters*, vol. 107, pp. 76-83, 2017. Available: 10.1016/j.sysconle.2017.07.010.

[8] D. Bauso, T. Mylvaganam and A. Astolfi, "Crowd-Averse Robust Mean-Field Games: Approximation via State Space Extension", *IEEE Transaction on Automatic Control*, vol. 61, no. 7, pp. 1882-1894, 2016. Available: 10.1109/tac.2015.2479927.

[9] D. Bauso and R. Pesenti, "Mean Field Linear Quadratic Games with Set Up Costs", *Dynamic Games and Applications*, vol. 3, no. 1, pp. 89-104, 2012. Available: 10.1007/s13235-012-0069-0.

[10] D. Bauso and H. Tembine, "Crowd-Averse Cyber-Physical Systems: The Paradigm of Robust Mean-Field Games", *IEEE Transactions on Automatic Control*, vol. 61, no. 8, pp. 2312-2317, 2016. Available: 10.1109/tac.2015.2492038.

[11] D. Bauso, H. Tembine and T. Başar, "Robust Mean-Field Games", *Dynamic Games and Applications*, vol. 6, no. 3, pp. 277-303, 2015. Available: 10.1007/s13235-015-0160-4.

[12] D. Bauso and H. Tembine and T. Başar, "Opinion Dynamics in Social Networks through Mean-Field Games", *SIAM Journal on Control and Optimization*, vol. 54, no. 6, pp. 3225-3257, 2016. Available: 10.1137/140985676.

[13] F. Blanchini, "Set invariance in control", *Automatica*, vol. 35, no. 11, pp. 1747-1767, 1999. Available: 10.1016/s0005-1098(99)00113-2.

[14] F. Blanchini, G. Chesi, P. Colaneri and G. Giordano, "Checking Structural Stability of BDC-Decomposable Systems via Convex Optimisation", *IEEE Control Systems Letters*, vol. 4, no. 1, pp. 205-210, 2019. Available: 10.1109/lcsys.2019.2922413.

[15] F. Blanchini and G. Giordano, "BDC-Decomposition for Global Influence Analysis", *IEEE Control Systems Letters*, vol. 3, no. 2, pp. 260-265, 2019. Available: 10.1109/lcsys.2018.2866903.

[16] S. Boccaletti, V. Latora, Y. Moreno, M. Chavez and D. Hwang, "Complex networks: Structure and dynamics", *Physics Reports*, vol. 424, no. 4-5, pp. 175-308, 2006. Available: 10.1016/j.physrep.2005.10.009.

[17] P. Bolzern, P. Colaneri and G. De Nicolao, "Opinion influence and evolution in social networks: A Markovian agents model", *Automatica*, vol. 100, pp. 219-230, 2019. Available: 10.1016/j.automatica.2018.11.023.

[18] A. Bressan, "Noncooperative Differential Games: A Tutorial", *J. Differential Equations*, vol. 248, 2010. Available: http://www.math.psu.edu/bressan/PSPDF/gamelnew.pdf.

[19] N. F. Britton, N. R. Franks, S. C. Pratt and T. D. Seeley, "Deciding on a new home: how do honeybees agree?", *Proceedings of the Royal Society of London. Series B: Biological Sciences*, vol. 269, no. 1498, pp. 1383-1388, 2002. Available: 10.1098/rspb.2002.2001.

[20] B. Brogliato, B. Maschke, R. Lozano and O. Egeland, "Kalman-Yakubovich-Popov Lemma", in *Dissipative Systems Analysis and Control. Communications and Control Engineering*. London: Springer, 2007.

[21] F. Bullo, *Lectures on Network Systems*. Create Space, 2018.

[22] M. Calabrese, "Hierarchical-Granularity Holonic Modelling". *Doctoral Thesis*. University of Milan, Italy, 2011.

[23] C. Camerer, *Behavioral Game Theory*. Princeton, NJ: Princeton University Press, 2003.

[24] C. Cameron, C. Patsios, P. Taylor and Z. Pourmirza, "Using Self-Organizing Architectures to Mitigate the Impacts of Denial-of-Service Attacks on Voltage Control Schemes", *IEEE Transactions on Smart Grid*, vol. 10, no. 3, pp. 3010-3019, 2019. Available: 10.1109/tsg.2018.2817046.

[25] D. Cheng, F. He, H. Qi and T. Xu, "Modeling, Analysis and Control of Networked Evolutionary Games", *IEEE Transactions on Automatic Control*, vol. 60, no. 9, pp. 2402-2415, 2015. Available: 10.1109/tac.2015.2404471.

[26] L. C. Coffman, R. F. Clayton and B. K. Judd, "A Model of Information Nudges", November 2015. Unpublished, Ohio State University: https://site.stanford.edu/sites/default/files/a_model_of_information_nudges_20151124.pdf.

[27] M. Corless, C. King, R. Shorten and F. Wirth, *AIMD dynamics and distributed resource allocation*. Philadelphia: Society for Industrial and Applied Mathematics, 2016.

[28] G. Craciun and M. Feinberg, "Multiple Equilibria in Complex Chemical Reaction Networks: I. The Injectivity Property", *SIAM Journal on Applied Mathematics*, vol. 65, no. 5, pp. 1526-1546, 2005. Available: 10.1137/s0036139904440278.

[29] G. Craciun and M. Feinberg, "Multiple Equilibria in Complex Chemical Reaction Networks: II. The Species-Reaction Graph", *SIAM Journal on Applied Mathematics*, vol. 66, no. 4, pp. 1321-1338, 2006. Available: 10.1137/050634177.

[30] P. Dai Pra, E. Sartori and M. Tolotti, "Climb on the Bandwagon: Consensus and Periodicity in a Lifetime Utility Model with Strategic Interactions", *Dynamic Games and Applications*, 2019. Available: 10.1007/s13235-019-00299-y.

[31] C. Du and W. H. Wong, "Stochastic Modeling and Statistical Inference of Intrinsic Noise in Gene Regulation System via Chemical Master Equation". In: arXiv:1610.07213 [q-bio, stat] (2016). arXiv: 1610.07213.

[32] M. Feinberg, "Chemical reaction network structure and the stability of complex isothermal reactors–I. The deficiency zero and deficiency one theorems", *Chemical Engineering Science*, vol. 42, no. 10, pp. 2229-2268, 1987. Available: 10.1016/0009-

2509(87)80099-4.

[33] M. Feinberg, "Chemical reaction network structure and the stability of complex isothermal reactors–II. Multiple steady-states for networks of deficiency one", *Chemical Engineering Science*, vol. 43, no. 1, pp. 1-25, 1988. Available: 10.1016/0009-2509(88)87122-7.

[34] M. Feinberg and F. J. M. Horn, "Dynamics of open chemical systems and the algebraic structure of the underlying reaction network", *Chemical Engineering Science*, vol. 29, no. 3, pp. 775-787, 1974. Available: 10.1016/0009-2509(74)80195-8.

[35] M. Feinberg and F. J. M. Horn, "Chemical mechanism structure and the coincidence of the stoichiometric and kinetic subspaces", *Archive for Rational Mechanics and Analysis*, vol. 66, no. 1, pp. 83-97, 1977. Available: 10.1007/bf00250853.

[36] G. Filatrella, A. Nielsen and N. Pedersen, "Analysis of a power grid using a Kuramoto-like model", *The European Physical Journal B*, vol. 61, no. 4, pp. 485-491, 2008. Available: 10.1140/epjb/e2008-00098-8.

[37] K. Fischer, M. Schillo and J. Siekmann, "Holonic Multiagent Systems: A Foundation for the Organisation of Multiagent Systems, *Lecture Notes in Computer Science*, Springer, vol. 2744, pp. 1083-1084, 2004.

[38] R. A. Fisher, *The Genetic Theory of Natural Selection*. Oxford: Clarendon Press, 1930.

[39] D. A. Gomes, J. Mohr and R. R. Souza, "Discrete time, finite state space mean field games", *Journal de Mathématiques Pures et Appliquées*, vol. 93, no. 3, pp. 308-328, 2010. Available: 10.1016/j.matpur.2009.10.010.

[40] D. A. Gomes, J. Mohr and R. R. Souza, "Continuous Time Finite State Mean Field Games", *Applied Mathematics & Optimization*, vol. 68, no. 1, pp. 99-143, 2013. Available: 10.1007/s00245-013-9202-8.

[41] D. A. Gomes and J. Saúde, "Mean Field Games Models – A Brief Survey", *Dynamic Games and Applications*, vol. 4, no, 2, pp. 110-154, 2014. Available: 10.1007/s13235-013-0099-2.

[42] D. A. Gomes and J. Saúde, "Numerical Methods for Finite-State Mean-Field Games Satisfying a Monotonicity Condition", *Applied Mathematics & Optimization*, 2018. Available: 10.1007/s00245-018-9510-0.

[43] D. A. Gomes, R. Velho and M. Wolfram, "Socio-economic Applications of Finite State Mean Field Games", Philosophical Transactions of the Royal Society A: Math-

ematical, Physical and Engineering Sciences, vol. 372, no. 2028, 2014. Available: 10.1098/rsta.2013.0405.

[44] D. González-Sánchez and O. Hernández-Lerma, "A survey of static and dynamic potential games", *Science China Mathematics*, vol. 59, no. 11, pp. 2075-2102, 2016. Available: 10.1007/s11425-016-0264-6.

[45] R. Gray, A. Franci, V. Srivastava and N. E. Leonard, "Multiagent Decision-Making Dynamics Inspired by Honeybees", *IEEE Transactions on Control of Network Systems*, vol. 5, no. 2, pp. 793-806, 2018. Available: 10.1109/tcns.2018.2796301.

[46] O. Gueant, J. M. Lasry and P. L. Lions, "Mean-Field Games and Applications", *Paris-Princeton Lectures*, Springer, pp. 1-66, 2010.

[47] W. D. Hamilton, "The genetical evolution of social behaviour. I", *Journal of Theoretical Biology*, vol. 7, no. 1, pp. 1-16, 1964. Available:10.1016/0022-5193(64)90038-4.

[48] W. D. Hamilton, "The genetical evolution of social behaviour. II", *Journal of Theoretical Biology*, vol. 7, no. 1, pp. 17-52, 1964. Available: 10.1016/0022-5193(64)90039-6.

[49] T. Harko, F. Lobo and M. Mak, "Exact analytical solutions of the Susceptible-Infected-Recovered (SIR) epidemic model and of the SIR model with equal death and birth rates", *Applied Mathematics and Computation*, vol. 236, pp. 184-194, 2014. Available: 10.1016/j.amc.2014.03.030.

[50] R. Hegselmann and U. Krause, "Opinion dynamics and bounded confidence models, analysis, and simulation", *Journal of Artificial Societies and Social Simulation*, vol. 5, no. 3, 2002.

[51] H. Hethcote, "The Mathematics of Infectious Diseases", *SIAM Review*, vol. 42, no. 4, pp. 599-653, 2000. Available: 10.1137/s0036144500371907.

[52] J. Hofbauer, "Deterministic Evolutionary game dynamics", in *Proceedings of Symposia in Applied Mathematics*, Karl S. editor, 2011.

[53] J. Hofbauer and K. Sigmund, "Evolutionary game dynamics", *Bulletin of the American Mathematical Society*, vol. 40, no. 4, pp. 479-520, 2003. Available: 10.1090/s0273-0979-03-00988-1.

[54] M. Y. Huang, P. E. Caines and R. P. Malhamé, "Individual and Mass Behaviour in Large Population Stochastic Wireless Power Control Problems: Centralized and Nash Equilibrium Solutions", *IEEE Conference on Decision and Control*, HI, USA,

pp. 98-103, 2003.

[55] M. Y. Huang, P. E. Caines, and R. P. Malhamé, "Large Population Stochastic Dynamic Games: Closed Loop Kean-Vlasov Systems and the Nash Certainty Equivalence Principle", *Communications in Information and Systems*, vol. 6, no. 3, pp. 221-252, 2006.

[56] M. Y. Huang, P. E. Caines, and R.P. Malhamé, "Large-Population Cost-Coupled LQG Problems With Nonuniform Agents: Individual-Mass Behavior and Decentralized ε-Nash Equilibria", *IEEE Transactions on Automatic Control*, vol. 52, no. 9, pp. 1560–1571, 2007. Available: 10.1109/tac.2007.904450.

[57] D. Kahneman and A. Tversky, "Prospect Theory: An Analysis of Decision under Risk", *Econometrica*, vol. 47, no. 2, pp. 263-291, 1979. Available: 10.2307/1914185.

[58] H. Khalil, *Nonlinear systems*. Upper Saddle River, NJ: Prentice Hall, 2002.

[59] A. Khanafer, Tamer Başar and B. Gharesifard, "Stability Properties of Infection Diffusion Dynamics over Directed Networks". *Proceedings of the 53rd IEEE Conference on Decision and Control*, pp. 6215-6220, 2014.

[60] W. O. Kermack and A. G. McKendrick, "A Contribution to the Mathematical Theory of Epidemics", in *Proceedings of the Royal Society of London A*, vol. 115, no. 772, pp. 700-721, 1927. Available: doi:10.1098/rspa.1927.0118.

[61] A. Koestler, *The Ghost in the machine*. London: Hutchinson, 1967.

[62] Y. Kuramoto, Editor: H. Araki, "Lecture Notes in Physics", *Proceedings of the International Symposium on Mathematical Problems in Theoretical Physics*, pp. 420. Berlin: Springer-Verlag, 1975.

[63] J. M. Lasry and P. L. Lions, "Jeux à champ moyen. I Le cas stationnaire", *Comptes Rendus Mathematique*, vol. 343, no. 9, pp. 619-625, 2006.

[64] J. M. Lasry and P. L. Lions, "Jeux à champ moyen. II Horizon fini et controle optimal". *Comptes Rendus Mathematique*, vol. 343, no. 10, pp. 679-684, 2006.

[65] J. M. Lasry and P. L. Lions, "Mean-field games", *Japanese Journal of Mathematics*, vol. 2, pp. 229–260, 2007.

[66] R. C. Lewontin, "Evolution and the theory of games", *Journal of Theoretical Biology*, vol. 1, no. 3, pp. 382-403, 1961. Available: 10.1016/0022-5193(61)90038-8.

[67] J. Li, B. Xia, X. Geng, H. Ming, S. Shakkottai, V. Subramanian and L. Xie, "Mean Field Games in Nudge Systems for Societal Networks", *ACM Transactions on Modeling and Performance Evaluation of Computing Systems*, vol. 3, no. 4, pp. 1-31,

2018. Available: 10.1145/3232076.

[68] Z. Li, Z. Duan, G. Chen and L. Huang, "Consensus of Multiagent Systems and Synchronization of Complex Networks: A Unified Viewpoint", *IEEE Transactions on Circuits and Systems I: Regular Papers*, vol. 57, no. 1, pp. 213-224, 2010. Available: 10.1109/tcsi.2009.2023937.

[69] R. Liu, C. Vellaithurai, S. Biswas, T. Gamage and A. Srivastava, "Analyzing the Cyber-Physical Impact of Cyber Events on the Power Grid", *IEEE Transactions on Smart Grid*, vol. 6, no. 5, pp. 2444-2453, 2015. Available: 10.1109/tsg.2015.2432013.

[70] K. A. Loparo and X. Feng, Editor: W. Levine, "Stability of Stochastic Systems", *The Control Handbook*. Boca Raton, Fla.: CRC Press, 2011.

[71] A. J. McKenzie, "Evolutionary Game Theory", *The Stanford Encyclopedia of Philosophy*, 2009 Edition, Edward N. Zalta (ed.). URL = https://plato.stanford.edu/archives/fall2009/entries/game-evolutionary/.

[72] Y. Moreno, R. Pastor-Satorras and A. Vespignani, "Epidemic outbreaks in complex heterogeneous networks", *The European Physical Journal B*, vol. 26, no. 4, pp. 521-529, 2002. Available: 10.1140/epjb/e20020122.

[73] T. Morstyn, N. Farrell, S. Darby and M. McCulloch, "Using peer-to-peer energy-trading platforms to incentivize prosumers to form federated power plants", *Nature Energy*, vol. 3, no. 2, pp. 94-101, 2018. Available: 10.1038/s41560-017-0075-y.

[74] T. Morstyn, A. Teytelboym and M. Mcculloch, "Bilateral Contract Networks for Peer-to-Peer Energy Trading", *IEEE Transactions on Smart Grid*, vol. 10, no. 2, pp. 2026-2035, 2019. Available: 10.1109/tsg.2017.2786668.

[75] R. B. Myerson, *Game Theory*. Cumberland: Harvard University Press, 2013.

[76] J. von Neumann and O. Morgenstern, *Theory of Games and Economic Behaviour*. New York: John Wiley and Sons, 1944.

[77] J. Newton, "Evolutionary Game Theory: A Renaissance", *Games*, vol. 9, no. 2, p. 31, 2018. Available: 10.3390/g9020031.

[78] A. Ortmann and J. Weibull, "Evolutionary Game Theory", *Southern Economic Journal*, vol. 63, no. 3, p. 834, 1997. Available: 10.2307/1061129.

[79] M. J. Osborne and A. Rubinstein, *A Course in Game Theory*. Cambridge, Mass.: MIT Press, 1994.

[80] D. Pais, P. Hogan, T. Schlegel, N. Franks, N. E. Leonard and J. Marshall, "A Mechanism for Value-Sensitive Decision-Making", *PLoS ONE*, vol. 8, no. 9, pp.

e73216, 2013. Available: 10.1371/journal.pone.0073216.

[81] K. M. Passino, "Honey Bee Swarm Cognition: Decision-Making Performance and Adaptation", *International Journal of Swarm Intelligence Research*, vol. 1, no. 2, pp. 80-97, 2010. Available: 10.4018/jsir.2010040105.

[82] K. M. Passino, T. D. Seeley and P. K. Visscher, "Swarm cognition in honey bees", *Behavioral Ecology and Sociobiology*, vol. 62, no. 3, pp. 401-414, 2008. Available: 10.1007/s00265-007-0468-1.

[83] D. Pichert and K. Katsikopoulos, "Green defaults: Information presentation and pro-environmental behaviour", *Journal of Environmental Psychology*, vol. 28, no. 1, pp. 63-73, 2008. Available: 10.1016/j.jenvp.2007.09.004.

[84] I. Poulakakis, G. F. Young, L. Scardovi and N. E. Leonard, "Information Centrality and Ordering of Nodes for Accuracy in Noisy Decision-Making Networks", *IEEE Transactions on Automatic Control*, vol. 61, no. 4, pp. 1040-1045, 2016. Available: 10.1109/tac.2015.2454373.

[85] A. Rantzer and M. E. Valcher, "A Tutorial on Positive Systems and Large Scale Control", in *IEEE Conference on Decision and Control (CDC)*, 2018.

[86] P. Rye, "Regional Development Plan, Walpole GSP - Peterborough (EPN)". *Version 2.0, Date 13/03/2014*.

[87] W. Saad, Z. Han, H. Poor and T. Başar, "Game-Theoretic Methods for the Smart Grid: An Overview of Microgrid Systems, Demand-Side Management, and Smart Grid Communications", *IEEE Signal Processing Magazine*, vol. 29, no. 5, pp. 86-105, 2012. Available: 10.1109/msp.2012.2186410.

[88] R. Salhab, R. P. Malhamé and J. Le Ny, "A dynamic game model of collective choice in multi-agent systems". *54th IEEE Conference on Decision and Control*, 2015, pp. 4444-4449.

[89] L. Samuelson, "Evolution and Game Theory", *Journal of Economic Perspectives*, vol. 16, no. 2, pp. 47-66, 2002. Available: 10.1257/0895330027256.

[90] A. Sarlette, R. Sepulchre and N. E. Leonard, "Autonomous rigid body attitude synchronization", *Automatica*, vol. 45, no. 2, pp. 572-577, 2009. Available: 10.1016/j.automatica.2008.09.020.

[91] T. Seeley, *Honeybee Democracy*. Oxford: Princeton University Press, 2010.

[92] J. M. Smith, "Game Theory and The Evolution of Fighting", *Evolution. Edinburgh University Press*, 1972. ISBN 0-85224-223-9.

[93] J. M. Smith and G. Price, "The Logic of Animal Conflict", *Nature*, vol. 246, no. 5427, pp. 15-18, 1973. Available: 10.1038/246015a0.

[94] V. Srivastava and N. E. Leonard, "Bio-inspired decision-making and control: From honeybees and neurons to network design", *American Control Conference*, 2017. Available: 10.23919/ACC.2017.7963250.

[95] S. Strogatz, "From Kuramoto to Crawford: exploring the onset of synchronization in populations of coupled oscillators", *Physica D: Nonlinear Phenomena*, vol. 143, no. 1-4, pp. 1-20, 2000. Available: 10.1016/s0167-2789(00)00094-4.

[96] S. H. Strogatz, *Nonlinear Dynamics and Chaos: with applications to physics, biology, chemistry, and engineering*. Westview press, 2014.

[97] S. Tan, J. Lu, G. Chen and D. Hill, "When Structure Meets Function in Evolutionary Dynamics on Complex Networks", *IEEE Circuits and Systems Magazine*, vol. 14, no. 4, pp. 36-50, 2014. Available: 10.1109/mcas.2014.2360790.

[98] H. Tembine, Q. Zhu and T. Başar, "Risk-Sensitive Mean-Field Games", *IEEE Trans. on Automatic Control*, vol. 59, no. 4, pp. 835-850, 2014. Available: 10.1109/tac.2013.2289711.

[99] R. Thaler and C. Sunstein, *Nudge*. New Haven, Conn.: Yale University Press, 2008.

[100] C. Vellaithurai, A. Srivastava, S. Zonouz and R. Berthier, "CPIndex: Cyber-Physical Vulnerability Assessment for Power-Grid Infrastructures", *IEEE Transactions on Smart Grid*, vol. 6, no. 2, pp. 566-575, 2015. Available: 10.1109/tsg.2014.2372315.

[101] P. K. Visscher, T. D. Seeley and K. M. Passino, "Group Decision Making in Honey Bee Swarms", *American Scientist*, vol. 94, no. 3, p. 220, 2006. Available: 10.1511/2006.3.220.

[102] K. Wang, Z. Ouyang, R. Krishnan, L. Shu and L. He, "A Game Theory-Based Energy Management System Using Price Elasticity for Smart Grids", *IEEE Transactions on Industrial Informatics*, vol. 11, no. 6, pp. 1607-1616, 2015. Available: 10.1109/tii.2015.2426015.

[103] Y. Wang, W. Saad, Z. Han, H. Poor and T. Başar, "A Game-Theoretic Approach to Energy Trading in the Smart Grid", *IEEE Transactions on Smart Grid*, vol. 5, no. 3, pp. 1439-1450, 2014. Available: 10.1109/tsg.2013.2284664.

[104] D. Watts and S. Strogatz, "Collective dynamics of 'small-world' networks", *Nature*, vol. 393, no. 6684, pp. 440-442, 1998. Available: 10.1038/30918.

[105] J. Webb, *Game theory*. London: Springer, 2007.

[106] G. Y. Weintraub, C. Benkard and B. Van Roy, "Oblivious Equilibrium: A mean-field Approximation for Large-Scale Dynamic Games", *Advances in Neural Information Processing Systems*, MIT Press, 2005.

[107] J. Wilk, "Mind, Nature and the Emerging Science of Change: An Introduction to Metamorphology". In: Cornelis G.C., Smets S., Van Bendegem J.P. (eds) *Metadebates on Science. EINSTEIN MEETS MAGRITTE: An Interdisciplinary Reflection on Science, Nature, Art, Human Action and Society*. Springer, Dordrecht: vol 6, pp. 71-87, 1999.

[108] E. O. Wilson, *Sociobiology*. Cambridge, Mass: Belknap Press of Harvard University Press, 2002.

[109] A. Wiszniewska-Matyszkiel, "Discrete Time Dynamic Games with a Continuum of Players I: Decomposable Games", *International Game Theory Review*, vol. 04, no. 03, pp. 331-342, 2002. Available: 10.1142/s0219198902000732.

[110] K. Y. M. Wong, D. Saad and C. H. Yeung, "Distributed Optimization in Transportation and Logistics Networks", *IEICE Transactions on Communications*, vol. 99, no. 11, pp. 2237-2246, 2016. Available: 10.1587/transcom.2016nei0003.

[111] C. H. Yeung, D. Saad and K. Y. M. Wong, "From the physics of interacting polymers to optimizing routes on the London Underground", *Proceedings of the National Academy of Sciences*, vol. 110, no. 34, pp. 13717-13722, 2013. Available: 10.1073/pnas.1301111110.

[112] H. Yin, P. G. Mehta, S. P. Meyn and U. V. Shanbhag, "Synchronization of Coupled Oscillators is a Game", *IEEE Transactions on Automatic Control*, vol. 57, no. 4, pp. 920-935, 2012. Available: 10.1109/tac.2011.2168082.

[113] W. Yu, G. Chen and M. Cao, "Consensus in Directed Networks of Agents With Nonlinear Dynamics", *IEEE Transactions on Automatic Control*, vol. 56, no. 6, pp. 1436-1441, 2011. Available: 10.1109/tac.2011.2112477.